

Adsorption and self-organization of CuOEP on heterogeneous surfaces: tuning the molecule-substrate interaction.

INAUGURALDISSERTATION

ZUR

Erlangung der Würde eines Doktors der Philosophie

vorgelegt der

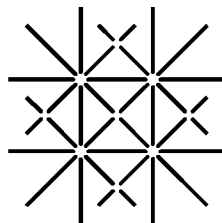
Philosophisch-Naturwissenschaftlichen Fakultät

der Universität Basel

VON

Luca Ramoino
aus Imperia (Italien)

Basel, 2005



UNI
BASEL

Genehmigt von der Philosophisch-Naturwissenschaftlichen Fakultät auf Antrag von:

Prof. Dr. H.-J. Güntherodt
Dr. T. A. Jung
Prof. Dr. E. Meyer

Basel, den 25. April 2005

Prof. Dr. Hans-Jakob Wirz, Dekan

Abstract

The adsorption and self-organization of copper(II) octaethyl porphyrin (CuOEP) have been studied in detail on heterogeneous surfaces by Scanning Tunnelling Microscopy (STM), Low Energy Electron Diffraction (LEED) and Ultraviolet Photoelectron Spectroscopy (UPS).

The research has been focussed both on the adsorption of CuOEP on clean metals as well as on ultrathin sodium chloride films grown on metals. For this reason, in a first stage, the growth of NaCl films on Cu(111), Ag(111) and Ag(001) has been carefully investigated. For submonolayer coverages the samples show the formation of NaCl islands with a characteristic rectangular shape, which coexist with clean metal regions. Salt structures 1 to 3 ML thick can be identified.

CuOEP molecules have been deposited on the so prepared heterogeneous salt-metal surfaces. STM reveals that the molecules self organize in ordered monolayers on the bare metal areas as well as on the NaCl islands. Series of observations performed by increasing the CuOEP coverage in steps from 0 to 1 ML revealed that the assembly develops in a hierarchical fashion. Molecules sequentially adsorb and assemble first on the bare metal, then on the 1-layer and 2-layer thick NaCl areas. From these observations it can be inferred that the adsorption energy of CuOEP decreases by introducing an insulator layer and by increasing its thickness. Moreover, the investigation of the STM appearance of CuOEP as a function of the bias voltage, indicates a weaker adsorbate-substrate interaction on the NaCl/metal system than on the bare metal.

The adsorption of CuOEP on the clean metal has been further investigated by LEED and UPS. Combining LEED and STM, the structure of the molecular layer formed on Cu(111), Ag(111) and Ag(001) is determined. Information on the adsorption conformation of CuOEP has also been gained by high resolution STM. In these measurements several intramolecular features can be recognized and they fit very well with simulated STM images based on DFT calculations. The theoretical predictions of the molecular orbital energies fit also very well with the UPS measurements. In particular the position and the relative intensity of HOMO and HOMO-1 levels show a very good agreement between experiment and calculation.

UPS has also been used to measure the work function change of the various metal substrates upon CuOEP adsorption. These experiments prove that, for all metal investigated, a charge transfer from the molecule to the substrate takes place. This charge transfer is found to depend on the work function of the substrate. In particular the comparison between the Ag(111) and Ag(001) cases demonstrates that the observed work function change does not depend only on the chemistry of the substrate but also on the details of the surface electronic structure.

Contents

Abstract	i
Abbreviations	v
1. Introduction	1
1.1. Motivation and Outline	1
1.2. Experimental Techniques	2
1.2.1. Scanning Tunnelling Microscopy	2
1.2.2. Low Energy Electron Diffraction	6
1.2.3. Photoelectron Spectroscopy	7
1.3. Instrumental Set-Up	9
1.3.1. The UHV System	9
1.3.2. Multipurpose Evaporation System	11
2. Growth of Sodium Chloride Ultra Thin Films on Metallic Substrates	13
2.1. Motivation	13
2.2. NaCl Thin Films Growth: State of the Art	14
2.3. Sample Preparation	16
2.4. STM Observations	17
2.4.1. Atomic Resolution	17
2.4.2. Island Borders and Shapes	20
2.4.3. Carpet Growth	22
2.5. LEED Measurements	23
2.5.1. NaCl on Cu(111)	23
2.5.2. NaCl on Ag(111)	26
2.5.3. NaCl on Ag(001)	28
2.6. XPS Measurements	29
3. CuOEP on Insulator Ultrathin Films	33
3.1. Motivation	33
3.2. Molecules on Insulators: State of the Art	34
3.3. First Attempts and Strategy	35
3.4. Sample Preparation	39
3.5. Assembly of CuOEP on NaCl	39

3.6. Layer Selective Adsorption	42
3.7. Theory of CuOEP Adsorption	45
3.8. Investigating the CuOEP-Substrate Electronic Coupling	47
4. CuOEP on Metals	51
4.1. Motivation	51
4.2. Determination of the Molecular Epitaxy	52
4.3. High Resolution STM Imaging and Voltage Dependence.	57
4.3.1. CuOEP on Ag(001)	57
4.3.2. CuOEP on Cu(111)	61
4.4. DFT Calculations	64
4.5. UPS Spectra: HOMO and HOMO-1 Positions	65
4.6. Work Function Change and Charge Transfer	67
4.7. Level Alignment: Substrate Dependence	69
5. Conclusion and Outlook	73
A. Triangular NaCl Structures	75
B. CuOEP on Metal: Collection of the UPS Data	78
Bibliography	82
List of Publications	94
Acknowledgments	96
Curriculum Vitae	97

Abbreviations

AES	Auger electron spectroscopy
AFM	Atomic force microscopy
CuOEP	Copper(II) octaethyl porphyrin
DFM	Dynamic force microscopy
DFT	Density functional theory
DOS	Density of states
EA	Electron affinity
EELS	Electron energy loss spectroscopy
EFM	Electrostatic force microscopy
ESCA	Electron spectroscopy for chemical analysis
HOMO	Highest occupied molecular orbital
IP	Ionization potential
LDOS	Local density of states
LEED	Low energy electron diffraction
LUMO	Lowest unoccupied molecular orbital
MFM	Magnetic force microscopy
ML	Monolayer
OLED	Organic light emitting diode
PES	Photoelectron spectroscopy
SNOM	Scanning Near Field optical microscopy
SEM	Scanning electron microscopy
SPM	Scanning probe microscopy
STM	Scanning tunnelling microscope
STS	Scanning tunnelling spectroscopy
SubPc	Chloro[subphthalocyaninato]boron(III)
UHV	Ultra-high vacuum
UPS	Ultraviolet photoelectron spectroscopy
vdW	van der Waals
XPS	X-ray photoelectron spectroscopy

1. Introduction

1.1. Motivation and Outline

The concept of molecule has historically been developed in the field of chemistry and for a long time molecules have almost exclusively been investigated by chemists. However, the development of powerful investigation tools as well as quantum theory allowed the scientists to gain a deep understanding of the physics at the molecular scale. Hence molecules started to be in the focus of physicists too.

Nature shows how much complexity can be borne in a very small space. A molecule is a remarkable example of an extremely small structure which has well defined characteristics and properties. Miniaturization is not only observed in nature but has been a constant trend in the technology development of our times. Researchers have continuously tried to engineer smaller and smaller devices. However so far the approach to miniaturization has mostly been quite different than the one used by nature. Scientists and engineers have mainly tried to shrink the size of objects which already exist and work at a larger scale. This approach proved to be very successful, nevertheless it is clear that there are limit to it. In fact scaling down processes which work at the macro- or micro-scale is going to face fundamental physical limits. For instance the ultimate limits for lithography processes employed in the silicon based electronics are not far from being reached[1].

The novelty of *nanoscience* consists in studying the properties and functionalities of nanoscale structures, often already known from chemistry or biology. Their understanding may lead to identify structures which can be directly used for applications or teach how to engineer new objects with the desired properties. Although very difficult, such an approach has a great potential. As pointed out by Richard P. Feynman in his famous talk “There’s plenty of room at the bottom – An invitation to enter a new field of physics” gaining the ability to control and address single atoms and single molecules would allow to extraordinarily accelerate most miniaturization processes.

Among the systems available in nature organic molecules look very appealing as they are small but simultaneously complicated and structured enough to comprise interesting functionalities. Therefore, in this thesis the attention will be focussed on organic molecules adsorbed on suitable supports with a relevance for potential applications in the field of *molecular electronics*.

The use of very small functional units poses many technological challenges. Among them a very relevant one is the difficulty to handle and interconnect different units which are needed to assemble any useful device. However, the observation of nature offers a very brilliant approach to this issue. Practically all systems in nature are somehow capable to self assemble.

1. Introduction

One of the goals of *nanoscience* is to understand and profitably use self assembly to form nanostructures with the desired functionalities. The smart combination of the so called *bottom up* approach (letting different substructures organize in more complicated ones) with the *top down* approach (scaling down system working at macro- and/or microscale) constitutes one of the most important peculiarities of *nanoscience* and *nanotechnology*. Of course understanding and reproducing the conditions necessary to address the self assembly in a desired way is a difficult task. Nevertheless, in recent years, the potential of such an approach triggered a lot of research in this direction. In particular, STM revealed itself to be a powerful tool to address, analyze and modify self assembled molecular structures as well as single atoms.

In this thesis different nanoscale structures have been produced, studied and combined. All the structures described have been produced following a *bottom up* scheme. As shown in the following, this indeed limits the control on the growth process. On the other hand, it has to be stressed that, due to this approach, the nanostructures investigated can be produced in a virtually countless number and in a comparably fast and cheap way. Exploiting this research direction looks therefore very important in order to open a way to the application of *nanotechnology* to any device of practical interest in everyday life.

1.2. Experimental Techniques

The experimental work described in this thesis has been carried out mainly by means of scanning tunnelling microscopy (STM), photoelectron spectroscopy (PES) and low energy electron diffraction (LEED). In this section a brief introduction about the working principles and some of the practical aspects of these instrumental techniques is given.

1.2.1. Scanning Tunnelling Microscopy

Introduction

Scanning Tunnelling Microscopy is a powerful tool invented at the IBM Zurich Research Laboratory in 1981 by Gerd Binnig and Heinrich Rohrer[2]. Very soon after its invention STM proved to be an extremely useful tool for the investigation of surfaces and in 1986 Binnig and Rohrer were awarded the Nobel Prize.

The STM working principle relies on the quantum mechanical tunnelling of electrons through a potential barrier between a conductive sample and a sharp metallic tip placed very close to each other (typically a few Å). A bias is applied between the tip and the sample and a tunnelling current is measured to flow across the tip-sample gap. The tip is then scanned over the sample by means of piezo-electric tubes. While moving the tip, the sample corrugation induces a variation of the sample-tip distance and therefore of the tunnelling current. The tip can be scanned on the sample at a fixed z -position above the sample while measuring the current (*constant height* mode). Alternatively a feedback system can be used to adjust the tip-sample distance in order to keep the tunnelling current constant. In this

second mode (*constant gap* or *constant current*) the most important signal recorded is the z -displacement of the tip needed to keep the current constant.

One of the key aspects of STM is the very strong dependence of the tunnelling current on the tip-sample distance. This implies that only the very end of the tip apex and a very small portion of the sample are significantly involved in the tunnelling process. Such a localized interaction is crucial in order to obtain a high spacial resolution. Binnig and Rohrer could observe for the first time features such as monoatomic steps, surface reconstructions[3] as well as atomic resolution of metal[4][5] and semiconductor[6] surfaces in real space.

The invention of STM turned out to be a landmark point in the advancement of surface science, allowing for the first time real space investigation of surfaces at the atomic scale. Moreover it triggered the development of a whole family of scanning probe microscopies (SPM) such as atomic force microscopy (AFM)[7], magnetic force microscopy (MFM)[8], electrostatic force microscopy (EFM)[9] and scanning near field optical microscopy (SNOM)[10][11].

A brief theory of STM

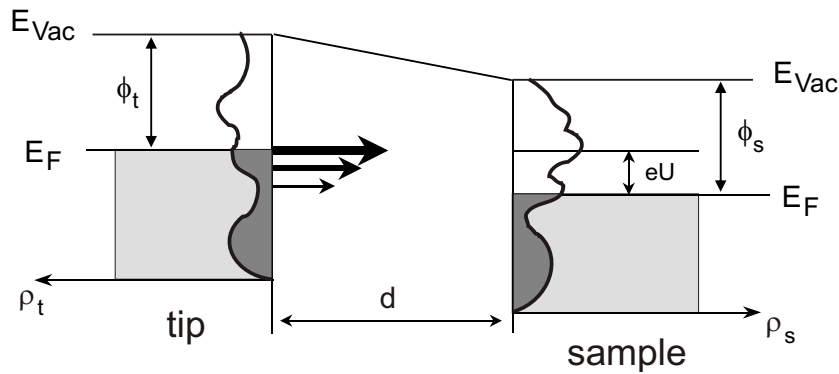


Figure 1.1.: Schematic 1-dimensional diagram of a tip-sample junction. In this representation a positive bias U has been applied to the sample. The size of the horizontal arrows indicates the different transmission coefficients (and therefore of the tunnelling probabilities) for electrons of different energies.

Developing a precise theory of the tunnelling process at the tip-sample gap is not feasible as very little is known about its detailed geometrical and chemical configuration. Overviews on this problem and the possible approaches to solve it are given in different books[12][13] as well as in review articles (see for example ref. [14]).

Despite this complexity, most of the aspects of scanning tunnelling microscopy can be explained considering the simple theory developed by Bardeen[15]. In this theory the specific geometry of the tip-sample junction is neglected and the tunnelling junction is modelled as a 1-dimensional system (fig. 1.1).

From basic quantum mechanics it follows that the probability for an electron with energy

1. Introduction

E to tunnel through a potential barrier of energy E_{bar} (with $E_{bar} > E$) is

$$T = e^{-\frac{2d\sqrt{2m(E_{bar}-E)}}{\hbar}} \quad (1.1)$$

where m and d are the electron mass and the barrier width, respectively.

In the approximation proposed by Bardeen the net tunnelling current between tip and sample measured while applying a bias U will simply be

$$I = \frac{4\pi e}{\hbar} \int_0^{e \cdot U} \rho_s(E) \rho_t(e \cdot U - E) T(E, e \cdot U, d) dE \quad (1.2)$$

where ρ_s and ρ_t are the density of states of the sample and of the tip while $T(E, e \cdot U, d)$ is the transmission coefficient from the tip to the sample for an electron with energy E . For this extremely simplified 1-dimensional model, as described in eq. 1.1, the transmission coefficient will be

$$T(E, e \cdot U, d) = e^{-\frac{2d\sqrt{2m(E_{bar}-E)}}{\hbar}} = e^{-\frac{2d\sqrt{2m}}{\hbar} \sqrt{\frac{\phi_s + \phi_t}{2} - \frac{e \cdot U}{2} - E}} \quad (1.3)$$

where ϕ_s and ϕ_t are the work function of the sample and of the tip. It is important to note that the expression 1.2 is just the integral of the transmission coefficient over the density of states of the tip and of the sample (indicated by the arrows in fig. 1.1) laying in the energy window allowed for tunnelling. This window corresponds to the energy range where the occupied states of the tip and the unoccupied states of the sample overlap each other. In the simplified model presented here, tip and sample have a perfectly symmetric role. Thus, the whole discussion applies the very same way for negative sample bias (i.e. for electrons tunnelling from occupied states of the sample to unoccupied states of the tip).

In reality the geometries of tip and sample are different and such an asymmetry significantly affects the system. As stated before, this complicates the situation significantly and makes it almost impossible to develop a first principles theory. Nevertheless many attempts have been made to treat the problem with approximations closer to the real situation. Among those the so called *s*-wave-tip model developed by J. Tersoff and D. R. Hamann[16][17] is definitely one of the most important. It models the tip apex as a little metal sphere, thus implying that only *s*-states of the tip take part in the tunnelling process. For low biases (much smaller than the tip work function ϕ_t), the current turns out to be proportional to the Fermi local density of states (LDOS) at the center of the sphere \mathbf{r}_0

$$I \propto eU \rho_s(E_{F,s}) \rho_t(E_{F,t}, \mathbf{r}_0) e^{-\frac{2d\sqrt{2m}}{\hbar} \sqrt{\frac{\phi_s + \phi_t}{2}}} \quad (1.4)$$

It is interesting to note that in this approximation the dependence of the current from the tip is expressed only by the factor $\rho_t(E_{F,t}, \mathbf{r}_0)$ which remarkably is just a constant. Therefore, in the frame of the Tersoff and Hamann theory, the variations of the tunnelling current while scanning the tip on the sample turn out to depend only upon local properties of the sample and not on the tip.

STM data handling

In STM the tip is typically scanned over a sample and the signal of interest is recorded at a fixed time/space interval. As the tip is usually raster scanned over a squared area, the natural output of an STM measurement is a two dimensional data array. While scanning more than one signal can be acquired, thus for each measurement different arrays can be generated. In the *constant current* mode (used throughout this thesis) the tunnelling current is kept constant by the feedback and the most interesting signal is the z -displacement of the tip. This signal is often called *topography* although it carries also information about the electronic structure of the sample surface. In addition to the z -displacement, the current signal can also give out useful information because of the limited reaction speed of the feedback. In fact, when the tip gets over a protrusion, a variation of the tip-sample distance and therefore of the tunnelling current is needed in order to induce the feedback reaction. Working with an integral feedback, the current signal represents the derivative of the topography and therefore highlights all the rapid variations of the z -displacement signal. Besides these considerations, the current signal is also very interesting in order to evaluate the efficiency of the feedback and for this reason is also called *error signal*. In certain experiments, also performed in this thesis, the bias voltage is changed repeatedly while scanning. For this kind of measurements the acquisition of the bias voltage is also very useful in order to keep track of its variations.

The two dimensional data arrays obtained as output of STM measurements are generally shown in an image format by using a color coding. Consequently very often for STM measurements the expression *STM images* is used. In practice each point of the array is converted to a pixel with a color corresponding to the recorded data value of the array. The most common code is the greyscale one, where bright and dark tones of grey are used for high and low values of the recorded signal. Other colored codings are also used, always according to the same convention about bright and dark tones.

If not explicitly otherwise indicated, all STM images reported throughout this thesis are topography images. Generally the data shown in the images are either raw data or processed through a plane subtraction. This is not the case for some of the images showing periodic structures. In some of these cases, in order to improve the resolution of a periodic structure, a so called *averaging procedure* has been employed. By using a special algorithm (developed by R. Hoffmann at the Institute of Physics of the University of Basel) it is possible to sample several copies of the unit cell of the periodic structure present in the image. The output of the procedure consists in an average of all the unit cells sampled from the original image. Another relevant filtering procedure employed for some of the images is the so called *flattening*. This procedure operates on the original data line by line. A polynomial of first order is fitted to each scan line of an image and successively it is subtracted to the original data. This procedure is specially useful to enhance the contrast in images which present significantly different z -displacements in different areas. For instance it is very helpful for images where the bias voltage is changed while scanning.

In order to emphasize specific features, the acquired data can also be presented in a so called pseudo 3D view. In addition to a color, an elevation is assigned to each point of the array. The resulting 3-dimensional structure is then represented in a perspective view.

1. Introduction

1.2.2. Low Energy Electron Diffraction

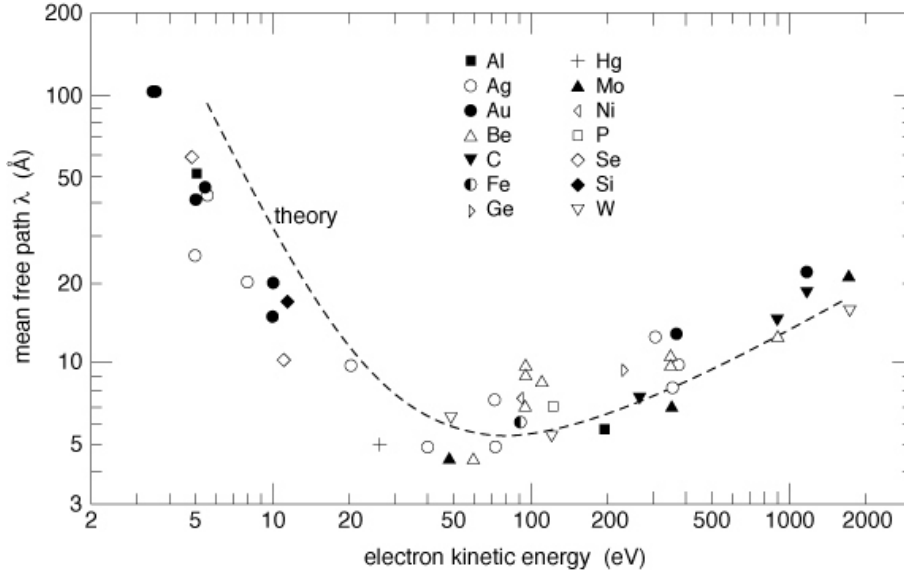


Figure 1.2.: Universal curve of electron mean free path. Adapted from ref. [18] and reference therein.

Along STM, another important experimental technique used in this thesis is low energy electron diffraction (LEED). The development of LEED was guided by Germer[19] some thirty years after his original experiment[20]. This technique relies on the observation that the de Broglie wavelength for electrons with low energy (in the order of tens of eV) is in the same range of the size of typical periodic structures studied in surface science (for example for electrons of $E = 10$ eV the de Broglie wavelength is $\lambda = \frac{h}{p} = \frac{h}{\sqrt{2mE}} = 3.88 \text{ \AA}$). This makes low energy electrons very well suitable for diffraction experiments on surfaces.

In LEED a beam of electrons, accelerated to the desired energy (from few to some hundreds eV), is directed towards the sample perpendicularly to its surface. The backscattered, diffracted electrons are then collected on a fluorescent screen placed in front of the sample surface (on the same side as the electron source). To ensure that only electrons that underwent an elastic process are collected, an energy filter is set in a way that only the electrons with an energy close to the one of the incident beam, are allowed to reach the fluorescent screen.

If the surface under investigation is characterized by some periodic structure this will be reflected in the diffraction pattern formed by the electrons collected on the screen. In detail it can be shown that such a pattern is the Fourier transformation of the periodic structure of the surface. More precisely the intensity recorded on the screen is proportional to the modulus of the reciprocal representation of the surface structure. For this reason the problem of inverting from LEED images to the direct space is not trivial and there is no direct method to solve it. Moreover, only a cut of the reciprocal surface can be imaged

through the fluorescent screen. In order to face these problems a big number of software tools have been developed, allowing to simulate the LEED pattern obtained from almost any possible periodic surface structure. In this thesis the LEEDSIM software by CreaPhys GmbH (Reinhardtsgrimma, Germany) has been used to simulate some of the LEED patterns observed.

A very important aspect of LEED is its very pronounced surface sensitivity. In fact the diffraction pattern obtained from LEED carries exclusively information of the periodic structures present in the few topmost layers of the sample. This is crucial in order to observe phenomena such as surface reconstruction or self assembly of adsorbate ultra-thin films.

This extreme surface sensitivity is achieved because of the very short mean free path of electrons in matter (not more than a few nanometers). This implies that only electrons penetrating a very short distance into the substrate can be elastically backscattered. Moreover, the mean free path of electrons does not depend much on their kinetic energy (fig. 1.2), thus allowing a great freedom in tuning the wavelength of the incident electrons. This property makes electrons very suitable for surface science investigations and indeed, besides LEED other powerful surface science techniques based on the short electron mean free path have been developed. Comprehensive overviews on LEED and its applications have been published in several books and articles (see for example the book of Van Hove *et al.*[21] or the review paper from Heinz[22]).

1.2.3. Photoelectron Spectroscopy

Another important experimental technique employed in this thesis is photoelectron spectroscopy (PES). As LEED, photoelectron spectroscopy is a non local method as it gives information integrated over a macroscopic area of the sample. The basis of this technique is the so called photoelectric effect discovered already in 1887 by Hertz[23] and theoretically explained in 1905 by Einstein[24]. This effect simply consists in the emission of electrons from a surface upon irradiation with electromagnetic radiation.

Given the frequency ν of the incident radiation, an electron emitted from the surface will have the kinetic energy

$$E_{kin} = h\nu - E_b - \phi \quad (1.5)$$

where E_b is the binding energy of the emitted electron (measured relatively to the Fermi energy) and ϕ is the work function of the sample.

In photoelectron spectroscopy, the excitation radiation is chosen to be monochromatic. Therefore, for each electron, it is possible to measure the energy of the level from which it has been emitted just by measuring its kinetic energy. The electrons emitted from the sample are collected on a detector which allows to measure the number of electrons for each kinetic energy $N(E_{kin})$. This allows to map the density of states (DOS) of the sample (fig. 1.3).

In order to excite the electrons from their bound states in the sample, different sources of electromagnetic radiation, operating at various energies, can be used. Generally two regimes are identified: X-ray photoelectron spectroscopy (XPS) for energies $h\nu \gtrsim 100$ eV and ultra-violet photoelectron spectroscopy (UPS) for energies $h\nu \lesssim 100$ eV. Although conceptually

1. Introduction

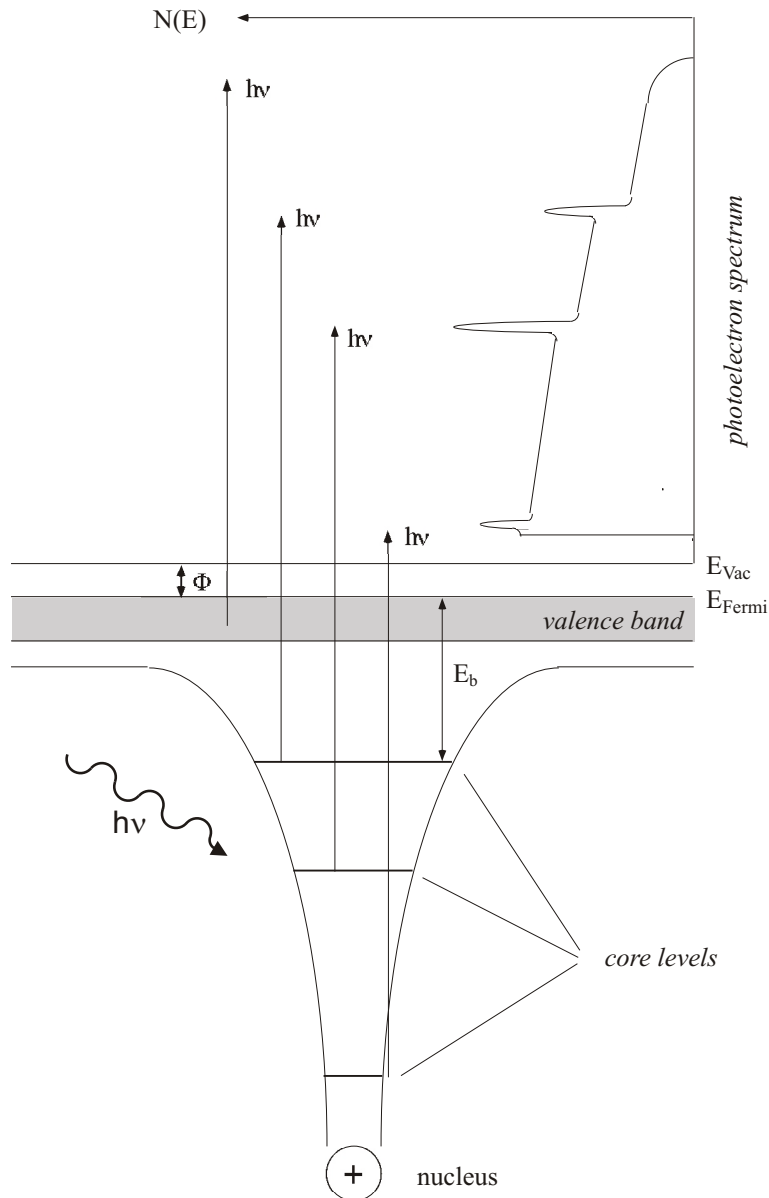


Figure 1.3.: Schematics of photoelectron spectroscopy measurement principle, showing the relation between the DOS of the sample and the photoelectron spectrum.

extremely similar, XPS and UPS measurements offer different kinds of information about the sample.

XPS allows to investigate the energy range corresponding to the atomic core levels and therefore gives information about the chemical composition of the sample. The intensity of the different peaks can be evaluated in order to determine the sample stoichiometry at the surface. Moreover, different chemical environments often induce slight modifications of the core level positions. These modifications, also known as *chemical shifts*, can be detected

by XPS and can be interpreted in terms of the interactions between the different chemical species present at the surface. This information is of special interest when investigating adsorbates as it allows to evaluate the adsorbate coverage and to learn about its interaction with the substrate.

The states investigated by UPS are the ones close to the Fermi level. The interpretation of these spectra is very interesting although more complicated than for the ones obtained by XPS. These low energy states are in fact very sensitive to the interactions between different compounds. UPS is therefore very useful to study the adsorption of molecules on surfaces as it allows to get deep insight in the molecule-substrate and molecule-molecule interactions. Moreover, by UPS it is possible to get a direct measurement of the sample work function and its change upon various surface modifications[25].

Common to UPS and XPS as well as to LEED, as described before, is the very high surface sensitivity due to the short electron mean free path. Electromagnetic radiation can penetrate deep into the sample but only electrons emitted in a region very close to the surface can leave it and reach the detector. Given the relevant role of photoelectron spectroscopy in surface science, a very large number of publications treat this topic in detail. For a comprehensive overview on the subject see for example the book of S. Hüfner[26].

1.3. Instrumental Set-Up

1.3.1. The UHV System

An extremely important requirement to study surfaces at the atomic or molecular scale is the ability to precisely control the conditions of the surface under investigation. In this perspective, ultra high vacuum (UHV) is a fundamental tool which allows to keep surfaces free of contaminations. All the experiments presented in this thesis have been performed in the NANOLAB at the Institute of Physics of the University of Basel. NANOLAB is a massive vacuum system consisting of seven chambers, each with a dedicated pumping system composed by turbomolecular, ion getter and titanium sublimation pumps. The base pressure for the system is in the low 10^{-10} mbar range. A fast entry air lock allows to insert or remove samples, STM tips as well as evaporation sources from the system, without breaking the vacuum. Two schematic representations of the NANOLAB multi-chamber system are shown in figs. 1.4 and 1.5. Samples are mounted on customized VG stubs that can be transferred through the entire vacuum system. The sample holders are equipped with a tungsten filament allowing to heat up the probe up to ca. 1100 K.

For the cleaning of metallic samples standard sputtering/annealing procedures have been employed[27]. For this purpose a sputtering gun operating with Ar gas is installed and the annealing of samples is performed by using the stub filament or by resistively heating the entire sample manipulator.

For the experiments described in this thesis it has been crucial to reliably deposit various molecules as well as NaCl on different substrates and with submonolayer precision. A flexible evaporation system has been specifically developed for the deposition of organic molecules. It is located in a dedicated chamber in order to keep the rest of the UHV system clean.

1. Introduction

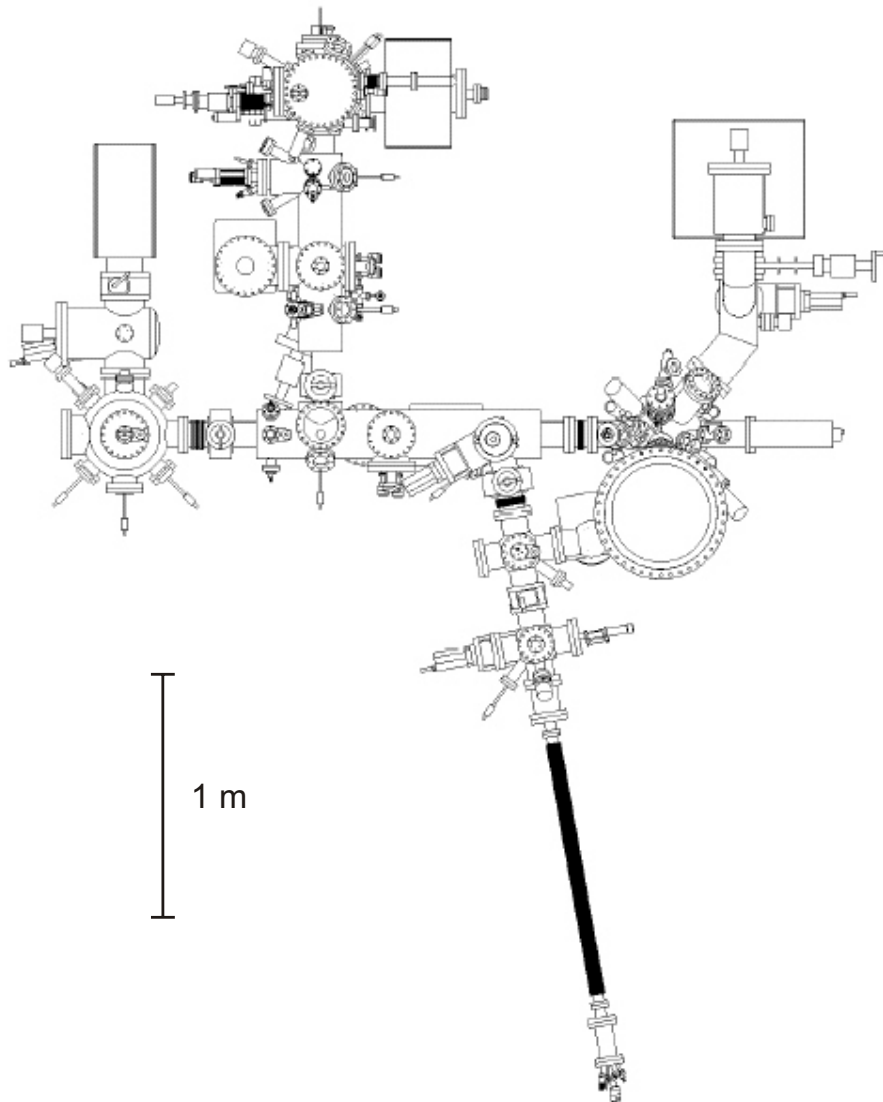


Figure 1.4.: Plan (topview) of the NANOLAB multi-chamber system. Drawing of A. Heuri.

The evaporation station can host up to twelve sources and four of them can be heated independently. Moreover, evaporation sources can be inserted and removed from the vacuum through the fast entry air lock. A detailed description of this evaporation system can be found in ref. [28]. Furthermore, for the deposition of insulator materials a specifically designed new evaporation system has been built (for further details see 1.3.2).

The most important instrument for sample investigation in the NANOLAB is the scanning tunnelling microscope (STM). The microscope is a home built instrument operating at room temperature. In order to obtain very low noise measurements the STM is mounted on a multistage damping system and is equipped with a preamplifier placed in vacuum very close (about 1 cm) to the tip-sample junction. For all experiments electrochemically etched

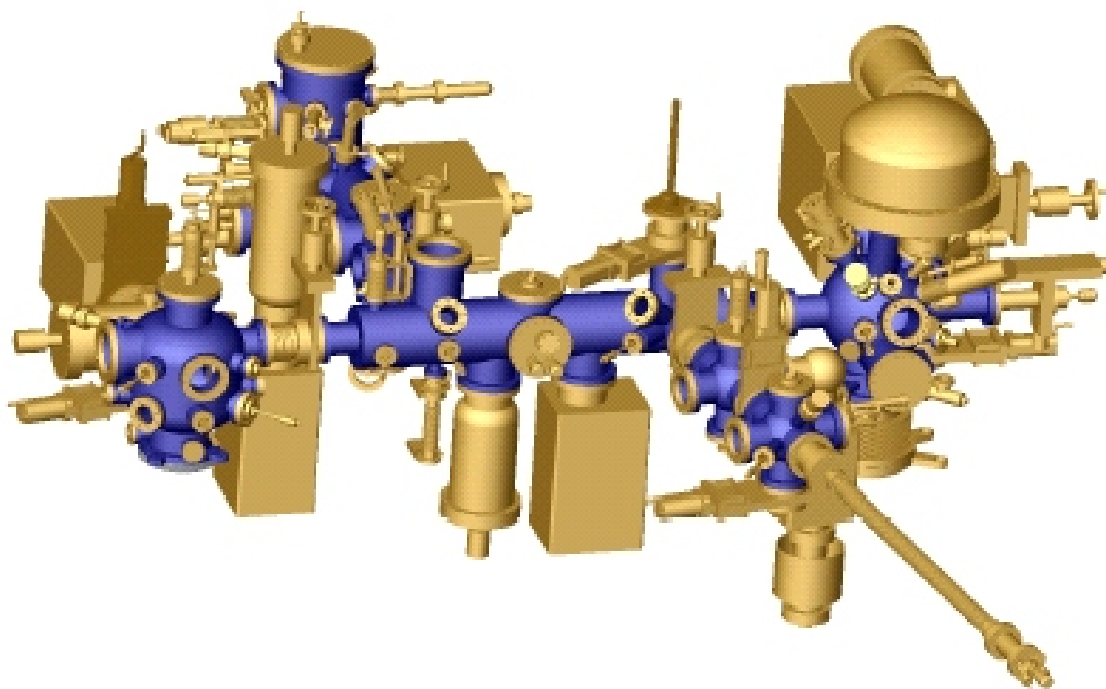


Figure 1.5.: 3D view of the NANOLAB. Drawing of A. Heuri.

tungsten tips are used. Moreover tips can be exchanged *in situ* and cleaned by means of high voltage electron bombardment. A more detailed description of the STM is given in ref. [29].

To investigate the electronic structure of samples, the NANOLAB is equipped with a dedicated ESCA (electron spectroscopy for chemical analysis) chamber hosting a commercial VG ESCALAB MKII system from Thermo Vacuum Generators (Hastings, United Kingdom). The detector is a hemispherical 150° analyzer with three channeltron electron counters. The source is a non monochromatized Mg/Al twin anode. Photon energies of the Mg and Al sources (K_α lines) are 1253.6 eV and 1486.6 eV, respectively. For the UV source, a He gas discharge lamp, that can be optimized either for the HeI_α (21.2 eV) or for the $HeII_\alpha$ (40.8 eV), has been used.

The system is also equipped with a commercial rear view low energy electron diffraction system (LEED) allowing the analysis of the crystal structure of sample surfaces. Further details about the NANOLAB system can be found in the following references[29][30][31][32][28].

1.3.2. Multipurpose Evaporation System

During this thesis the UHV system has been used to deposit many different materials, i.e. several organic molecules as well as sodium chloride, magnesium and gold. For this reason a new multipurpose evaporation system has been developed (fig. 1.6). A very distinctive feature of this system is the ability to heat up the source by electron bombardment.

1. Introduction

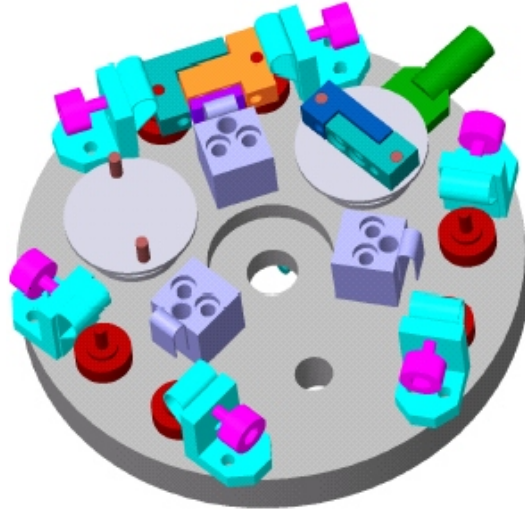


Figure 1.6.: 3D view of the newly developed multipurpose evaporation station. Drawing of A. Heuri.

To ensure maximum flexibility the evaporators can be transported through the entire UHV system (including the fast entry air lock) by means of a modified stub. Each evaporator is a small metallic plate consisting of three electrically isolated parts. These parts are kept together by a proper combination of screws and ceramic washers. On the other hand each evaporation station is equipped with two vertical conductive pins and a third spring contact. The evaporator plate fits on the two pins in a way that each of its three isolated parts are connected to different electric contacts (the two pins and the spring contact). Such a special mounting can be employed in a very versatile way. A filament can be welded between the two parts connected to the vertical pins and therefore resistively heated. The filament is wrapped in a coil shape around a boron nitride crucible containing the material to be evaporated.

The third contact is high voltage compatible in order to use it for electron bombardment. In this configuration the source material, that has to be conductive, is fixed to the part of the plate connected to the third contact while again a filament is placed between the two parts connected to the vertical pins of the station. The filament current can be raised until electron thermoionic emission[33] occurs. The emitted electrons are then accelerated onto the source material placed at positive high voltage. This electron bombardment technique allows to reach high temperatures in a very short time.

A peculiar detail of the station is the fact that for space reasons the evaporators, the modified stub for the evaporator transport as well as regular samples have to be handled with a single wobble stick. For this reason the station hosts two specially designed tools (a special fork and an Allen key) that can be mounted *in situ* at the wobble stick end. All these specifications enable the evaporation station to combine in a very flexible manner different types of evaporators, all fully transferrable in a limited amount of space.

2. Growth of Sodium Chloride Ultra Thin Films on Metallic Substrates

One of the principle goals of the research performed in this thesis has been to extend the application of the surface science tools available in the NANOLAB to the investigation of non conductive surfaces. As a model system for non conductive surfaces it has been chosen to work with ultra-thin sodium chloride films grown on various metallic substrates. In this chapter the growth and the characterization of these films is described in detail.

2.1. Motivation

In the last decades a huge interest has been devoted to surface science. The development of many instrumental techniques and methods triggered great achievements in this field and led to findings which played a key role in some of the most important technology advancements of our era. Although there has been such a great development, insulating surfaces historically have been much less investigated than the conductive ones. There are several reasons that can explain such a situation but certainly it has been crucial that many powerful experimental techniques do work only on conductive samples. Among them STM, LEED, PES, AES, SEM are just some of the most known and widely used.

To overcome these limitations, the choice of insulator thin layers looks like an interesting compromise. On these systems many experimental techniques not working on bulk insulators can be successfully applied, allowing to access many interesting physical properties. However, it has to be remarked that some of the properties of a bulk insulator may be significantly modified when considering the special case of ultra thin films. Clearly this element sets some limitations to the strategy of using insulating thin layers as substitutes for *normal* insulators. On the other hand, thin films disclose the very interesting opportunity to build structures with novel properties, possibly tunable just by acting on the film thickness. A very appealing aspect is that, in the ultrathin regime, material properties may significantly change just by adding or removing a single layer. This would allow to build structures with well defined, stepwise variation of their properties.

The potential to overcome some of the experimental limitations normally present in the case of bulk insulators has already been shown in many different cases for insulator thin film. In the following some of the most relevant and/or most closely related examples are given.

Already in 1988 Barjenbruch *et al.*[34] grew NaCl and KCl films on germanium substrates in order to investigate their electronic properties by means of UPS and EELS. Alkali halides and NaCl in particular are indeed among the most widely studied insulator thin films and

2. Growth of Sodium Chloride Ultra Thin Films on Metallic Substrates

a more complete review about this specific topic will follow in sec. 2.2. Another insulator material which has been in the focus of intense investigation at the ultra thin film regime is CaF_2 . Viernow *et al.*[35] showed that upon deposition on $\text{Si}(111)$, CaF_2 forms a first layer of semiconductive CaF_1 followed by the growth of insulating CaF_2 . They demonstrated how STM can be used as a chemically sensitive imaging tool for insulators. In another publication[36], the same group showed how the growth of semiconductive and insulating CaF_1 and CaF_2 nanostructures can be controlled in a bottom up approach.

The biggest part of the studies on insulator thin films definitely concerns metal oxide surfaces. Among them one of the most widely studied is MgO which has been grown on different substrates such as $\text{Fe}(001)$ [37][38], $\text{Mo}(001)$ [39][40][41] and $\text{Ag}(001)$ [42][43][44]. From these studies a detailed understanding of the structural, electronic and chemical properties of MgO thin films has been gained. A comprehensive collection of the work published about MgO thin films is presented in a review paper by Schintke *et al.*[45]. The same publication offers also an overview on other metal oxide systems. Among them a relevant role has been played by Al_2O_3 . The growth of ordered alumina thin films has been studied by STM on various substrates, including different NiAl alloy surfaces[46][47][48][49][50] as well as metal surfaces like $\text{Re}(0001)$ [41] and $\text{Nb}(110)/\text{sapphire}(0001)$ [51]. EELS measurements have been reported for Al_2O_3 films grown on $\text{NiAl}(110)$ [52] and on $\text{Re}(0001)$ [53]. NiO has also been investigated by STM[54][55][56] and Bäumer *et al.* published a combined LEED/STM study[57]. Similar attention has been devoted to CoO layers which have been studied by STM[55][58] as well as by EELS[59][60]. A relatively less investigated metal oxide is Ga_2O_3 , which has been grown on $\text{CoGa}(100)$ and studied by STM[61]. Finally, STM has been used to investigate a CeO_2 thin film grown on $\text{Pt}(111)$ [62].

The short overview reported here demonstrates the vast interest in insulator thin films which has mainly been rising in the last decade. A relevant part of this thesis is dedicated to the study of NaCl thin films. In particular STM has been used to access properties of the crystal and electronic structures of sodium chloride layers. Special attention is given to the use of these surfaces for the adsorption and self organization of organic compounds.

2.2. NaCl Thin Films Growth: State of the Art

The choice of the insulator material to use in our research has been the first important step of the experimental work. The key point in favor of NaCl has been the fact that it allows a great flexibility in the choice of the substrate on which the salt film can be grown. Substrates successfully used for the growth of NaCl include semiconductors as $\text{Ge}(001)$ [34][63][64][65], $\text{Ge}(111)$ [63], as well as metals such as $\text{Cu}(111)$ [66][67], $\text{Al}(111)$ and $\text{Al}(100)$ [68], $\text{Pd}(100)$ and $\text{Pt}(111)$ [69].

In the here reported experiments, NaCl ultra-thin films have been grown on $\text{Cu}(111)$, on $\text{Ag}(111)$ and on $\text{Ag}(001)$. While the first system has already been studied by other groups[70][66][67], in the literature we did not find any report of NaCl grown on silver.

In most cases reported, NaCl growth is achieved by means of practical and simple techniques. NaCl melts at (1074 K) and reaches a comparably high vapor pressure at quite low

2.2. NaCl Thin Films Growth: State of the Art

temperature (i.e. 10^{-4} mbar at about 800 K). Therefore, in a UHV environment, it can easily be sublimated at a comparably low temperature. It is interesting to note that upon sublimation NaCl dimers are formed[71][69], thus guaranteeing the conservation of stoichiometry in the film growth.

The growth is not much influenced by the underlying substrate. In fact, the strong ionic bond of NaCl (cohesive energy of 7.94 eV per ion pair for the bulk case[72]) clearly drives the growth process. In all the experimental works published so far, NaCl thin films always form a squared crystal lattice where the ions are arranged in the same way as on the (001) surface of the NaCl bulk crystal. As expected, due to the predominance of the Coulomb interaction between the ions, the structure which minimizes the energy for the thin film case is the same of the bulk NaCl. The only modification reported is a relaxation of the 2D crystal, characteristic of each substrate. Small increases of the Na-Cl in-plane distance (e.g. on Pt(111)[69]) as well as decreases (e.g. on Cu(111)[66]) are reported, but the change of the lattice constant is never bigger than a few percent. The observation of these crystal relaxations fits well to the well known high compressibility of alkali halides (NaCl bulk modulus is $0.24 \cdot 10^{11}$ N/m² [72]).

Another observation related to the mismatch between the substrate and the NaCl lattice is the so called *carpet growth*. In the neighborhood of substrate step edges, the NaCl lattice is deformed over the length of several lattice constants in order to allow a growth across two adjacent terraces. The formation of such NaCl *carpets* extending across substrate steps often seems to be energetically favorable. In fact on various substrates (i.e. Ge(001)[64][65], Al(111)[68], Cu(111)[67]) steps edges appear to be preferential nucleation sites for the growth of NaCl islands.

The ionic bond is also playing a crucial role in determining the shape of the NaCl structures that are grown. In order to minimize the ionic interaction, island borders are aligned to the $\langle 100 \rangle$ directions of the NaCl bulk crystal, implying an alternation of Na⁺ and Cl⁻ ions along the border. Such an orientation of the borders leads to a rectangular shape of the NaCl islands. Due to the strength of the ionic interaction this characteristic shape of the NaCl structure is observed virtually on every substrate.

Concerning the growth, it is interesting to note that some authors report that the first layer formed on the substrate is a double layer. This has been reported for different substrates such as Ge(001)[34][65], Al(111)[68] and Cu(111)[67]. The discrimination of the real thickness of the first layer is not trivial and it has not been in the focus of this thesis.

The investigation of the structural properties described above has been pursued with different experimental techniques. A lot of studies have been carried out with LEED to gain information about the orientation of the NaCl lattice with respect to the underlying substrate[34][63][64][66][69][73]. An intensive analysis of the electronic structure of thin and ultra-thin NaCl films has been carried out by means of EELS and PES[34][63][73]. Also scanning probe microscopy, namely STM[65][68][74][67][75] and AFM[70][76] proved to be useful to improve the understanding of these salt structures.

2. Growth of Sodium Chloride Ultra Thin Films on Metallic Substrates

	sputtering	annealing
Cu(111)	800 eV, 1.7 μ A, 17 min	1000 K, 60 min
Ag(111)	800 eV, 1.6 μ A, 17 min	1100 K, 55 min
Ag(001)	700 eV, 1.5 μ A, 17 min	900 K, 50 min

Table 2.1.: Summary of the parameters chosen for the sputtering and annealing cycles employed to prepare the metallic substrates.

2.3. Sample Preparation

NaCl ultra-thin layers have been deposited on three different metallic substrates: Cu(111), Ag(111) and Ag(001). All substrates used are single crystals (Mateck GmbH - Jülich, Germany) cut along the specified crystallographic direction with an accuracy better than 0.4° . These crystals have been prepared *in situ* according to regular surface science techniques by several cycles of Ar^+ ion bombardment (sputtering) and annealing. Between each experiment the substrates have been treated again with two Ar^+ sputtering-annealing cycles using the parameters specified in table 2.1.

The recipes described here, allow to produce atomically flat and clean metallic substrates. The quality of the pure metallic substrates has periodically been checked by means of STM, XPS and LEED. STM images show atomically flat terraces with a typical size in the order of hundred nanometers. Practically no contamination can be identified and atomic resolution repeatedly shows a perfect crystal structure. The latter has been crosschecked by LEED which shows very well defined interference patterns. LEED also proves that the substrates are really formed by a single crystallographic domain. The absence of contamination on the surfaces has also been carefully checked by means of XPS. Analysis of the 285 eV 1s peak of carbon, which is known to be the most common contaminant for the surfaces used[27], led to determine a carbon contamination level below 0.03 ML.

NaCl has been deposited on the metallic substrates by sublimation, using the evaporation system described in sec. 1.3.2. As source material a NaCl fine free-flowing powder (purity $\geq 99.5\%$, Fluka) has been used. The evaporator is formed by a boron nitride cylinder that can be heated through a tungsten filament wrapped around it (see sec. 1.3.2). The heating process can be easily controlled by regulating the current flowing through the tungsten filament. The operation temperature for the source cannot be measured directly but is estimated to be between 650 K and 700 K[66]. The deposition is monitored by means of a quartz crystal microbalance placed few centimeters aside the manipulator holding the sample. Various deposition rates have been tested but, for the great majority of the experiments described in this thesis, samples have been prepared using a rate around 1 $\text{\AA}/\text{min}$.

During deposition the temperature of the substrate can be controlled by resistive heating of the sample manipulator which is equipped with a thermocouple. Temperature control proved to be useful in order to tune the average size of the sodium chloride islands formed on the metallic substrate. Mostly temperatures between 300 K and 400 K have been used.

2.4. STM Observations

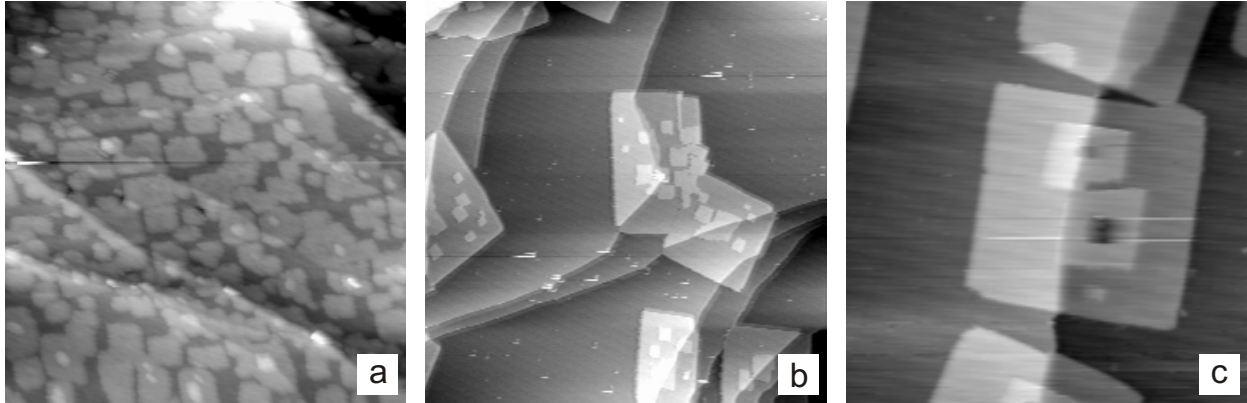


Figure 2.1.: NaCl on different substrates. (a) NaCl on Cu(111) ($145 \text{ nm} \times 145 \text{ nm}$, $U = 1.8 \text{ V}$, $I = 30 \text{ pA}$): many relatively small NaCl islands are visible; (b) NaCl on Ag(111) ($150 \text{ nm} \times 150 \text{ nm}$, $U = -1.1 \text{ V}$, $I = 10 \text{ pA}$): some large salt islands can be identified. On top of them several smaller second layer features are visible as well; (c) NaCl on Ag(001) ($200 \text{ nm} \times 200 \text{ nm}$, $U = 4.0 \text{ V}$, $I = 15 \text{ pA}$): an extended salt island is present in the middle of the image. On top of it second and third layers are also present. Remarkably in this image the third layer structures appear as a depression, in contrast with the real topography. In all three images it can be noted that islands are preferentially located across substrate step edges.

The investigation of the NaCl growth on the various metal substrates has mainly been carried out by STM. This tool proved to be very efficient in order to localize the areas of the sample covered by NaCl and to reveal many interesting properties of the salt structures formed. Typical results are collected in fig. 2.1 where three images, one for each of the different metal substrates used, are shown. The presence of NaCl can easily be inferred from characteristic rectangular shapes of the structures formed. Nothing similar is observed on any of the metallic surfaces before NaCl deposition and, in agreement with literature[65][68][74][67][75][70][76], it can be concluded that these structures are indeed composed of NaCl. A further prove of this conclusion can be obtained also by achieving atomic resolution (see sec. 2.4.1). In the images shown in fig. 2.1 the three samples look quite different especially concerning the size of the NaCl islands. These differences are mainly related to different growth parameters and not to the different types of metallic substrates used. Most of the observation performed are qualitatively the same for all the three substrate used: Cu(111), Ag(111) and Ag(001). Because of this homogeneity, the results obtained on all three metal substrates are discussed together.

2.4.1. Atomic Resolution

As pointed out before, direct atomic resolution decisively proves that the structures imaged are NaCl islands. Moreover it provides insight into the crystalline structure of the salt islands

2. Growth of Sodium Chloride Ultra Thin Films on Metallic Substrates

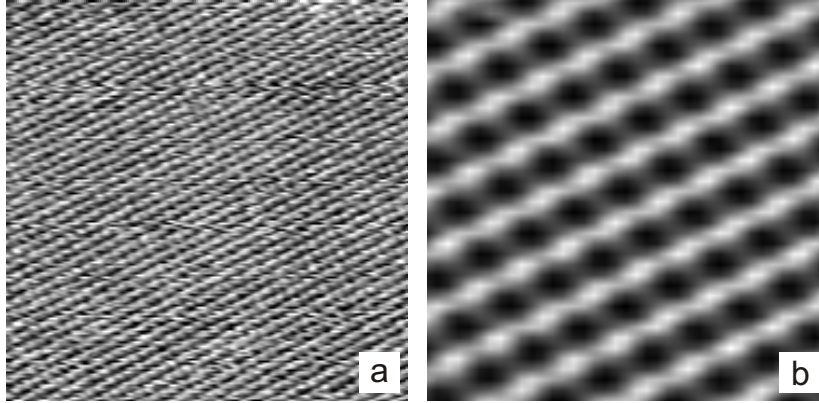


Figure 2.2.: NaCl on Ag(001). Image (a) ($14.5 \text{ nm} \times 14.5 \text{ nm}$, $U = 1.24 \text{ V}$, 40 pA) shows the atomic resolution achieved on a NaCl island; a closer look on the atomic structure (obtained from (a) by applying an averaging filter) is shown in image (b) ($3.4 \text{ nm} \times 3.4 \text{ nm}$).

present on the surface. In image 2.2 (a) an example of atomic resolution achieved on a salt island is shown. An even better resolution of the atomic pattern can be obtained from the same image through an averaging procedure (see sec. 1.2.1) as displayed in fig. 2.2 (b). The imaged atomic structure consists of a square lattice and, although NaCl is formed by an alternation of anions and cations, all protrusions present in the images look the same. The distance between two protrusions is 3.76 \AA while the lattice constant for bulk NaCl is 5.65 \AA . These results may appear surprising, but they can all be coherently explained and agree well with what is known from literature for similar systems.

In order to better understand this problem, it is useful to refer to the scheme shown in fig. 2.3. On the left, the 3D drawing represents a unit cell of the NaCl crystal lattice while, on the right, a scheme of its (001) surface is shown. It becomes clear that the unit cell of the surface lattice does not correspond with the one of the bulk and its basis vectors are directed along the $[110]$ and $[\bar{1}\bar{1}0]$ directions. Moreover the surface lattice constant is smaller than the bulk one (5.65 \AA) by a factor of $\sqrt{2}$.

All our observations fit very well with the assumption that Na^+ and Cl^- ions arrange on the metal substrate in the same way as on the (001) surface of bulk NaCl as reported numerous times for similar systems (see references of sec. 2.2). The surface lattice constant is then expected to be $a_0/\sqrt{2} = 5.65/\sqrt{2} \text{ \AA} = 4.00 \text{ \AA}$. A summary of the periodicities found is reported in table 2.2. The values found are only few percent off from the expected ones. As already mentioned in sec. 2.2, small relaxations of the sodium chloride lattice in the thin film regime have been already observed on other substrates[69][66]. For the three substrates used, slightly different relaxations of the lattice constant are observed but only for Ag(001) the relaxation (6%) exceeds the measurement uncertainty.

The fact that all protrusions present in the images look the same although the lattice is formed by ions with opposite charges can be explained assuming that only the ions of one type are imaged as maxima. That is in agreement with what is reported in literature[65][68][67]. However, from the STM images alone, one cannot identify which one of the two types of

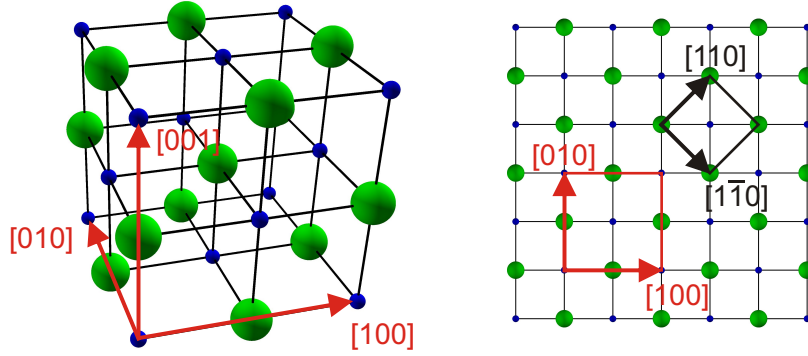


Figure 2.3.: Crystal structure of NaCl. On the left a unit cell of the sodium chloride lattice and its basis vectors are shown. On the right the (001) surface is displayed in detail. The relation between the unit cell of the (001) surface and the unit cell of the bulk is highlighted.

	surface periodicity	corresponding 3D lattice constant	relaxation
Cu(111)	3.88 Å	5.49 Å	-3%
Ag(111)	3.91 Å	5.53 Å	-2%
Ag(001)	3.76 Å	5.32 Å	-6%

Table 2.2.: NaCl lattice constant relaxations. The NaCl shows a tendency to adapt to the underlying substrate and therefore a slight relaxation of its lattice constant can be observed. Among the three substrate investigated in this work only Ag(001) induces a remarkable variation of the lattice constant. Due to the comparably low accuracy of STM in determining distances, an uncertainty of the measured lattice constants of about 2% can be estimated.

atoms is imaged as a maximum. In principle this may also depend on the bias voltage applied as shown for GaAs by Feenstra *et al.*[77]. For NaCl, in a quite handwaving way, it can be expected that the protrusions observed must be Cl^- ions as their van der Waals radius is significantly bigger than the one of Na^+ ($r_{\text{Na}^+} = 95$ pm, $r_{\text{Cl}^-} = 181$ pm [78]). Hebenstreit *et al.*[68] carefully analyzed the case of NaCl on Al(111). Based on ab initio calculation, they show that for both positive and negative sample bias a protrusion should be observed in correspondence with the Cl^- ions. Measurements, showing NaCl atomic resolution for opposite biases on the same sample area, indicate that in both cases always the same atomic species appears as protrusion.

The nature of the tunnelling mechanism on an insulator thin film is still quite unclear. Despite the fact that the band gap of sodium chloride is about 8.5 eV, it is possible to image NaCl island with bias voltages relatively close to zero and with both polarities. This implies that it is possible to tunnel from/to occupied/unoccupied states which lie inside the sodium chloride band gap. This may suggest that electrons tunnel through the salt layer directly

2. Growth of Sodium Chloride Ultra Thin Films on Metallic Substrates

from the tip to the sample and viceversa. However, by zooming on one island the proper atomic structure of NaCl can be resolved. This proves that atomic states of the sodium chloride layers are imaged and therefore the tunnelling really involves NaCl states. The fact that these states lie at an energy which completely disagrees with the electronic structures of bulk NaCl can have different explanations. As discussed by Schintke *et al.*[44] for MgO on Ag(001), the electronic structure of an insulator ultra thin films can be significantly different than the one of the bulk and the appearance of states within the gap is reported. Moreover, Tegenkamp *et al.* carefully discussed the role played on the thin film electronic structure by the presence of defects at the insulator-metal interface[73].

2.4.2. Island Borders and Shapes

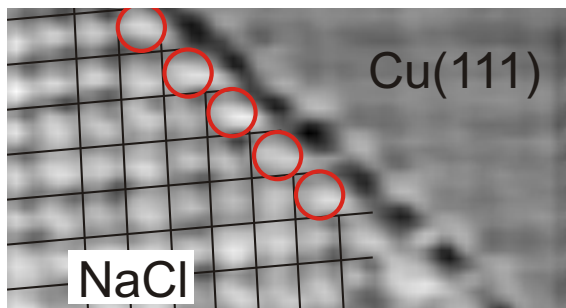


Figure 2.4.: Border of a NaCl island on Cu(111) (6.0 nm \times 3.7 nm, $U = -1.5$ V, 60 pA). Atomic resolution near the salt edge is achieved, allowing to identify the atomic structure of a NaCl island border. The most external ions visible are circled while a grid is superimposed in order to better identify the NaCl lattice structure.

STM also allows to get insight about additional details of the sodium chloride islands. As described in sec. 2.2, the coulombian interaction between the Na^+ and Cl^- ions is by far the dominating force in the assembly process. The borders of the islands and therefore their shapes are also strongly influenced by that. It can be found that the borders which minimize the coulombian surface energy of a NaCl monolayer are aligned along the $\langle 100 \rangle$ directions (fig. 2.3). Indeed, this agrees with what can be observed in real space through high resolution images of NaCl island borders. In fig. 2.4 atomic resolution is achieved right near the island border allowing to identify its exact atomic structure. As only one atomic species is imaged by STM, the island borders appear to have a characteristic sawtooth shape (see also scheme in fig. 2.6 (b)).

The $\langle 100 \rangle$ directions along which NaCl island borders tend to align are obviously orthogonal. That is decisive in causing the typical rectangular shape observed for sodium chloride islands on many different substrates. Fig. 2.5 illustrates how the choice of borders aligned along $\langle 100 \rangle$ directions leads to rectangularly shaped islands.

As described before, the observed alignment of the island borders is the one needed to minimize the coulombian surface energy. This argument holds in general, unless at the corner

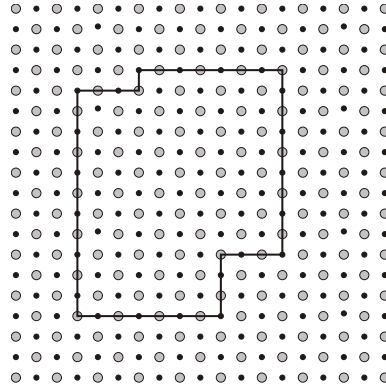


Figure 2.5.: NaCl islands shape and borders. For energetic reasons the borders of salt islands order parallel to the $\langle 100 \rangle$ directions of the NaCl crystal. Consequently the islands tend to adopt the characteristic rectangular shape shown here.

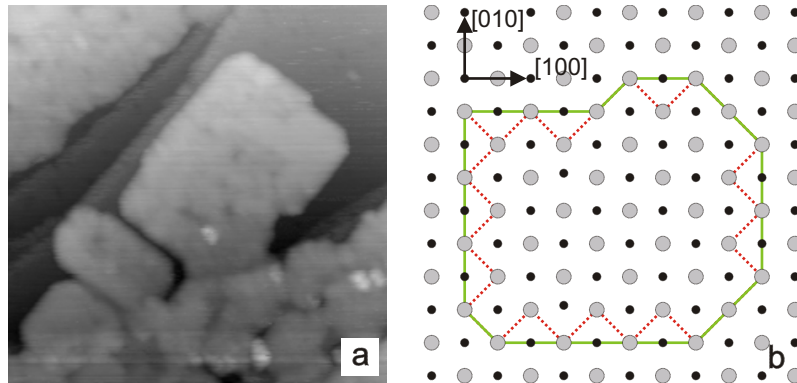


Figure 2.6.: NaCl on Cu(111). The islands imaged in (a) ($79 \text{ nm} \times 79 \text{ nm}$, $U = 3.5 \text{ V}$, 20 pA) show a slight deviation from the typical squared shape described before. At the corners, the island edges are aligned along the $\langle 110 \rangle$ directions therefore forming an angle of 45° with the main border directions. In (b) a schematic interpretation at the atomic scale of this phenomenon is presented. The solid line schematically shows the $\langle 100 \rangle$ oriented island border while the dashed one shows the corresponding appearance in an STM image, where only one type of ions is imaged.

of an island. As shown in fig. 2.6 (b), the corners of an island are highly polar sites and it may be energetically favorable to cut those ions away. This tendency is indeed found in the STM images (fig. 2.6 (a)). It is evident that the island shown in the image has no sharp corners. The typical length scale of these *corner cut* is between 5 and 10 nm, which means that only very few ions are missing to complete a perfectly rectangular island.

Another prominent feature observed by STM imaging of NaCl islands is the higher appearance of the ions placed at the island border (fig. 2.7). This effect critically depends on the tip shape and can be quite strong, with an enhancement of the border apparent height between 10% and 30%. A very similar observation performed by means of dynamic force

2. Growth of Sodium Chloride Ultra Thin Films on Metallic Substrates

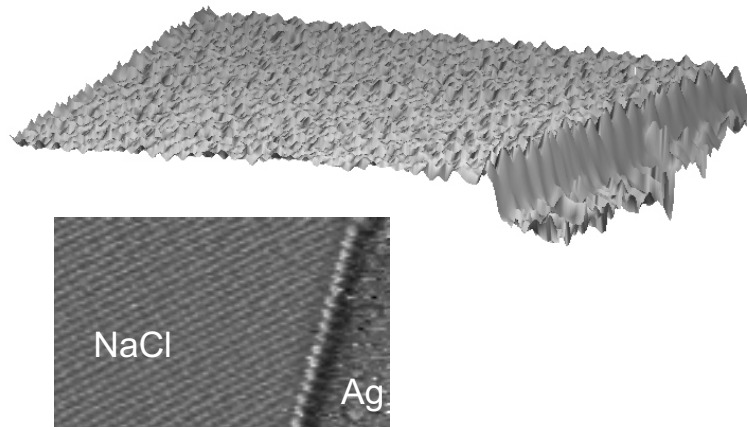


Figure 2.7.: Apparent height of NaCl island border. NaCl on Ag(001) ($6.2 \text{ nm} \times 11.4 \text{ nm}$, $U = 1.2 \text{ V}$, 25 pA). Ions placed at the border of a salt island show an enhanced apparent height.

microscopy (DFM) has been reported by Bennewitz *et al.*[76]. In that case a numerical calculation was carried out and led to the conclusion that an important role is played by a relaxation phenomenon, i.e. the ions at the edge of an island, characterized by a lower coordination, are slightly displaced due to the interaction with the tip. In STM, scanning at low tunnelling current (typically few tens of pA), the tip-sample distance should be relatively large (some Å). Therefore, in our observations, it can be expected that the relaxation induced by the tip-sample interaction does not play a significant role. More likely, the lower coordination of the ions at the borders leads to a distortion of the electronic states of these atoms, which may explain the increase of their apparent height.

2.4.3. Carpet Growth

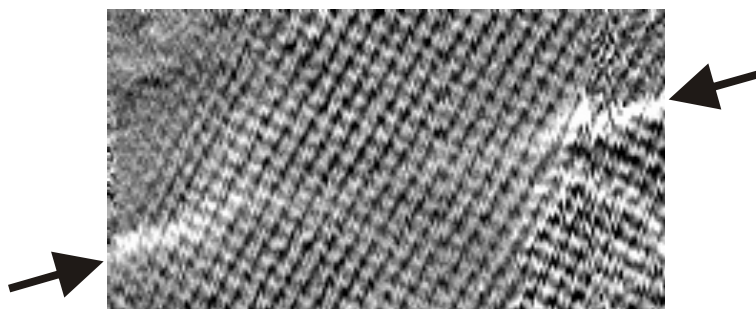


Figure 2.8.: NaCl on Cu(111). In this image ($11.5 \text{ nm} \times 6.3 \text{ nm}$, $U = -0.7 \text{ V}$, 40 pA) atomic resolution is obtained on an island grown across a copper step edge. The strain extends over several unit cells and no relevant deformation of the atomic lattice can be observed in the neighborhood of the step.

An interesting feature of the NaCl island growth observed is the tendency to grow across step edges of the underlying metal substrate. This phenomenon has already been reported in literature and is commonly called *carpet growth*[64][65][68][67]. As shown in fig. 2.1 (a), (b) and (c) many islands are lying across one or even several steps of the substrate. Also the growth of 2nd and 3rd layer structures seems preferentially to take place starting from step edges. Quite surprisingly this behavior is observed on many different surfaces and therefore it should not be related to a specific matching between the substrate and the salt atomic lattices. NaCl seems indeed to form an elastic *carpet* across the steps as discussed by Schwennicke *et al.*[64]. A proof of this is well visible in fig. 2.8 where atomic resolution has been achieved on a NaCl island extending over two terraces of its Cu(111) substrate. The atomic lattice structure looks extremely uniform throughout the whole image and no distortion can be observed around the underlying step edge. This clearly indicates that the island is not *broken* at the step edge and suggests that any deformation needed to adapt the island to the step extends over several unit cells.

2.5. LEED Measurements

In order to further exploit the way the NaCl islands grow on the different metallic substrates and specifically to learn about the relative orientation between the salt layer and the substrate, systematic LEED measurements have been carried out. A careful analysis of these measurements, as described in the following, allows to determine the effective orientation of the NaCl islands for all the investigated samples.

2.5.1. NaCl on Cu(111)

The LEED pattern obtained for NaCl grown on Cu(111) is shown in fig. 2.9. The lowest order of diffraction is composed of twelve spots. This observation can be explained by the well known NaCl squared structure (giving four spots) repeated three times, as it can be expected based on the 3-fold symmetry of the Cu(111) surface. This argumentation is explained in detail in fig. 2.10. Scheme (a) simply shows the LEED pattern for a squared lattice grown on a surface with hexagonal symmetry. The figure shows the case where the squared lattice is aligned to one of the main crystallographic directions of the substrate lattice. For Cu(111) surface there are three equivalent crystallographic directions separated by angles of 60°. Therefore, the squared pattern can be repeated three times by successive rotation of 60°, as shown in fig. 2.10 (a).

While the maxima of the twelve spots are indeed equally distributed every 30° according to the model of three square domains rotated by 60°, eight of the twelve spots visible in fig. 2.9 are quite elongated along the azimuthal direction. Notably the elongation is asymmetric. The eight spots are mainly stretched in the direction of the nearest round shaped spot. As shown in fig. 2.10 (c), this can be explained by a certain dispersion in the orientations of the NaCl islands. Remarkably, this dispersion is observed only for domains aligned to two of the three main crystallographic orientations of the Cu(111) surface. Moreover, as

2. Growth of Sodium Chloride Ultra Thin Films on Metallic Substrates

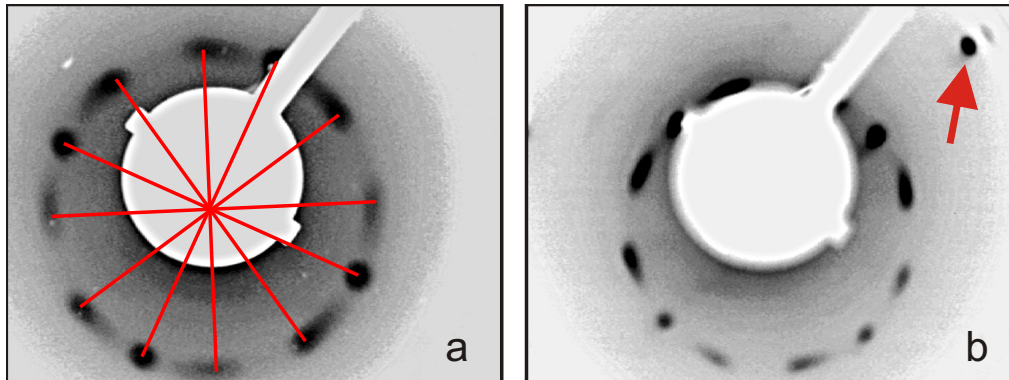


Figure 2.9.: NaCl on Cu(111): LEED patterns measured at 30 eV (a) and at 37 eV (b). For the first order of diffraction there are four round shaped spots plus eight spots which are clearly elongated. The spot maxima are distributed at intervals of 30° as highlighted by the lines drawn in image (a). The shape of the eight elongate spots is not symmetric: from the maximum of intensity it extends toward the nearest round shaped spot. The arrow in image (b) indicates a spot belonging to the hexagonal pattern of the Cu(111) substrate. Note that this spot is aligned with one of the four symmetric spots of the NaCl pattern.

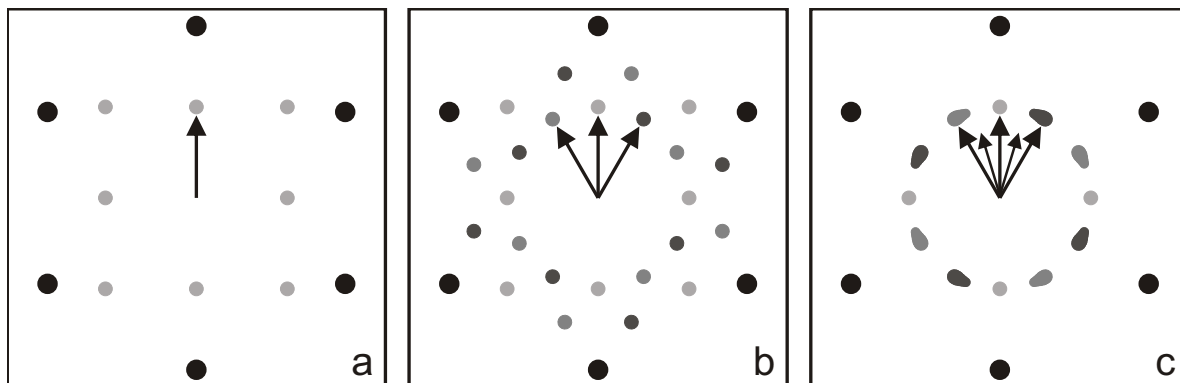


Figure 2.10.: LEED patterns for the growth of NaCl on Cu(111). Scheme (a) shows the diffraction pattern of a squared lattice on a hexagonal substrate. The relative orientation is chosen in order to keep the squared lattice aligned to one of the main crystallographic directions of the substrate. Scheme (b) shows the result obtained by superimposing three times the pattern represented in (a) for all the three equivalent orientations. Scheme (c) highlights the observed asymmetric elongation of eight of the diffraction spots. While the domain aligned to one of the main crystallographic directions of the substrate yields four round spots, the other domains are characterized by a significant dispersion in their orientation (see the small arrows). Remarkably, this dispersion is asymmetric: each elongate spot stretches towards the nearest round shaped spot. In (c) only the spots of the lowest order of diffraction are represented.

schematically shown in fig. 2.10 (c), the misalignment is only oriented to one side of the respective crystallographic axis.

Considering the position of the maxima of the diffraction pattern our results perfectly agree with what has been reported in literature for the same system[66] and for other surfaces with the same symmetry as for example Pt(111)[69]. On the other hand, the observation of the asymmetrically elongated spots has never been reported to date. Only Bennewitz *et al.*[66] report a non uniform distribution among the three (theoretically equivalent) domains for low coverages of NaCl on Cu(111). Moreover the same publication shows that, decreasing the substrate temperature during the deposition, NaCl starts to grow in all directions and the twelve LEED spots merge into a ring.

It is interesting to note that, for a unique sample preparation, a single NaCl domain orientation (fig. 2.11) has once been obtained. The only remarkable difference in the growth parameter was a deposition rate of 0.45 Å/min instead of a value around 1 Å/min. For this case the LEED pattern obtained agrees very well with scheme (a) of fig. 2.10.

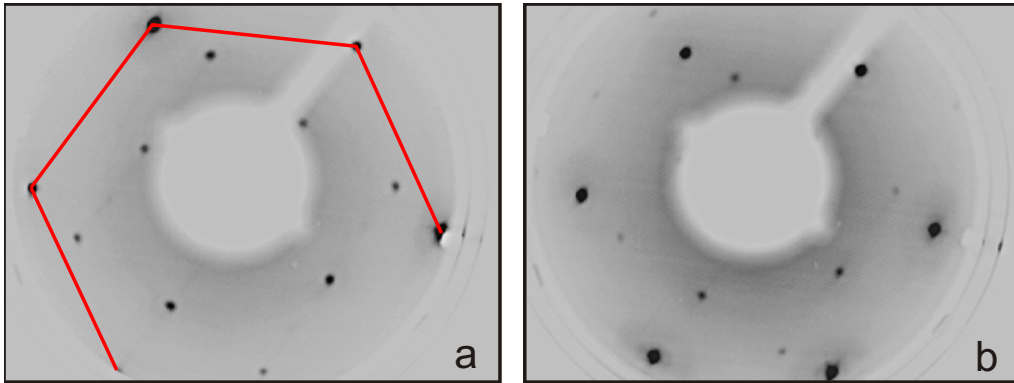


Figure 2.11.: NaCl on Cu(111): LEED patterns measured at 49 eV (a) and at 64 eV (b). In the external part of the images the spots of the hexagonal diffraction pattern of Cu(111) are visible (in (a) they are highlighted by a line linking five of them). In the middle the standard diffraction pattern of the NaCl(001) surface is identifiable. The relative alignment is the same observed in fig. 2.9 and described in fig. 2.10 (a).

This observation together with the result reported by Bennewitz *et al.*[66] for low coverages and for different substrate temperatures points out that the growth conditions can strongly affect the orientation of the NaCl islands. Although this is an interesting topic, it has not been further investigated because the main goal of this thesis was the growth of NaCl structures as suitable template for the adsorption of organic molecules and not a comprehensive characterization of the NaCl growth process.

In summary, it can be concluded that NaCl islands on Cu(111) have mainly three equivalent orientations. The basis vectors of the NaCl surface lattice are oriented parallel to one of the main crystallographic axis of the Cu(111) surface (fig. 2.12). In addition a slight misalignment from these orientations has been observed depending on the growth conditions. All these observations are consistent with the fact that the growth is mainly driven by the strong ionic interaction between Na^+ and Cl^- ions and tends therefore to be practically independent from the substrate.

2. Growth of Sodium Chloride Ultra Thin Films on Metallic Substrates

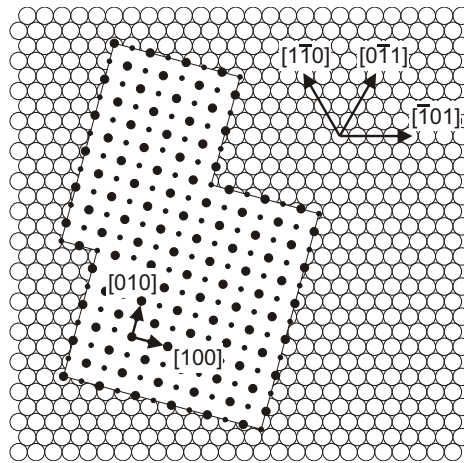


Figure 2.12.: NaCl on Cu(111). Schematic representation of the orientation of a NaCl island on Cu(111) as identified by LEED. All interatomic distances are drawn to scale although the position of the island barycenter has been chosen randomly.

2.5.2. NaCl on Ag(111)

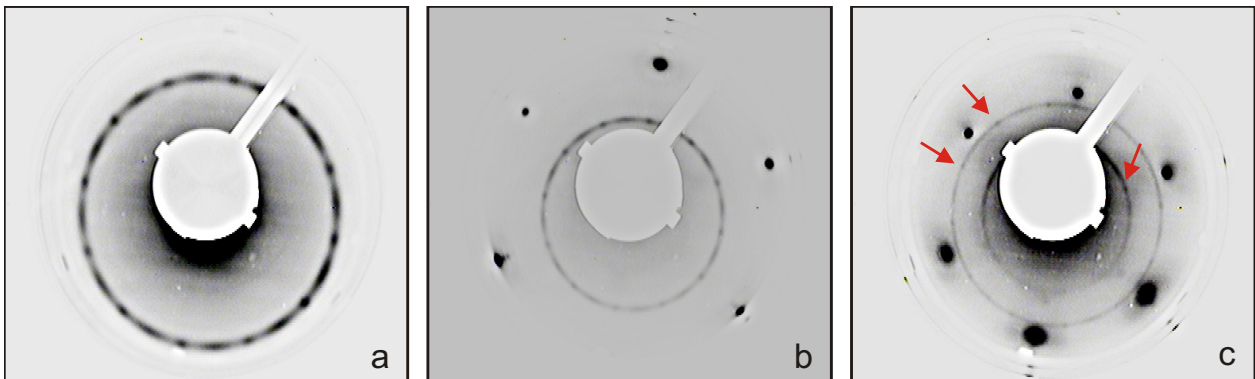


Figure 2.13.: NaCl on Ag(111): LEED patterns measured at 19 eV (a), 37 eV (b) and 53 eV (c). In (a) only the lowest order is visible. Twelve round spots are alternated to twelve elongate spots, all positioned on the same circumference. In the external part of image (b) the six spots belonging to the Ag(111) diffraction pattern are visible. In (c) the second order of diffraction produced by the NaCl can be identified as well. The arrows remark the relative alignment between some of the round spots of the NaCl diffraction pattern and the six spots of the Ag(111) pattern.

The result obtained for the NaCl orientation on Ag(111) is remarkably different from the situation on Cu(111). As shown in fig. 2.13, the lowest order of diffraction consists of 24 spots, which is twice the number observed on Cu(111). The pattern is composed by an alternation of round and elongate spots. The explanation of this pattern is possible whereas assuming that there are two non-equivalent NaCl domains, both with squared lattice structure. Each

of them can exist in three different orientations (forming 60° angles between them) due to the 3-fold symmetry of the Ag(111) surface. The elongated shape of half of the spots can again be explained assuming that, for one of the non-equivalent domains, the NaCl islands are not precisely aligned along the same direction but they are distributed around a main orientation. On Ag(111) the spread in the orientation is symmetric around the maximum of the angular distribution.

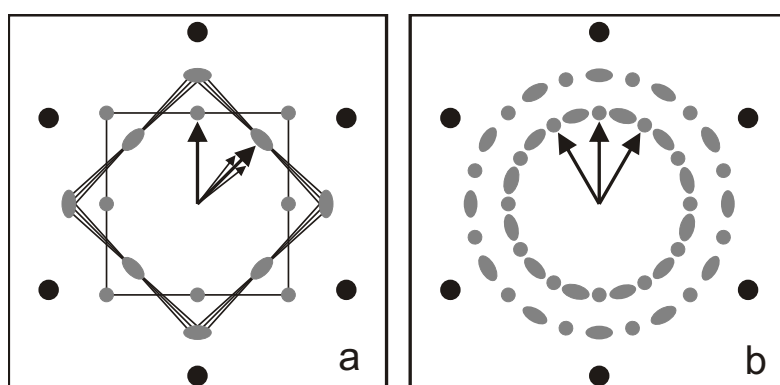


Figure 2.14.: LEED patterns for the growth of NaCl on Ag(111). Scheme (a) shows the diffraction pattern obtained from the superposition of two domains. For the first one the alignment is the same as described above for NaCl on Cu(111) (figs. 2.10 (a) and 2.12). The second domain is rotated by 45° . Moreover, for the latter a moderate angular dispersion can be assumed, as indicated by the small arrows. Scheme (b) shows the result obtained superimposing three times the pattern represented in (a) for all the three equivalent orientations of the substrate.

The consistency of this model is proved in fig. 2.14. Scheme (a) shows the pattern obtained by superimposing the two domains described above. For the first one the NaCl(001) surface lattice primitive vectors are aligned parallel to one of the main crystallographic orientations of Ag(111). The second domain is rotated by 45° and an angular dispersion in its orientation is taken into account as well. The presence of a spread in the orientations only for the second domain can be proved by a close analysis of fig. 2.13 (b) and (c). For the NaCl first order of diffraction, six among the round spots, but none of the elongate ones, are aligned with the spots of Ag(111). Exactly the opposite happens for the NaCl second order. As highlighted by the arrows in fig. 2.15 (b) our model truly reproduces also this detail of the LEED measurements.

These results are summarized in fig. 2.15 where two NaCl islands, each belonging to one of the two inequivalent domains, are drawn. The one on the left has the same orientation also found for NaCl on Cu(111) (fig. 2.12). On the other hand, the one on the right (rotated by 45°) shows an orientation not observed on Cu(111). The bent double arrow recalls that for this class of islands there is not a unique orientation but a distribution of orientations.

2. Growth of Sodium Chloride Ultra Thin Films on Metallic Substrates

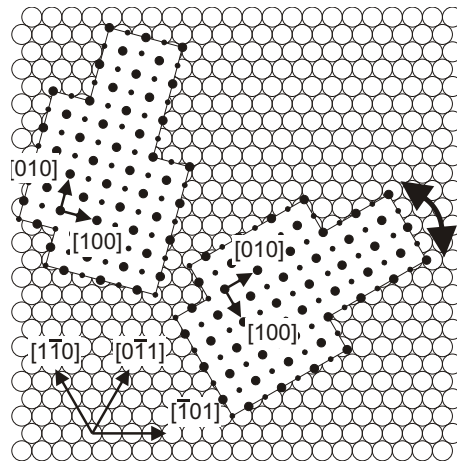


Figure 2.15.: NaCl on Ag(111). Schematic representation of the two possible orientations of NaCl islands on Ag(111) as identified by LEED. All interatomic distances have been drawn to scale, however, the positions of the island barycenters have been chosen randomly. The bent double arrow aside the island on the right shows that, for this domain, islands are not very well aligned but are characterized by an angular dispersion.

2.5.3. NaCl on Ag(001)

The LEED pattern interpretation for NaCl on Ag(001) is quite different from the two (111) surfaces described before, as this surface is characterized by different symmetry properties. An example of the obtained LEED patterns is shown in fig. 2.16 (a). In the inner part, there are eight diffraction spots: four round shaped and four elongated (indeed in the image shown here only three of the elongate spots are visible as one of them lies in the shadow of the electron source). This can be easily explained by the presence of two domains, one rotated by 45° with respect to the other. Again for one of the domains a disperse distribution of orientations around a maximum is observed. This time the spread in the orientation is observed for the islands whose primitive vectors are aligned along the main crystallographic directions of the Ag(001) surface, while the other islands are turned by 45° and are all well aligned. The pattern obtained according to these assumptions agrees very well with the diffraction pattern acquired (fig. 2.16).

Because of the 4-fold symmetry of the Ag(001) surface, for each of the two non-equivalent domains, four equivalent orientations can be obtained by turning the islands by 90° , 180° and 270° . However these cases are not distinguishable due to the fact that the NaCl(001) has the very same 4-fold symmetry. Fig. 2.17 gives a real space representation of the orientation of the NaCl islands for the two domains observed. For the island on the right the primitive surface lattice vectors are parallel to the substrate's crystallographic directions, for the one on the left they are tilted by 45° .

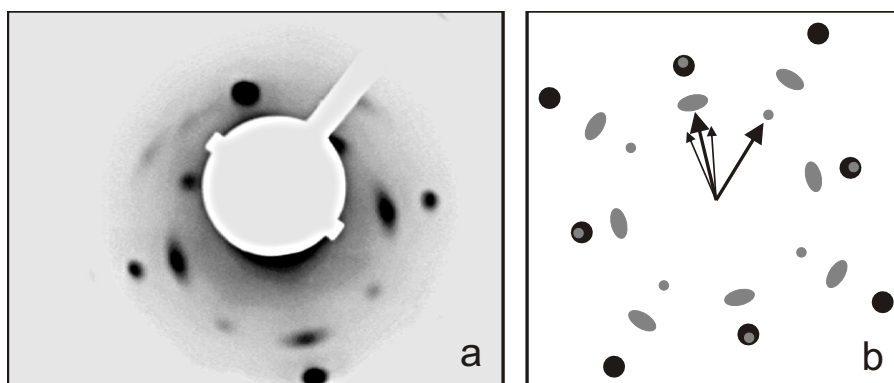


Figure 2.16.: NaCl on Ag(001). (a) shows the LEED pattern obtained at 35 eV. The scheme in (b) agrees very well with the measurements. It is obtained assuming two NaCl domains: one whose surface unit cell vectors are parallel to the main crystallographic directions of the Ag(001) surface, the other rotated by 45° . For the first, the presence of an angular dispersion is taken into account as well. The whole pattern has been then rotated to help the comparison with (a).

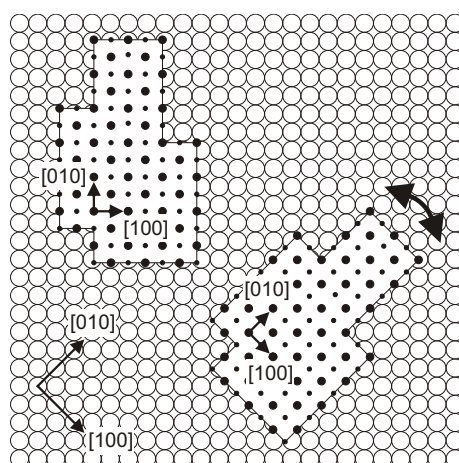


Figure 2.17.: NaCl on Ag(001). Schematic representation of the two possible orientations of NaCl islands on Ag(001) as identified by LEED. All interatomic distances have been drawn to scale, however, the positions of the island barycenters have been chosen randomly. The bent double arrow aside the island on the right shows that for this domain islands are not very well aligned but are characterized by an angular dispersion.

2.6. XPS Measurements

To characterize the NaCl films, X-ray photoelectron spectroscopy has also been used as a complementary tool. By XPS the stoichiometry of the salt structures and the presence of potential contaminants can be checked. After a detailed analysis of an overview spectrum (fig. 2.18) it was concluded that all the detected peaks correspond either to sodium, chlorine or to the metallic substrate (i.e. copper or silver). Furthermore an analysis specifically

2. Growth of Sodium Chloride Ultra Thin Films on Metallic Substrates

	sample 1	sample 2	ratio
Quartz microbalance	1.6 Å	2.0 Å	1.25
Cl2p _{1/2} + Cl2p _{3/2}	0.92 Å	1.18 Å	1.28
Na1s	1.34 Å	1.77 Å	1.32

Table 2.3.: NaCl/Cu(111): comparison of the salt coverage values measured by the quartz microbalance during the salt deposition and by the analysis of the Cl2p and the Na1s XPS peaks. For all measurements reported in the table the estimated uncertainty is ± 0.10 Å. The third column reports the ratio between the coverage obtained on sample 1 and 2, respectively.

targeted to reveal the most common contaminants such as carbon or sulfur, shows that their presence is below the detection limit (about 0.03 ML).

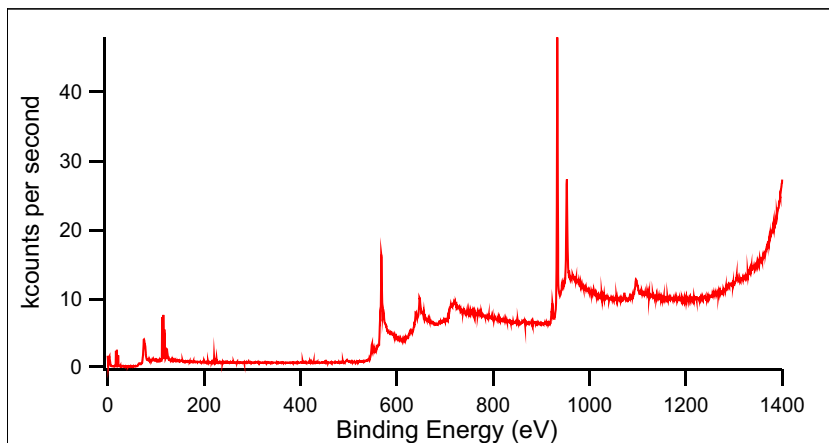


Figure 2.18.: XPS overview spectrum. The spectrum has been measured on a Cu(111) substrate covered with about 0.5 ML of NaCl

The amount of the different atomic species present on the surface has been quantified according to standard procedures[79]. Fig. 2.19 shows the details of the Cl2p, Na1s and Cu2p_{1/2} peaks used for the quantitative determination of the NaCl coverage on a Cu(111) substrate.

For alkali halides it is known that X-ray irradiation can induce the desorption of anions, consequently leading to the formation of defects as color centers[80][81]. In fact, in our XPS measurements, it is regularly observed that the amount of chlorine is significantly lower than the amount of sodium. Therefore, only the Na peak can reliably be used to estimate the NaCl coverage.

In table 2.3 the results for two sets of measurements performed on two NaCl/Cu(111) samples with different coverages are given. Note that the coverage obtained from the analysis of the chlorine peak is always underestimated. The NaCl coverage obtained from the sodium peak turns out to be lower with respect to the value measured by means of the quartz

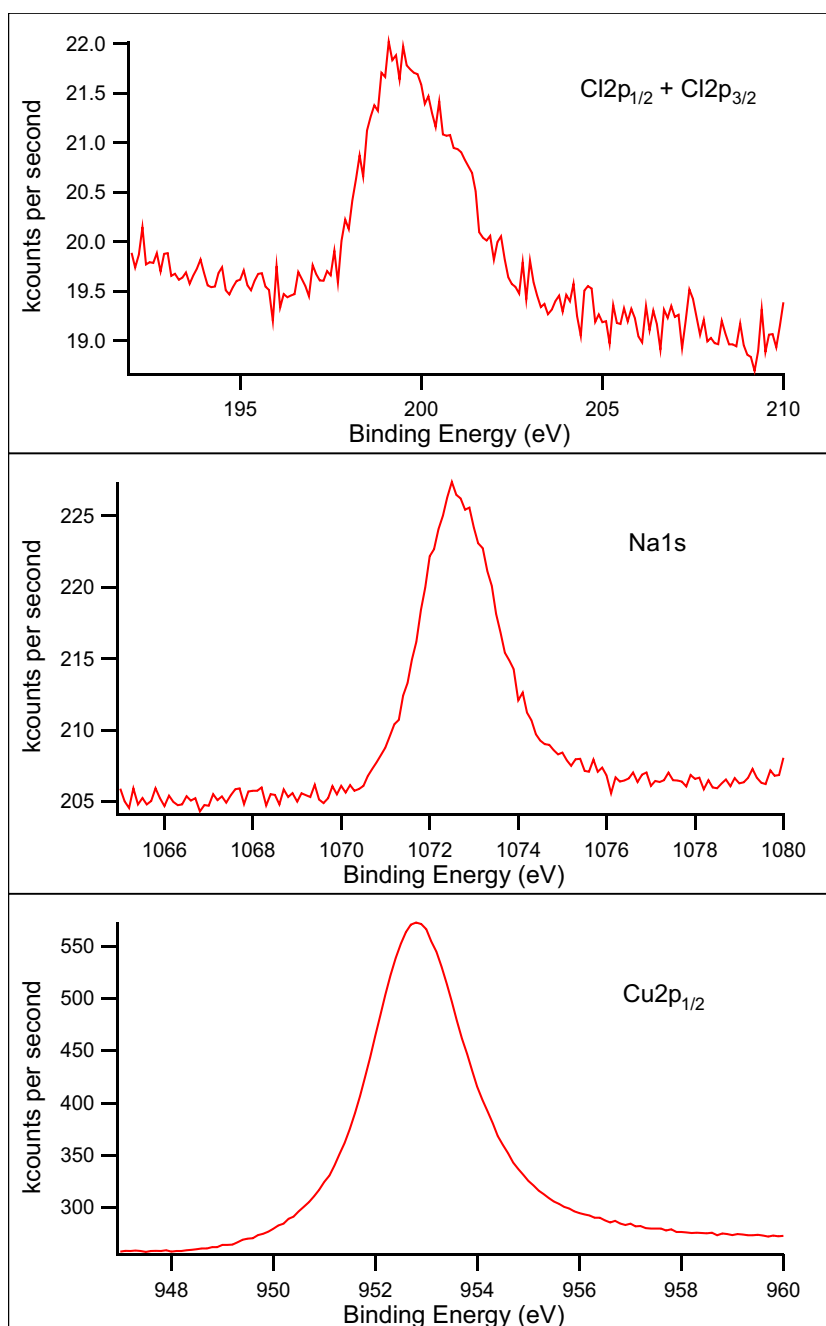


Figure 2.19.: NaCl/Cu(111): detail of the XPS spectrum for Cl2p, Na1s and Cu2p_{1/2} peaks measured on the same sample of fig. 2.18 (NaCl coverage \sim 0.5 ML).

microbalance. This can be explained by the fact that, during the deposition, the quartz and the substrate are not placed in a position symmetric with respect to the salt source. Therefore, together with STM, the quantitative analysis carried out by XPS can be conveniently used to calibrate the thickness measurements provided by the quartz microbalance normally

2. Growth of Sodium Chloride Ultra Thin Films on Metallic Substrates

used to monitor the deposition.

From a detailed analysis of the Na and Cl peaks (fig. 2.19) the following positions of the peaks can be obtained: Na1s 1072.5 eV, Cl2p_{1/2} 199.2 eV, Cl2p_{1/2} 200.9 eV. All these peak positions are perfectly consistent with the value expected for NaCl[82]. Especially the chemical shift of the Na1S peak speaks clearly in favor of a positive charging of the Na atoms as expected for an ionic crystal as NaCl.

3. CuOEP on Insulator Ultrathin Films

As described in the previous chapter ultra thin insulator layers can be grown on various metal substrates and with variable thickness. An important goal set for this Ph. D. project was to study the adsorption and self-assembly of organic molecules on these structures. This goal has been achieved by depositing Copper Octaethyl Porphyrin on NaCl thin films. In the following a detailed description of the analysis performed on this novel system is presented.

3.1. Motivation

Organic molecules on surfaces have been in the focus of vast and intense investigations. The research in this field is very heterogeneous and has developed into several branches. Different reasons justify the huge interest in investigating molecules on surfaces. A solid substrate is a very convenient support for molecules to organize, to assemble or to react. It also provides a favorable environment to interface and integrate molecules in more complex devices as it has been achieved for example in the field of organic light emitting diodes (OLED)[83][84][85] or thin film transistors[86][87]. Molecules on surfaces are also interesting in the context of heterogeneous catalysis[88], where the substrate surface offers a special environment for chemical reactions to occur.

Another very interesting branch of research which has been drawing a big interest to organic molecules on surfaces is *molecular electronics*. As first proposed by A. Aviram and M. A. Ratner[89], single or small groups of molecules can hypothetically be used in order to perform electronic functions. In recent years countless efforts have been made to develop such a revolutionary idea and *molecular electronics* has become a research field of primary interest[90][91].

To match the needs of *molecular electronics*, among others, special attention has been drawn on large organic molecules and in particular on molecules with highly delocalized electron systems. In the last decade countless publications dealing with such molecules adsorbed on metal and semiconductor surfaces appeared[92][93][94].

On the other hand much less is known about the adsorption of large organic molecules on insulator substrates. As already described in sec. 2.1, insulating substrates are less studied because many experimental surface science techniques can only be applied to conductive surfaces. Nevertheless, insulating substrates are of great interest in the context of *molecular electronics*. In fact they offer the unique possibility to electronically decouple the molecular structure from the supporting substrate. This is a key issue towards the use of molecules in planar electronic structures.

Therefore, the main goal set for this thesis has been to study the adsorption of large

3. CuOEP on Insulator Ultrathin Films

organic molecules on non conductive substrates. Ultrathin insulator films on metal substrates represent ideal model systems for such investigations as, in contrast to bulk insulators, many important surface analysis tools (e.g. STM, STS, and PES) can be applied.

Moreover, in recent years it has been shown that already few layers of an insulator can provide a significant decoupling from the substrate. For example for MgO it has been reported that for a thickness ≥ 3 layers the system exhibits the same gap as the bulk.[44]. Single adsorbates on ultra-thin films have also been studied. It has been shown how the charge state of an Au atom adsorbed on NaCl/Cu(111) can be controlled by means the STM tip[95]. This result is very interesting because it implies that an ultra-thin NaCl film is able to electronically decouple the Au atom from the Cu substrate. In addition, STS experiment have been performed with large organic molecules such as porphyrin[49] and phthalocyanine[96] adsorbed on Al₂O₃/NiAl(110). In both these cases it has been demonstrated how a monolayer of alumina is able to significantly reduce the molecule-substrate coupling. Very recently similar observations have been reported for pentacene adsorbed on NaCl/Cu(111)[97].

3.2. Molecules on Insulators: State of the Art

As mentioned in the previous section, the knowledge about organic molecules adsorbed on insulators is quite limited, especially for the case of large organic molecules. In fact quite a number of publications discuss the adsorption of smaller molecules on various substrates. Two examples relevant in the context of this thesis are CO₂[98][99] and CH₄,[100][101][102] adsorbed on NaCl. In both cases, upon adsorption, the molecules grow epitaxially on the salt forming ordered structures. Remarkably, for these molecules also the formation of ordered monolayers is reported.

The situation is very different for larger molecules. As a general trend these molecules seem to be very mobile on insulator surfaces and stable structures are observed only for relatively thick films or when large molecular crystallites are formed. Epitaxially grown multilayers are formed by various porphyrin molecules on KCl[103][104][105], on KBr[105] and by perylene on KCl[106]. The formation of large 3D crystallites, where only a very small fraction of the molecules are in contact with the surface, is observed for C₆₀ on NaCl[107]. Similar observations are reported for para-phenylene on the (001) surface of various alkali halides and on mica[108] as well as for perylene-tetracarboxylic-dianhydride (PTCDA) on the (001) surfaces of NaCl and KCl[109].

In summary, large organic molecules seem not to adsorb strongly enough to form organized structures in the monolayer regime. This is also suggested by observations of CuTBPP on KBr(001), where molecules tend to cluster at step edges and pile up in relatively thick structures[110]. Moreover, even large multilayer islands of C₆₀ on NaCl have been proven to be weakly bound to the substrate and could be easily moved as intact entities by means of an AFM tip[107]. From these experiments it has been extrapolated that the energy required to slide a single C₆₀ molecules over a NaCl unit cell is only 0.25 meV[107].

Few observations of single molecules on ultra-thin insulator films have been reported

3.3. First Attempts and Strategy

as for example porphyrin[49] and phthalocyanine[96] on $\text{Al}_2\text{O}_3/\text{NiAl}$, and pentacene on $\text{NaCl}/\text{Cu}(111)$ [97]. It is important to note that all these experiments have been performed at low temperature. Of course these conditions favor the stability of even very weakly bound adsorbates. Another relevant experiment dealing with thin films is the study of di(propyl)perylene (DPP) adsorbed on a $\text{Si}(111)$ substrate partially covered by a semiconducting Si-CaF_1 monolayer and by an insulating CaF_2 bi-layer[111]. Confirming the tendency discussed above, DPP preferentially adsorbs on the semiconducting Si-CaF_1 monolayer. Consistent results are obtained in a UPS study comparing the adsorption of 4-hydroxy-thiophenol (HTP) on $\text{Ag}(001)$ and on NaCl multilayers grown on $\text{Ge}(100)$ [112]. A careful analysis of the UPS spectra shows that, while HTP bounds to silver through its thiol group, nothing similar happens on NaCl , where molecules are bound to the surface by a weak van der Waals interaction.

All in all, at room temperature, there is basically no example of a large organic molecule stably adsorbing on an insulator at coverages of a single layer or below. One exception to this has been reported in a recent publication which demonstrates the adsorption and self assembly of chloro-[subphthalocyaninato]boron-(III) (SubPc) molecules on $\text{KBr}(001)$ [113]. However, the assembly can be observed only for SubPc molecules confined in very small (less than 15 nm) pits artificially produced in the KBr surface. The fact that no organization can be observed for non-confined SubPC molecules seems to confirm the general trend discussed above.

3.3. First Attempts and Strategy

From the previous remarks it becomes clear that it is not trivial to achieve adsorption of large organic molecules in ordered structures on insulator materials. This is confirmed by the experience gained during this thesis. Different molecules did not provide the results awaited. However, some of these attempts showed interesting results and have been useful in order to identify a system matching the specific needs.

The first molecule investigated has been C_{60} . Fullerene, after its discovery[114] and especially after the development of efficient methods for its synthesis[115], has been in the focus of intensive researches. The adsorption and growth of C_{60} layers on various surfaces has also been studied in detail[116][117] and, among large organic adsorbates, C_{60} today is one of the best known systems. In addition C_{60} can practically be handled in a very reliable way. Therefore it has been a natural choice for our experiments. In fact, having to deposit in sequence NaCl layers and molecules, significantly enhances the difficulties of the sample preparation. Consequently a poor control in a single step of the sample preparation may be highly detrimental to the whole experiment.

A short summary of the essential results obtained with C_{60} on NaCl/metal samples is shown in fig. 3.1 (a). C_{60} molecules do organize on the bare $\text{Cu}(111)$ surface (fig. 3.1 (b)) while the NaCl layer looks clean; no sign of the presence of molecules can be observed and atomic resolution of the salt is achieved (fig. 3.1 (c)). This confirms previous observations describing a very unstable adsorption of fullerene on bulk NaCl [107].

3. CuOEP on Insulator Ultrathin Films

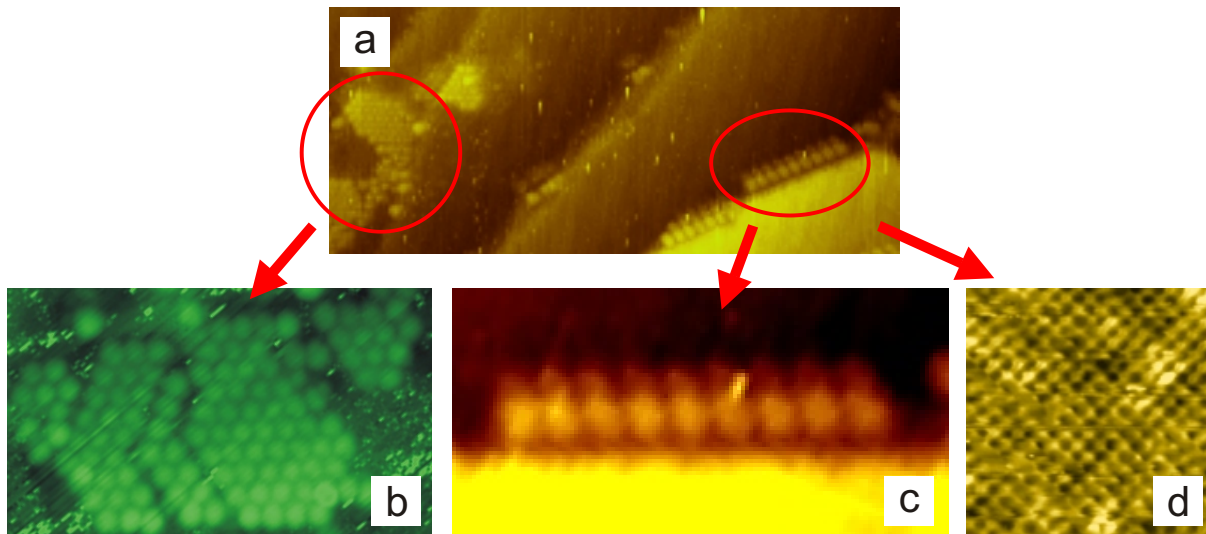


Figure 3.1.: $C_{60}/NaCl/Cu(111)$ annealed to 450 K. Image (a) (32×74 nm, $U = -3.1$ V, $I = 5$ pA) shows a part of a NaCl island and some clean metal. On the left side, on top of the bare copper, the formation of a C_{60} island can be noted. A closer view on the fullerene island is shown in (b) (11×19 nm, $U = -2.0$ V, $I = 10$ pA). In (a) and in more detail in (c) (17.7×8.8 nm, $U = -3.1$ V, $I = 5$ pA), it can be observed that some C_{60} molecules order along the border of the NaCl island. In (d) (5×5 nm, $U = -1.5$ V, $I = 50$ pA) by zooming-in on the NaCl area, atomic resolution of the NaCl lattice can be achieved.

An interesting feature can be observed at the border of NaCl islands (fig. 3.1 (d)). After annealing the sample to 450 K, C_{60} molecules tend to arrange in a row at the side of a salt island. Remarkably the distance between two molecules is about 1.5 nm, which is significantly larger than the one observed for the standard hexagonal packing of C_{60} on metal surfaces. For example from fig. 3.1 (b) an intermolecular distance of about 1 nm is obtained, which is in good agreement with the distance reported in literature for $C_{60}/Cu(111)$ [118]. The same distance of about 1 nm has also been reported for C_{60} molecules adsorbed on other metallic surfaces such as Au(111) and Ag(111)[119]. Clearly the NaCl plays a key role in sustaining such a large distance between two neighboring molecules.

In a next step molecules with a large dipole moment, which should interact more strongly with an ionic NaCl layer, have been investigated. Chloro-[subphthalocyaninato]boron-(III) (SubPc) is an interesting candidate whose adsorption on Ag(111) has already been carefully investigated by STM and PES[120][121][28].

The interpretation of the results obtained for SubPc on NaCl/metal is not straightforward. Surface areas densely covered by molecules coexist with clean regions (fig. 3.2). At the same time, different structures with borders which are straight and form right angles, can be identified. These evidences clearly indicate the presence of NaCl structures on the surface. Although molecules and NaCl structures can be simultaneously imaged, from the STM data it is not possible to reveal whether the SubPC molecules are adsorbed on the free metal regions or on top of the salt islands.

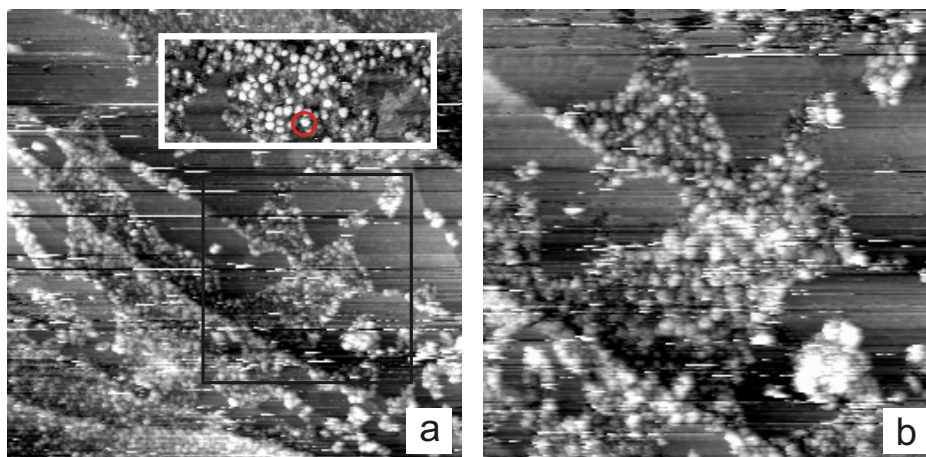


Figure 3.2.: SubPc/NaCl/Cu(111). Image (a) (200×200 nm, $U = 2.85$ V, $I = 30$ pA) shows an overview where the presence of some NaCl structure as well as several molecules can be identified. The top right inset (12.1×7.8 nm) offers a closer view where single molecules can be identified (as highlighted by the circle). Image (b) (100×100 nm, $U = 2.85$ V, $I = 30$ pA) shows a more detailed view (corresponding to the black frame of image (a)) where the typical borders of a NaCl structure can be identified.

The interpretation of the STM results is complicated by the fact that the molecules stick on some areas of the surface but they do not organize in any ordered structure. In addition each molecule has a different appearance in STM images, suggesting the coexistence of several different adsorption configurations. These observations are consistent with a strong adsorbate-substrate interaction, which *freezes* the molecules upon their adsorption, without giving them the possibility to move and arrange in an ordered and energetically favored structure.

Although stable adsorption of SubPc molecules on NaCl structures cannot be excluded, the fact that it is not possible to observe any ordered molecular layering, indicates that SubPc is not appropriate to achieve the desired result.

Based on these experiences, porphyrin molecules have been chosen. These molecules are especially interesting because they can interact with the substrate in different ways. Both, their extended π -system and the central metal ion – which, depending on its chemical nature and oxidation state, can interact in the direction perpendicular to the porphyrin plane – may favor the adsorption on the salt substrate. Moreover, a big variety of porphyrins with a number of different peripheral substituents are commercially available. These *legs* are expected to play a significant role in determining the distance of the porphyrin core from the substrate and therefore affecting the interactions described above. The possibility to act on these two different degrees of freedom (i.e. the central ion group, and the side substituents) makes porphyrin molecules ideal candidates for experiments where a delicate balance of the molecule-substrate and molecule-molecule interactions plays a crucial role. The concept of this operational strategy is schematically shown in fig. 3.3. A further advantage of porphyrin

3. CuOEP on Insulator Ultrathin Films

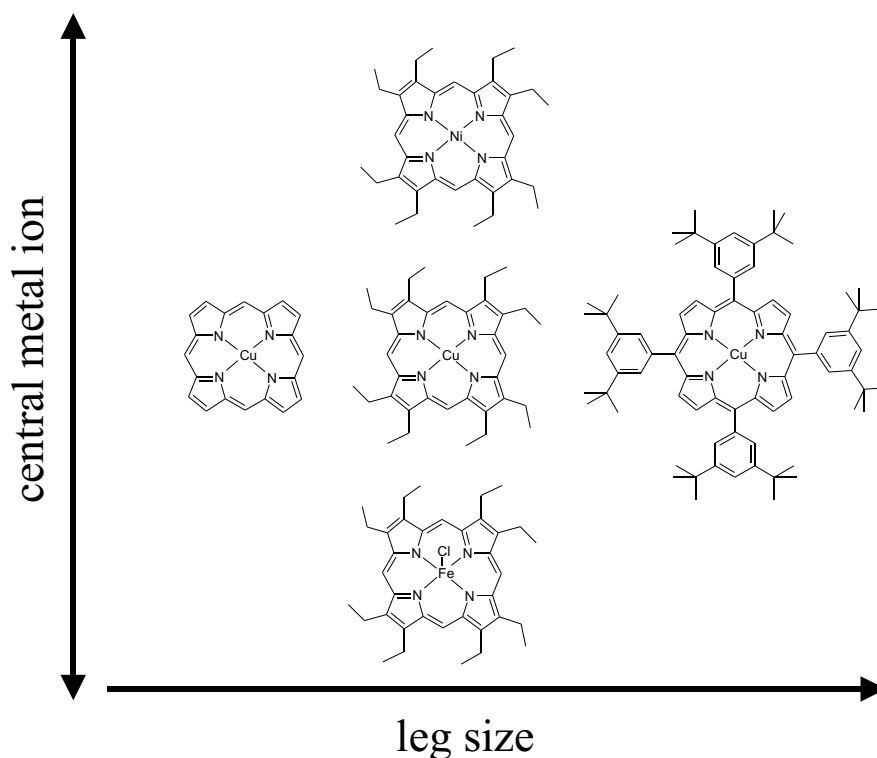


Figure 3.3.: Scheme of the research plan. Porphyrin are available with a large number of central ion groups as well as side substituents. A systematic investigation of molecules chosen by varying these parameters may allow to study the role played in the adsorption by each part of the molecule.

molecules is the fact that a lot is already known about their evaporation as they have already been largely investigated on metallic substrates[122][123][124].

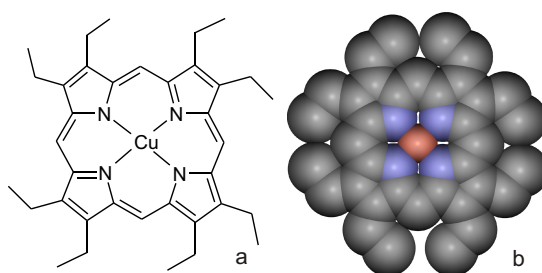


Figure 3.4.: CuOEP molecule. a) Structural formula. b) space filling CPK representation.

From the research plan schematically shown in fig. 3.3, two porphyrin molecules have been investigated: iron(III)chloride octaethyl-porphine (FeClOEP) (CAS 28755-93-3, Fluka) and copper(II) octaethyl-porphine (CuOEP) (CAS 14409-63-3, Fluka). Experiments with FeClOEP were successful and the formation of an ordered monolayer of molecules on top

	rate	current	temperature
C ₆₀	3-4 Å/min	1.70 A	300 K
SubPc	2-3 Å/min	1.10 A	300 K
FeClOEP	1-2 Å/min	1.05 A	300 K
CuOEP	1-2 Å/min	1.05 A	300 K

Table 3.1.: Evaporation parameters (evaporation rate, current used to heat up the crucible, and substrate temperature during deposition) employed for the different molecules studied.

of NaCl islands has been observed. However the big majority of the experiments performed during the Ph.D. and described in the thesis have been performed with CuOEP. A schematic representation of its chemical structure is reported in fig. 3.4.

3.4. Sample Preparation

The sample preparation and all the measurements have been performed in the system described in sec. 1.3. The molecules have been sublimated from home made tantalum crucibles, using a quartz microbalance to monitor the evaporation rate. A summary of the typical evaporation parameters used for different molecules is presented in table 3.1. The substrates have been prepared as described in sec. 2.3, depositing NaCl on Cu(111), Ag(111) and Ag(001). For the experiments described in this chapter, samples with a NaCl coverage between 0.3 and 0.7 ML have been prepared. Before the deposition of the molecules, these samples have been investigated by STM to check their quality and the NaCl coverage. During the molecule deposition all substrates have been kept at room temperature.

3.5. Assembly of CuOEP on NaCl

Upon deposition of about 1 ML of CuOEP, the molecules are observed to organize in an ordered pattern on the bare metal areas as well as on the sodium chloride islands as shown in fig. 3.5. From this zoom-in sequence of STM images a comprehensive understanding of the behavior of CuOEP on the surface can be gained.

Although the sample is covered with a layer of CuOEP, in the large overview (a) several NaCl islands can be identified. They have typical squared shapes and a characteristic size of about 100 nm. Islands are scattered on the surface with various orientations, and show a tendency to grow across the step edges of the substrate. Furthermore the formation of adlayer structures can be observed on top of many of the islands. A better understanding of these structures can be gained by zooming-in as shown in (b): adlayers can be identified as second and smaller third layer structures. Further zooming-in allows to resolve the molecules adsorbed on the surface (c).

3. CuOEP on Insulator Ultrathin Films

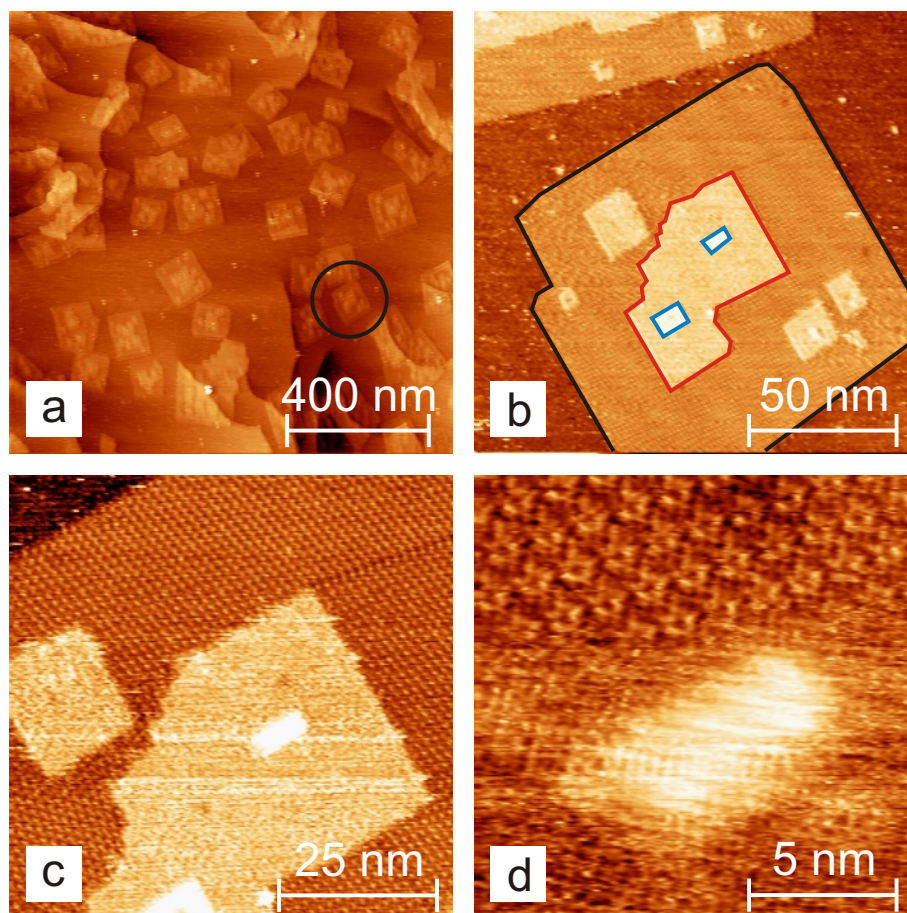


Figure 3.5.: CuOEP on NaCl/Ag(111). Zoom-in sequence of STM images referring to the same sample area. (a) Overview ($1.25 \times 1.25 \mu\text{m}$, $U = -0.25 \text{ V}$, $I = 49 \text{ pA}$): NaCl islands of characteristic square shape. (b) Zoom-in ($150 \times 150 \text{ nm}$, $U = -0.34 \text{ V}$, $I = 57 \text{ pA}$) on the island encircled in (a): for clarity, the border of the NaCl island and some of its second and third layers are highlighted. The distinctive islands shape allow to univocally identify sample regions of defined NaCl layer thickness, even upon deposition of 1 ML of CuOEP. (c) ($70 \times 70 \text{ nm}$, $U = -0.34 \text{ V}$, $I = 57 \text{ pA}$) Resolution of individual CuOEP molecules self-assembled on the first NaCl layer. The observation of dislocation lines indicates that there is a CuOEP/NaCl registry. (d) Close up view ($15 \times 15 \text{ nm}$, $U = -0.25 \text{ V}$, $I = 81 \text{ pA}$), centered on the third NaCl layer: the second layer is partially covered by a molecular assembly.

The key point of this sequence of images is that the large overviews allow to prove that the imaged molecules are indeed adsorbed on top of a NaCl layer. The same observations have been made on all substrates tested: Cu(111), Ag(111) and Ag(001). In all these cases molecules adsorb with their aromatic core parallel to the substrate and form an ordered pattern. The fact that domains form only specific angles with the island borders and the presence of dislocation lines suggest the existence of a registry between the molecular pattern and the underlying NaCl layer. This means that the growth of the molecular assembly is

epitaxial. Independently of the underlying metal substrate, the CuOEP molecules form a close packed, slightly distorted hexagonal pattern on top of the NaCl layer. To our knowledge, the observed molecular superstructure represents the first observation of an extended 2D molecular assembly of large organic molecules on an insulator surface.

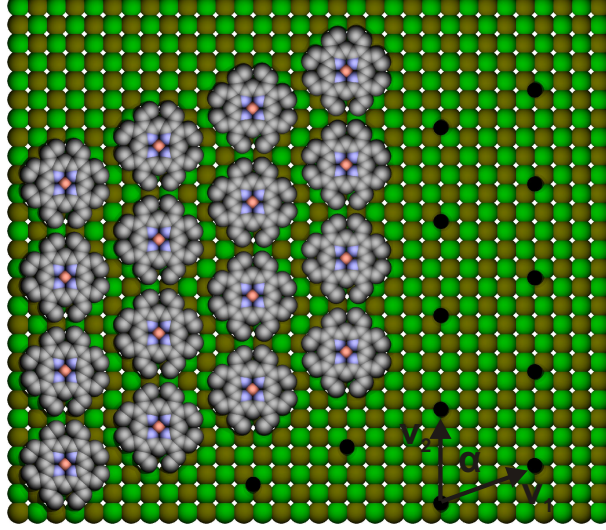


Figure 3.6.: Proposed model for the superstructure of CuOEP adsorbed on a NaCl layer. For clarity the position of some of the molecules is indicated by a black dot. Concerning the CuOEP orientation and its adsorption site within the NaCl(001) unit cell the picture shows only one of the possible choices.

	model	experiment
v_1	14.6 Å	14.3 ± 0.3 Å
v_2	13.5 Å	13.5 ± 0.3 Å
α	68.2°	$69.0 \pm 1^\circ$

Table 3.2.: CuOEP on NaCl/Ag(001). Comparison between the intermolecular distances and angles predicted by the model of fig. 3.6 and measured by STM.

Based on the intermolecular distances and angles measured by STM, for CuOEP on NaCl/Ag(001), the superstructure model presented in fig. 3.6 is suggested. This model is described by the epitaxy matrix $M = \begin{pmatrix} \frac{5}{2} & 1 \\ 0 & \frac{5}{2} \end{pmatrix}$, where the [100] and [010] primitive vectors of the NaCl bulk crystal unit cell have been chosen as basis vectors. Table 3.2 shows the good agreement between the proposed model and the measurements. The model accounts for the relative position of the molecule centers in the pattern but does not define

3. CuOEP on Insulator Ultrathin Films

the molecular orientation on the surface. Similarly, the precise adsorption site within a unit cell of the substrate cannot be determined although, based on a symmetry argument, some preferential sites can be identified.

The proposed model assumes a registry between the molecules and the substrate yet the two structures are not commensurate. This means that not each molecule is adsorbed on an equivalent substrate site but there is a coincidence only every second molecule (this situation has been defined as *point-on-line* coincidence by Hooks et al.[93]). On the other hand, all the CuOEP molecules within the pattern look identical. Therefore, adsorption on top of one ion seems unlikely, as it would imply molecules to adsorb on highly inequivalent sites (i.e. alternately on top of anion and cations). Adsorption above hollow sites (or above bridge sites) instead, would lead to a higher symmetry configuration, where the same adsorption energy has to be expected for each molecule.

The molecules arrange in a quite densely packed fashion. The here described adsorption model predicts an area of 183 \AA^2 per molecule which is comparable to the densities measured for CuOEP adsorbed on various bare metal surfaces (see discussion in sec. 4.2). This density is close to the maximum which is possible when packing the molecules in one plane. For instance in the (001) plane of the CuOEP bulk crystal structure a slightly higher density is observed (164 \AA^2 per molecule)[125]. However, it has to be remarked that in the crystal the molecules have more room as they are tilted by about 45° with respect to the (001) plane.

The high density of the molecular pattern suggests that the assembly of the ordered CuOEP layer is mainly driven by the balancing between the repulsive intermolecular interactions and the energy gained by each CuOEP upon adsorption. Moreover, the fact that the CuOEP superstructure is not commensurate to the NaCl lattice, but only a *point-on-line* coincident epitaxy is observed, suggests that the lateral stiffness of the molecular overlayer significantly exceeds the shear strength of the overlayer-substrate interface[93]. Further evidence supporting this hypothesis is given in section 3.6.

3.6. Layer Selective Adsorption

In order to gain deeper insight into the discovered system and specifically about the formation of the extended molecular assemblies on the different surface regions, each of the NaCl/metal systems has been studied by systematically increasing the CuOEP coverage from 0 to 1 ML.

The observed behavior is schematically illustrated in fig. 3.7. Interestingly, the CuOEP adsorption takes place in a hierarchical fashion, first on the clean metal areas, than on the 1- and 2-layer thick NaCl islands respectively. Initially, at very low coverage, no assembly is observed in any area of the sample. By increasing the coverage, although no ordered CuOEP structure can be observed yet, the presence of a significant amount of molecules on the metal areas becomes evident. Molecules are quite mobile on the surface but can nevertheless be identified by characteristic streak patterns in the STM images[126][120]. After a further coverage increase, the assembly of ordered molecular structures is observed. Very remarkably at this stage they appear only on the salt-free metal areas, while the NaCl islands are still clean (see for example fig. 3.8).

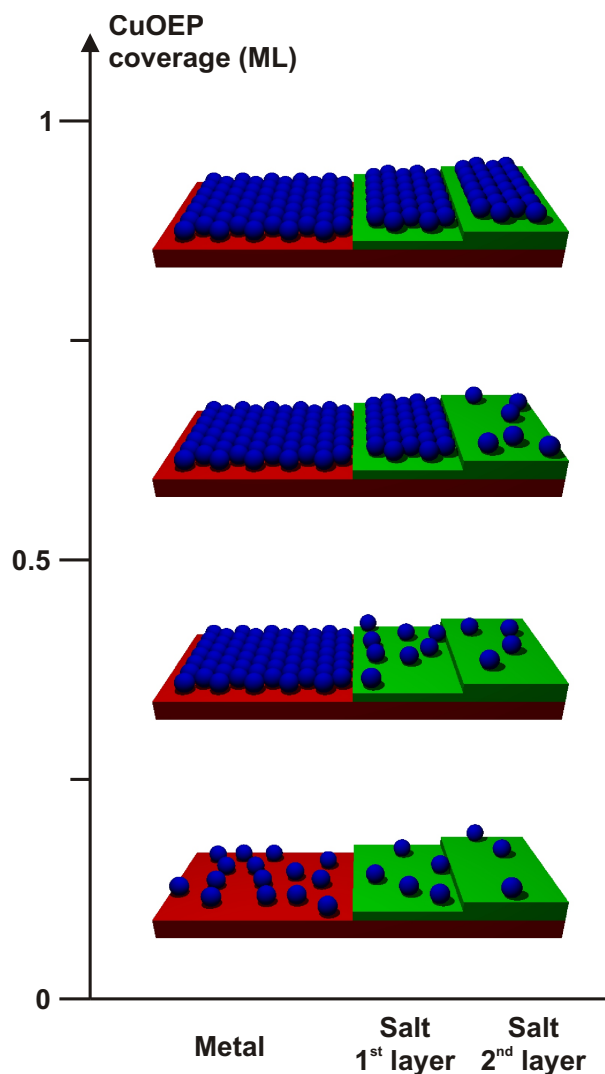


Figure 3.7.: Schematic depiction of the layer selective hierarchical assembly of CuOEP on NaCl/metal as a function of CuOEP coverage. Epitaxial filling occurs successively on metal, first and second NaCl layer. Note that stable ordered assemblies are observed on each layer only once it is almost full. This process is governed by the stepwise decrease in the adsorption energy of CuOEP when going from metal to first and second NaCl layer.

For higher coverages, all metal areas are covered by an ordered CuOEP layer and molecules also appear on salt, first in the form of the characteristic streak pattern in the STM images and finally as molecular assembly with an ordered superstructure. A very similar behavior is found on the 2-layer thick NaCl islands, once the first NaCl layer is almost completely covered with molecules.

The growth kinetic of these 2-dimensional CuOEP assemblies is probably governed by specific across-step diffusion coefficients between different sample regions and/or by a lower sticking coefficient on the NaCl layers compared to the metal substrate. However, over the

3. CuOEP on Insulator Ultrathin Films

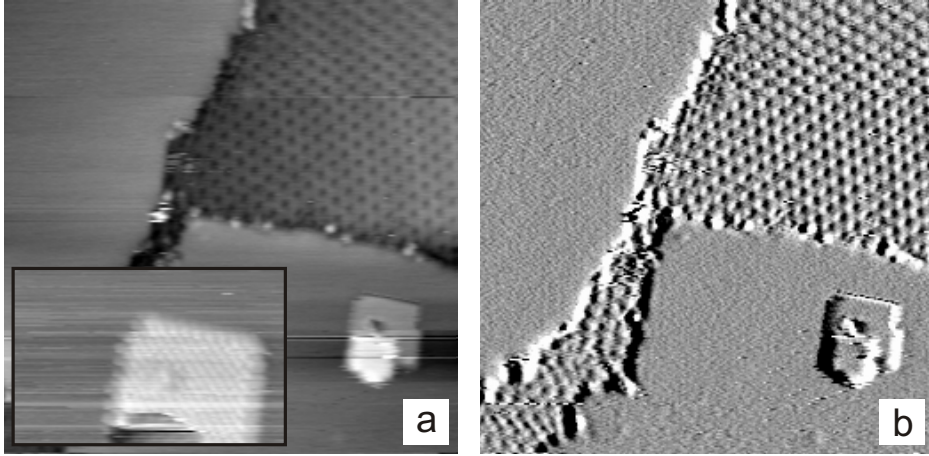


Figure 3.8.: CuOEP/NaCl/Ag(001). Image (a) and (b) show the topography and current signal of the same STM scan (40×40 nm, $U = -2.9$ V, $I = 45$ pA). The images show that the salt free metal area is covered by an ordered layer of CuOEP molecules. On the salt islands no molecule can be imaged and in the current signal (b) a regular pattern, most likely corresponding to the NaCl lattice, can be identified. On the small, 2-layer thick salt island atomic resolution is clearly achieved, as shown in the inset of the topography image (12.1×7.8 nm, $U = -2.6$ V, $I = 45$ pA).

time span between the molecule deposition and the STM measurements it is reasonable to assume that thermal equilibrium between different sample areas is reached. Consequently, the different populations observed on the diverse sample areas as a function of the mean coverage allow to determine the following inequalities between the respective adsorption energies

$$E_{ads}^{(metal)} > E_{ads}^{(1^{st} \text{ layer NaCl})} > E_{ads}^{(2^{nd} \text{ layer NaCl})} \quad (3.1)$$

Moreover, the fact that no formation of 3D structures is observed up to the completion of the first CuOEP layer indicates that

$$E_{ads}^{(1^{st} \text{ layer NaCl})} > E_{ads}^{(1^{st} \text{ layer CuOEP})} \quad (3.2)$$

In a first approximation $E_{ads}^{(1^{st} \text{ layer CuOEP})}$ can be replaced by the cohesive energy for the CuOEP crystal, therefore leading to the relation

$$E_{ads}^{(1^{st} \text{ layer NaCl})} > E_{coh}^{(CuOEP \text{ crystal})} \quad (3.3)$$

The last approximation offers an interesting term of comparison for the observed adsorption energies. However, it has to be remarked that this estimate may be quite inaccurate, because, opposite to what observed for the adsorbed molecules, in the 3D crystal the CuOEP aromatic cores lie all in different planes[125].

The relations between the adsorption energies for CuOEP on different sample areas seem to confirm the general trend described in literature (see sec. 3.2): adsorption on insulators is unfavored compared to the adsorption on metals. However, the relation between the

adsorption energy of CuOEP on NaCl and on a molecular layer (see eqs. 3.2 and 3.3) represents a significant exception to what is known in literature where the formation of molecular crystallite is often reported (see discussion in sec. 3.2).

3.7. Theory of CuOEP Adsorption

For non polar molecules with an aromatic core parallel to the substrate, a significant contribution to the adsorption energy is expected from van der Waals (vdW) interactions. Similarly for the molecular crystal, E_{coh} is dominated by the vdW attraction between parallel molecules arranged in stacks[125]. For the somewhat larger Cu-phthalocyanine, for instance, the corresponding contribution to E_{coh} (2.95 eV) has been estimated to be 2.47 eV, assuming pairwise interatomic potentials[127].

In general, vdW interactions scale with the effective electronic polarizabilities of the interacting atoms. Therefore, a first evaluation of the vdW forces between adsorbates and different substrates can be performed considering the relative Hamaker constants[128][129] which are a measure of the polarizability of a medium. For example, Hamaker constants calculated according to Lifschitz theory[130][131][129] for the materials of interest are the following: $H_{NaCl}=0.4$ eV[132], $H_{Cu}=2.5$ eV and $H_{Ag}=1.25-3.1$ eV[133]. This trend of the Hamaker constants and therefore of the polarizabilities of these media, already suggests that vdW interaction between an adsorbate and the substrate is likely to be weaker for NaCl than for a metal. This is well in line with the measured adsorption energies of methane, which is one of the few molecules which has been studied on both metal and ionic crystal surfaces. For CH_4 the measured physisorption energies are 130 meV on NaCl(001)[100][102], 160-190 meV on Cu(001)[134] and 220 meV on Ag(110)[135]. Of course for CuOEP with eight peripheral ethyl groups and a central core comprising four N and twenty C atoms, one expects significantly stronger binding on metal as well as on salt. Moreover, for the case of CuOEP we can neglect effects of lateral intermolecular interactions on the adsorption energy. These effects are important for CH_4 [102][136] but should be relatively weak for CuOEP, a large flat molecule lying parallel to the substrate.

The vdW attraction between a chemically inert species at a distance d from a flat substrate is approximately C_3/d^3 . The d^{-3} dependence only holds at distances large compared to the interatomic spacing but has nevertheless successfully been used to describe physisorption of inert species[136]. For a given adsorbate at a fixed distance d , this dependence predicts the difference between the vdW attraction to a metal (m) and to the same metal covered by an insulator (i) of thickness t to be:

$$(C_{3,m} - C_{3,i}) \left[\frac{1}{d^3} - \frac{1}{(d+t)^3} \right] \quad (3.4)$$

The strength of the C_3 coefficients for CuOEP are not known. Although, to get a rough estimation of the relation between adsorption energies on metal and insulator surfaces, it seems reasonable to consider the C_3 coefficients measured for rare gases which are quite well known[136]. According to Vidali *et al.*[136] $C_{3,m}$ on Ag(111) is only slightly larger than on

3. CuOEP on Insulator Ultrathin Films

Cu(111), but is more than twice $C_{3,i}$ on NaCl and other alkali halide (001) surfaces for all the rare gas adatoms. Then, from eq. 3.4 clearly follows that the adsorption energy of CuOEP on NaCl/metal is lower than on the clean metal and it decreases monotonically with the salt layer thickness t . In detail, the difference between the adsorption energies of CuOEP on NaCl layers of different thickness t_1 and t_2 ($t_1 < t_2$) is given by:

$$(C_{3,m} - C_{3,i}) \left[\frac{1}{(d + t_2)^3} - \frac{1}{(d + t_1)^3} \right] \quad (3.5)$$

This is in good agreement with the experimental observation of a sequential absorption, on the first and then on the second NaCl layer. It is important to note that in eqs. 3.4 and 3.5 the thicknesses (t, t_1, t_2) can adopt only discrete values, which again can vary only in steps of the same order of magnitude of the adsorbate-substrate distance d . Therefore the adsorption energy difference expressed by eq. 3.5 will decrease very rapidly by increasing the number of salt layers t_1 and t_2 . This means that the limit-case of adsorption on bulk NaCl is approached after relatively few layers.

Eqs. 3.4 and 3.5 only hold under the approximation that the distance between the adsorbate and the substrate is the same. This is not trivial, especially as CuOEP is a large molecule which can adopt various conformations upon adsorption[122]. It is therefore interesting to analyze how eq. 3.4 changes when assuming two different adsorption distances, d_m for CuOEP on metal and d_i for the adsorption on NaCl/metal. Assuming $d_m = d_i + \Delta d$, in a first order approximation for $\Delta d \ll d_i, d_m, t$ the following expression is obtained:

$$(C_{3,m} - C_{3,i}) \left[\frac{1}{d_i^3} - \frac{1}{(d_i + t)^3} \right] - \frac{3C_{3,m}}{d_i^4} \Delta d \quad (3.6)$$

Therefore, for $\Delta d < 0$, that is for $d_m < d_i$, a positive term has to be added to the difference in the adsorption energies of eq. 3.4. On the other hand, for $d_m > d_i$ the correction term becomes negative and a more detailed quantitative analysis is needed. This is a quite delicate issue and indeed there are evidences that for inert adsorbates it may happen that $d_m > d_i$. For instance Vidali *et al.*[136] report that, within the scatter of the data, measured adsorption energies of many rare gas atoms are quite similar on both ionic and metal substrates although in the latter case significantly larger C_3 coefficient are reported. In the case of metals it seems that a stronger repulsion is balancing the larger vdW attractive interaction. Vidali *et al.* attribute this to the steeper variation of the repulsion interaction due to electronic overlap, on ionic crystal compared to metal surfaces.

This effect should be negligible once one NaCl layer is present. Furthermore, the conformation of CuOEP on NaCl/metal should not depend significantly on the number of salt layers. Therefore, the approximation of a constant substrate-adsorbate distance d for different NaCl layer thickness implied in eq. 3.5 should hold.

The whole discussion above has been carried out considering only the vdW contribution to the molecule-surface interaction. However, coverage dependent UPS measurements of CuOEP adsorbed on the three metal surfaces (see sec. 4.6) reveal significant work function changes. These prove a relevant electron transfers from the molecules to the substrate,

3.8. Investigating the CuOEP-Substrate Electronic Coupling

consistent with the well established donor character of porphyrins[25]. Hence, ionic bonding between CuOEP and the metal surface seems to occur. Such a bonding directly contributes to the adsorption energy of CuOEP on metal ($E_{ads}^{(metal)}$). Moreover it may influence the substrate-adsorbate distance and consequently also the strength of the vdW interaction.

In principle electrons can tunnel through a few insulator layers[68][44][137] which would result in a net charge transfer between the molecules and the metal also in the presence of a salt layer. However, the broadening of the molecular energy levels is proportional to the tunnelling exponent which governs the decay of the metal local density of states (LDOS) through the insulator. According to fig. 3 (b) of ref. [68], the latter decreases about a hundred times for each new monolayer of NaCl. As a consequence, the HOMO of CuOEP, which lies about 2 eV below the Fermi level (see sec. 4.5), already for 1 ML NaCl is so narrow that it cannot donate any electron to the metal.

To summarize, the differences in the adsorption energies of CuOEP on metals covered by different numbers of NaCl monolayers are most likely explained by two mechanisms. A charge transfer leading to ionic bonding of the molecules directly adsorbed on the metal is the cause for the difference between the 0-layer and the 1-layer cases. Whenever more NaCl layers are present, adsorption energy differences can be explained in the frame of pure vdW interaction (see eq. 3.5).

3.8. Investigating the CuOEP-Substrate Electronic Coupling

After the observation of different adsorption energies of CuOEP on NaCl/metal systems, bias dependent STM experiments have been envisaged for a first assessment of the electronic structure of the adsorbed molecules. For instance, Viernow *et al.* showed how STM can conveniently be used to locally identify differences in the LDOS of insulator thin films[35]. In detail, the appearance of CuOEP molecules adsorbed on NaCl and on metals has been studied at different bias voltages.

Pursuing this goal by means of STM at room temperature is very challenging because of several experimental complications. In particular the STM imaging process strongly depends on the tip conditions, which can easily undergo slight changes. Therefore, it is not easy to reliably compare fine details from images scanned at different times. Moreover, layers of CuOEP molecules, as already reported for other large organic molecules[138][139][140], are not very stable and it happens relatively often that molecules jump from the sample to the tip or vice versa. This means that tip changes are not rare and that it is difficult to keep the same tip conditions on the time scale of several STM images.

Given these circumstances, we decided to acquire STM images scanning across the border between a NaCl island and a salt-free metal area (see for example fig. 3.9 and 3.10). In an ideal case the fast scan direction is perpendicular to the salt-metal step, so that, at each scan line, the tip images both areas to be compared. In this way it can be guaranteed that molecules on both areas are imaged with exactly the same tip and images eventually affected by tip changes can easily be identified and discarded.

3. CuOEP on Insulator Ultrathin Films

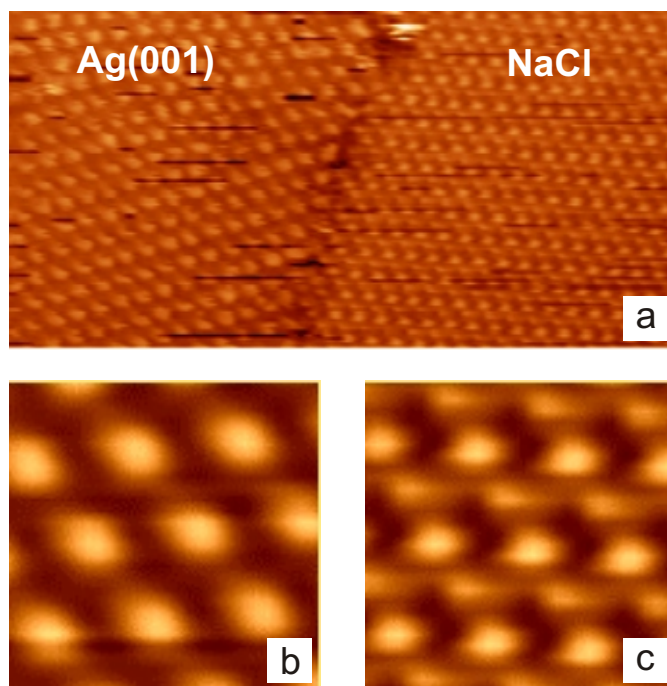


Figure 3.9.: CuOEP on NaCl/Ag(001). (a) STM image ($40 \text{ nm} \times 20 \text{ nm}$, $U = -1.76 \text{ V}$, $I = 40 \text{ pA}$) taken across a NaCl-metal step. Images (b) and (c) (both $4.3 \text{ nm} \times \text{nm}$) are extracted from the left (CuOEP/Ag(001)) and right (CuOEP/NaCl/Ag(001)) part of image (a) by averaging over several unit cells. Clearly, the molecular appearance differs depending on the underlying substrate.

A representative example of a direct comparison of the appearance of CuOEP molecules on metal and on NaCl thin film is shown in fig. 3.9 (a). In this STM image each molecule adsorbed on the salt layer shows two separate maxima. On the other hand, under the same scanning conditions, the molecules directly adsorbed on Ag(001) are characterized by a single maximum. A closer view on the different molecular appearances can be obtained by applying the averaging filter described in sec. 1.2.1 (fig. 3.9 (b) and (c)). Undoubtedly the different substrates specifically affect the molecule appearance.

Moreover, it can be observed that the substrate does not only determine the molecular appearance, but also its dependence on the bias voltage. Image 3.10 shows an experiment where the bias voltage has been repeatedly changed while moving the tip in the slow scanning direction. The image has been acquired scanning across the same metal-salt step of image 3.9 (a). The appearance of molecules adsorbed on NaCl/metal significantly depends on the applied bias voltage while the appearance of the molecules directly adsorbed on metal stays almost unaffected. This behavior has been repeatedly observed for bias variations between -0.5 V and -2.0 V . In fig. 3.10, at -1.9 V the molecules on salt and on metal share quite similar appearances. However, upon a decrease of the bias to -1.6 V , only the molecules adsorbed on the NaCl layer change their appearance significantly and the image of each molecule consists of two distinct protrusions.

3.8. Investigating the CuOEP-Substrate Electronic Coupling

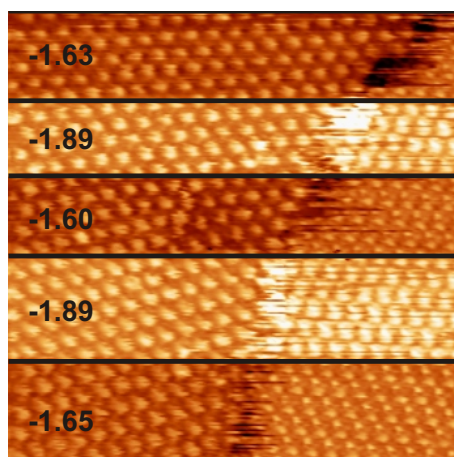


Figure 3.10.: CuOEP on Ag(001) vs CuOEP on NaCl/Ag(001) ($30 \text{ nm} \times 30 \text{ nm}$, $I = 40 \text{ pA}$). Bias voltage has been changed while moving the tip along the slow scanning direction. Its value (in volt) is directly indicated on each image section. The image has been acquired scanning across the same salt-metal border of fig. 3.9 (Ag(001) on the left and NaCl on the right). The two different substrates do not only affect the way the molecules look like but also the dependence of their appearance as a function of the bias. Changing the bias from -1.6 V to -1.9 V the appearance of CuOEP on silver is almost unaffected while the two dots belonging each molecule adsorbed on salt merge in a single bigger spot.

The observed contrast cannot be the result of a convolution with the underlying NaCl ion pattern. As explained in sec. 3.5, the CuOEP assembly on NaCl/Ag(001) is not commensurate with the underlying NaCl lattice but there is a coincidence only every second molecule (see figure 3.6). Therefore, any feature arising from a convolution between the molecular pattern and the substrate should appear with a periodicity double the one of the CuOEP pattern. Furthermore, in separate experiments on clean NaCl layers (not shown here), no significant changes for corresponding bias values have been observed. Thus, the different molecular appearances and their bias dependence reflect an inherent difference between the two substrates.

It is important to note that such observations of a pronounced voltage dependence of the appearance of the molecules adsorbed on salt is confirmed by several measurements performed with different tips.

At the current state there is no comprehensive understanding of these interesting observations. In order to gain a deeper insight, detailed molecular orbital calculations and low temperature STM/STS measurements are needed. Nevertheless, the observed results are well in line with the weak binding to the substrate found for CuOEP on NaCl (see sec. 3.6 and 3.7).

It has already been shown that the appearance of atomic adsorbates in STM images can be strongly affected by the adsorbate-substrate interaction[141]. The effects on the adsorbate electronic structure seem to be even more significant for organic adsorbates. For instance, this has been shown for 4-hydroxy-thiophenol adsorbed on Ag(001) and on NaCl/Ge(100)[112].

3. *CuOEP on Insulator Ultrathin Films*

In the latter case, opposite to what observed on the pure metal, it has been found that the molecular electronic structure resembles very much the one calculated for a free molecule. Similarly, for porphyrin[49] and phthalocyanine[96] adsorbed on $\text{Al}_2\text{O}_3/\text{NiAl}(110)$ only a small broadening and/or delocalization of the molecular electronic states has been observed.

In the frame of these observations, it seems plausible to assume that the different appearances of CuOEP on metal and on salt are due to different adsorbate-substrate interactions. Especially the tendency of CuOEP to show a more pronounced dependence on the bias voltage on salt than on metal suggests that in the latter case a more pronounced broadening of the molecular electronic states occurs, i.e. the interaction is stronger.

4. CuOEP on Metals

In the previous chapter the growth and the self assembly of Copper Octaethyl Porphyrin on salt/metal heterostructures have been presented. In order to offer a term of comparison, we intensively studied the same molecules also on pure metal substrates. In particular, the adsorption and self organization has been intensively investigated by STM, LEED and UPS on Cu(111), Ag(111) and Ag(001). Furthermore, a deep insight on the interaction intervening at the organic-metal interface is obtained by comparing the STM and UPS results with DFT calculations performed for a free CuOEP molecule.

4.1. Motivation

The investigation of Copper Octaethyl Porphyrin on salt/metal heterostructures described in the previous chapter leads to very interesting conclusions. As explained in sec. 3.5 and 3.8, a key point of that experimental approach has been the use of substrates showing bare metal as well as salt covered areas at the same time. This allows for a direct comparison of STM measurements on both type of surfaces. On the other hand, such an approach severely limits the potential of non-local probe techniques, which integrate over macroscopic sample regions (e.g. PES, LEED). Therefore, other possible approaches would have been to study CuOEP on a full NaCl layer or directly on a bare metal surface. In this chapter the latter approach is described.

Working with a uniform substrate it is possible to take full advantage of measurement techniques such as LEED and UPS. Moreover, measurements on the CuOEP/metal system are technically easier to carry out, especially concerning the sample preparation, allowing a high degree of control on the experiments. Therefore, the analysis of CuOEP on metals represents a promising direction of research in order to extend the investigations discussed in the previous chapter.

On the other hand, organic molecules on metal surfaces are an interesting and intensively investigated topic for different reasons. In this chapter, the attention is focussed on the properties of the organic-metal interface. This is currently a field of high interest in the context of the development of hybrid organic-inorganic electronic and optical devices such as OLEDs[83][84][85] and thin film transistors[86][87]. A good understanding of the electronic structure at the organic-metal interface is very important in order to control the charge carrier injection between metals and organic semiconductors.

In detail, we investigated the formation of an interface dipole layer at the organic-metal interface, which is induced by charge transfer upon molecular adsorption. It has been shown that changing the chemical composition of specific molecular substituent groups, can signifi-

4. CuOEP on Metals

cantly influence the ionization potential and/or the electron affinity, thus the acceptor/donor character of a molecular adsorbate. For example Peisert *et al.*[142][143] have shown that the fluorination of copper phthalocyanine leads to an increase of the ionization potential of the molecular solid by up to 1.1 eV, which substantially influences the interfacial dipole moment. Controlling this interfacial dipole moment is very interesting because it influences the energy level alignment and therefore the carrier injection process[144][145].

4.2. Determination of the Molecular Epitaxy

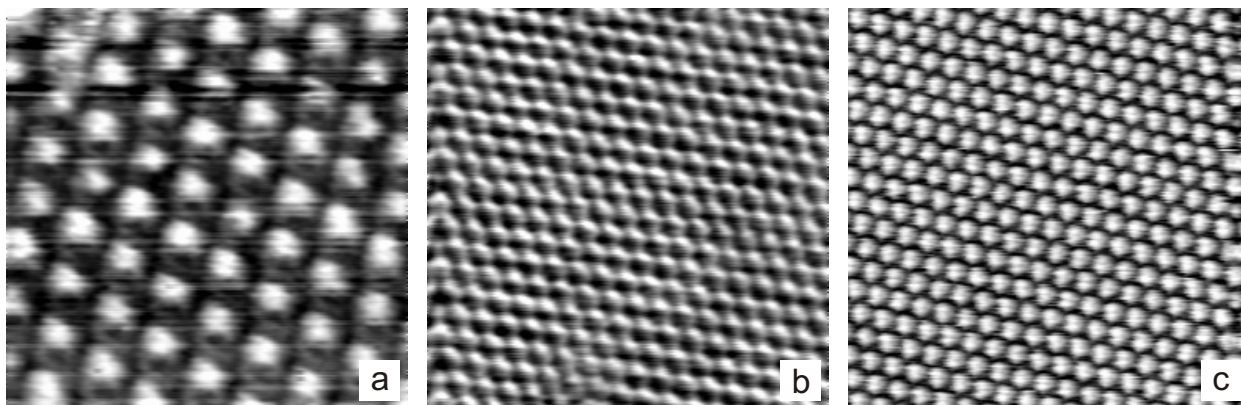


Figure 4.1.: CuOEP on different metal substrates. (a) Cu(111) (10 nm \times 10 nm, $U = -2.0$ V, $I = 20$ pA); (b) Ag(111) (25 nm \times 25 nm, $U = -0.8$ V, $I = 16$ pA); (c) Ag(001) (25 nm \times 25 nm, $U = -1.4$ V, $I = 10$ pA).

As reported in sec. 3.5, CuOEP molecules self assemble in ordered monolayers on the NaCl/metal surface. The formation of ordered patterns is observed on both the bare metal and the salt covered areas. Upon deposition of about 1 ML of CuOEP on pure metal, the structure of the molecular layer can very conveniently be investigated by LEED. By combining the information obtained by real space (STM) and reciprocal space (LEED) measurements, a complete understanding of the molecular pattern has been gained for Cu(111), Ag(111) and Ag(001) substrates.

As a first observation, STM images show that CuOEP molecules organize in a nearly hexagonal pattern on all three substrates. However, due to drift and hysteresis of the piezoelectric actuators, STM does not allow a very precise determination of distances and angles. In order to improve the accuracy of the measured intermolecular distances and angles within the CuOEP pattern, distances and angles have been determined by averaging over four images acquired for different scanning directions. This procedure allows to limit the error below 5% for intermolecular distances and below 2° for angles. The results obtained for the three metal substrates are summarized in table 4.1.

For Cu(111) and for Ag(001) the observed deviation from the hexagonal arrangement is clearly larger than the experimental uncertainty. As explained in the following, the LEED

4.2. Determination of the Molecular Epitaxy

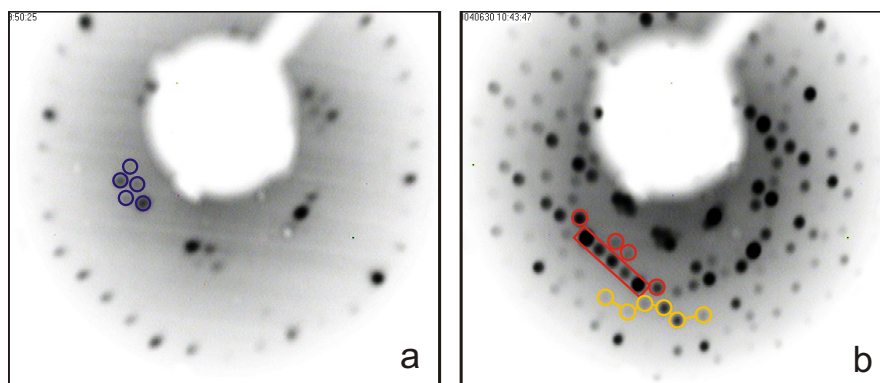


Figure 4.2.: CuOEP on Cu(111): LEED patterns measured at 7 eV (a) and at 19 eV (b). In both images some of the spots are highlighted by circles and other characteristic geometric shapes, in order to simplify the comparison with the simulated pattern in fig. 4.3 (b).

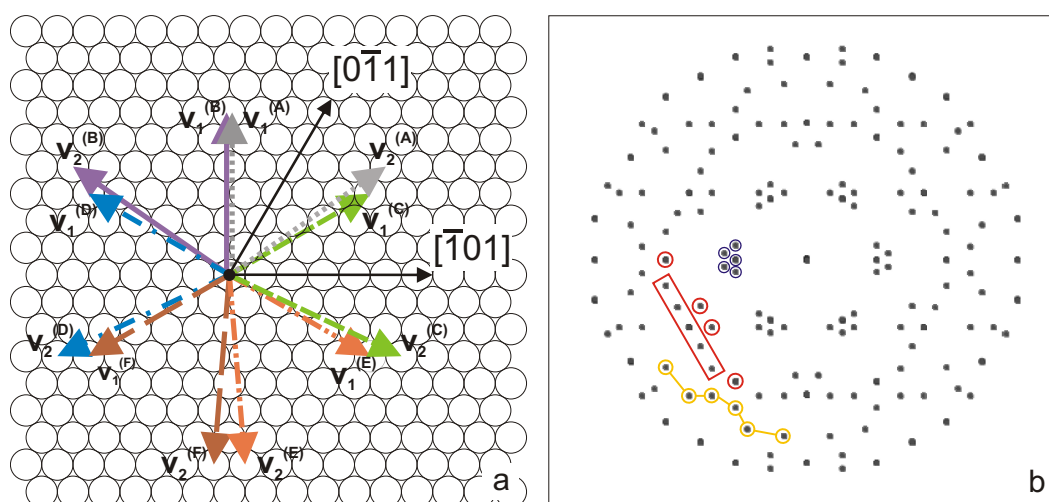


Figure 4.3.: CuOEP on Cu(111). In (a) the basis vectors of the six inequivalent CuOEP domains formed on Cu(111) are shown. The corresponding simulated LEED pattern is shown in (b). To help the comparison between model and experiment some of the spots have coherently been highlighted in the simulated pattern (b) and in the measured ones (fig. 4.2). Five small circles identify a group of spots at the first order of diffraction. Other circles and lines mark spots of higher diffraction orders.

measurements confirm these STM observations. Due to the low symmetry of the self assembled 2D crystal formed by CuOEP, the interpretation of the LEED patterns is not straightforward. For this reason a simulation software (see sec. 1.2.2) has been used. Based on the symmetry of the observed LEED patterns and on the intermolecular distances and angles measured by STM, different epitaxy models have been assumed and then tested by means of the LEED simulation software. For all the three investigated substrates this procedure led to the identification of the proper epitaxy models. In the following, these models are

4. CuOEP on Metals

presented and their simulated LEED patterns are compared with the measured ones.

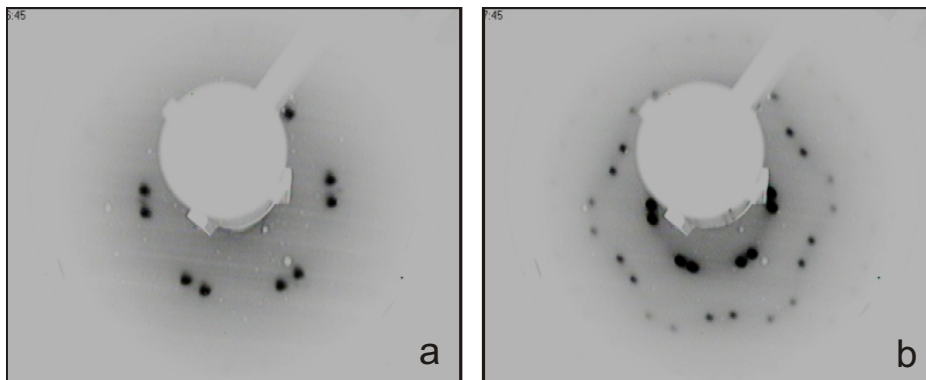


Figure 4.4.: CuOEP on Ag(111): LEED patterns measured at 5 eV (a) and at 11 eV (b). For this substrate much less spots than on Cu(111) are visible. This is explained by a higher symmetry for the epitaxy of CuOEP on Ag(111).

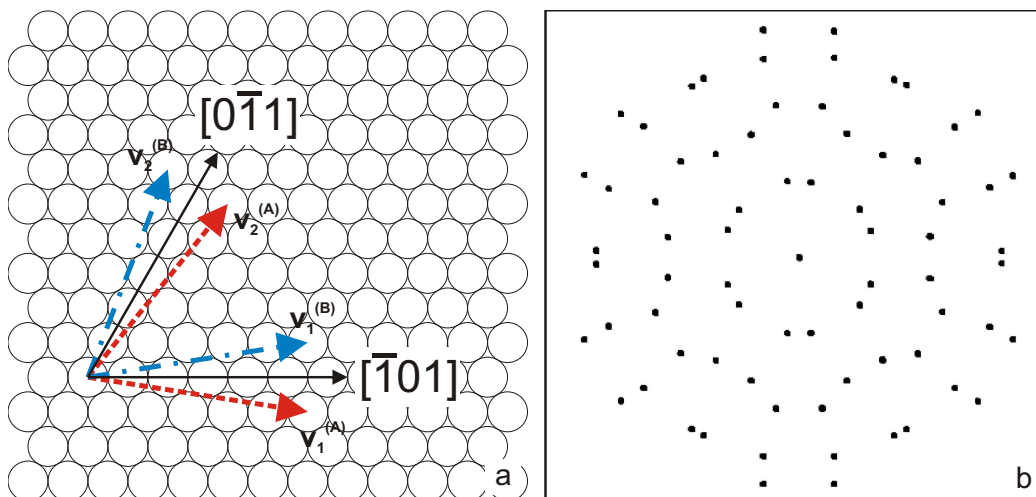


Figure 4.5.: CuOEP on Ag(111). In (a) the basis vectors of the two inequivalent domains formed on Ag(111) are shown. The corresponding simulated LEED pattern is shown in (b). The agreement between the simulated pattern and the experimental results (fig. 4.4) is perfect.

Figure 4.2 shows the experimental LEED pattern obtained for CuOEP on Cu(111). As anticipated, the numerous spots visible indicate a low symmetry of the 2D crystal formed by the CuOEP molecules. The analysis carried out (fig. 4.3 (a)) shows that only one domain type is formed on the surface. The epitaxy matrix for it (domain A of fig. 4.3 (a)) is $M = \begin{pmatrix} -3 & 6 \\ 3 & 4 \end{pmatrix}$. Due to its low symmetry, this domain is not invariant under three of the symmetry operations proper for the Cu(111) surface (rotation by 60° and 120° and reflection with respect to one of the main crystallographic directions). As a consequence, from a single

4.2. Determination of the Molecular Epitaxy

domain type, six inequivalent domains are generated (fig. 4.3 (a)). The simulated LEED pattern for this adsorption model is shown in fig. 4.3 (b). The comparison with the measured data clearly proves that the model found is the correct one. To help in the comparison between simulated and measured data some of the spots have been highlighted. Five circles identify a bunch of five LEED spots at the first order of diffraction. Other circles and lines have been used to highlight some of the spots of higher diffraction orders (figs. 4.2 and 4.3 (b)).

Figure 4.4 shows the LEED pattern obtained for CuOEP on Ag(111). At the first order of diffraction (fig. 4.4 (a)) only twelve spots are visible, being an indication of a comparably high symmetry of the CuOEP structure. The analysis confirms that the molecules assemble in a hexagonal structure slightly rotated with respect to the main axis of the Ag(111) surface. For this reason two mirroring domains are present on the surface. More precisely the CuOEP forms on top of Ag(111) a $\sqrt{31} \times \sqrt{31} R(\theta)$ structure (where $\theta = \pm \tan^{-1} \frac{\sqrt{3}}{11} \simeq \pm 8.95^\circ$). This arrangement is schematically shown in fig. 4.5 (a). The simulation of the LEED pattern for this model (fig. 4.5 (b)) agrees perfectly (at least for the first three orders of diffraction) with the measured patterns (fig. 4.4).

The LEED pattern for CuOEP on Ag(001) (fig. 4.6), similarly to the one on Cu(111), shows many spots (24 for the first order of diffraction alone). Again, the CuOEP assembles in a single type of domain with a fairly low symmetry. Its epitaxy matrix (domain A of fig. 4.7 (a)) is $M = \begin{pmatrix} 1 & 5 \\ 5 & 2 \end{pmatrix}$. This domain is not invariant under two of the symmetry operations proper for the Ag(001) surface (rotation by 90° and reflection with respect to one of the main crystallographic directions). Hence, from a single domain, four different domains are generated (fig. 4.7 (a)). The LEED pattern calculated for this epitaxy model is shown in fig. 4.7 (b). Again, to help the comparison between the simulation and the measurements, some groups of spots have been conveniently highlighted (figs. 4.6 and 4.7 (b)).

Table 4.1 shows the good agreement between the intermolecular distances and angles measured by STM and those determined from the epitaxy models described above. The good agreement obtained by combining two independent methods like LEED and STM puts the suggested models on a very solid ground.

On all investigated substrates (Cu(111), Ag(111) and Ag(001)), CuOEP grows epitaxially and forms patterns which are commensurate to the underlying surface. However, except for the case of Ag(111), the CuOEP superstructure does not reflect the symmetry of the substrate. It is interesting to note, that for CuOEP on NaCl, the correspondence between the CuOEP pattern and the salt surface is even lower (see sec. 3.5) and only a *point-on-line* coincidence is observed. According to the criteria suggested by Hooks *et al.*[93], this is a further indication of a stronger molecule-substrate interaction on the metal surfaces than on the salt layer, as already stated in the previous chapter.

Furthermore, it is interesting to compare the molecular densities of CuOEP on the different investigated substrates. According to the epitaxy models described above, each molecule occupies a surface area of 169.29 \AA^2 on Cu(111), 224.55 \AA^2 on Ag(111) and 192.37 \AA^2 on Ag(001). These numbers can be compared to the density measured on NaCl (183 \AA^2 per

4. CuOEP on Metals

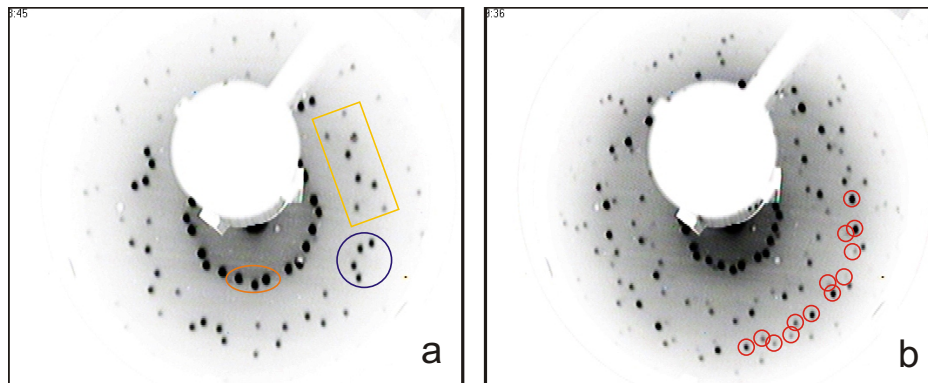


Figure 4.6.: CuOEP on Ag(001): LEED patterns measured at 11 eV (a) and at 20 eV (b). In both images some spots are highlighted by characteristic geometric shapes (a) and by circles (b), in order to simplify the comparison with the simulated pattern in fig. 4.7 (b).

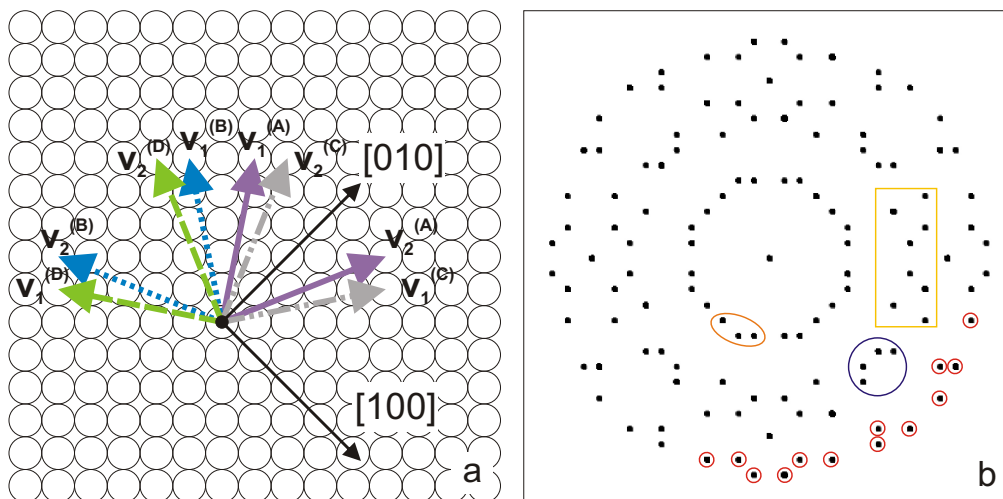


Figure 4.7.: CuOEP on Ag(001). In (a) the basis vectors of the four inequivalent domains formed on Ag(001) are shown. The corresponding simulated LEED pattern is shown in (b). To help the comparison between model and experiment, some of the spots have coherently been highlighted in the simulated pattern (b) and in the measured ones (fig. 4.6). An ellipse, a circle and a rectangle are used to identify groups of spots at the lower orders of diffraction. Higher order diffraction spots are marked by a series of small circles.

molecule, see sec. 3.5). Moreover, in the (001) plane of the CuOEP crystal, a density of 164 \AA^2 per molecule is reported[125]. However, it has to be remarked that in the 3D crystal the molecules have significantly more room, as they are tilted by about 45° with respect to the considered plane. In all cases CuOEP adsorption leads to remarkably high densities. This indicates that, upon adsorption, CuOEP molecules gain a significant amount of energy and therefore tend to pack closely. The remarkable spread observed for the molecular densities on different metal surfaces shows that the substrate plays a relevant role in the adsorption

4.3. High Resolution STM Imaging and Voltage Dependence.

	Cu(111)		Ag(111)		Ag(001)	
	STM	model	STM	model	STM	model
v_1 (Å)	12.44	13.264	15.81	16.102	15.20	14.639
v_2 (Å)	15.05	15.527	15.26	16.102	15.43	15.574
v_3 (Å)	12.77	13.507	15.36	16.102	14.55	14.460
α (deg)	73.4	68.77	59.5	60.00	56.5	56.89
β (deg)	53.9	59.80	61.5	60.00	60.5	58.67
γ (deg)	52.5	51.43	59.0	60.00	62.5	64.44

Table 4.1.: CuOEP self assembly on various metal surfaces. The table compares the intermolecular distances and angles measured by STM with those obtained by the epitaxy models described. For the STM measurements the uncertainty on the distances is below 5%, while for angles an accuracy of $\pm 2\%$ can be assumed.

and assembly mechanism. On the other hand, the effect of the central metal ion seems to be negligible as CoOEP[146], ZnOEP[147], NiOEP[124] and FeClOEP[148] adsorbed on Au(111) all have nearly the same density (around 190 \AA^2 per molecule).

4.3. High Resolution STM Imaging and Voltage Dependence.

STM and LEED measurements allow to determine the precise structure of the CuOEP layers formed on Cu(111), Ag(111) and Ag(001). However, not much can be inferred about the structure of a single molecule on the surface and its adsorption conformation. In order to investigate these topics, high resolution STM images have been acquired.

In detail bias dependent STM images allow to gain an insight about the electronic structure of CuOEP adsorbed on the metal surfaces investigated. The interpretation of these measurements is also based on the results of a DFT calculation performed for a free CuOEP molecule (for details about the calculation method see sec. 4.4). In the following the CuOEP/Ag(001) and the CuOEP/Cu(111) systems are described in detail.

4.3.1. CuOEP on Ag(001)

For CuOEP on Ag(001) the highest resolution STM images at negative sample bias (i.e. tunnelling from the occupied states of the sample into the tip) are systematically obtained for bias voltages between -1.5 V and -2 V . The molecular appearance for these biases is shown in fig. 4.8. Mainly the peripheral part of each molecule (corresponding to the ethyl legs) is imaged as a protrusion, while the inner core appears dimmer. For each molecule four elongate protrusions can clearly be identified and a closer analysis reveals that each of them

4. CuOEP on Metals

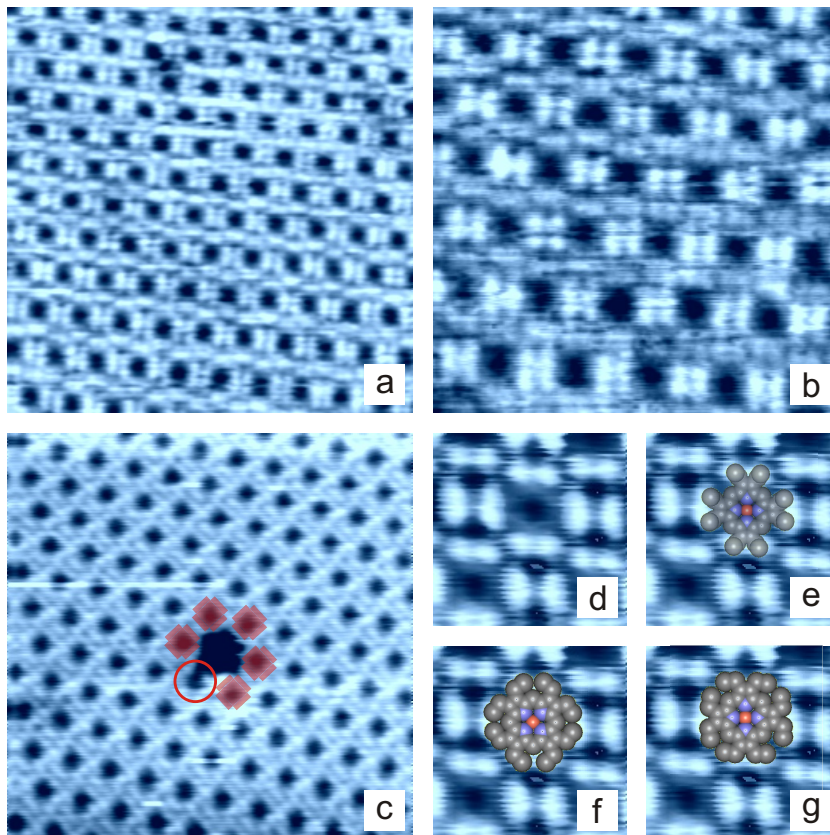


Figure 4.8.: CuOEP on Ag(001). Image (a) (15×15 nm, $U = -2.2$ V, $I = 25$ pA) shows the overlayer formed by CuOEP molecules. Zoom-in image (b) (8×8 nm, $U = -1.9$ V, $I = 25$ pA) shows that each minimum is surrounded by 4 elongate protrusions, which comprise two separate maxima. In image (c) (15×15 nm, $U = +0.45$ V, $I = 20$ pA) a pattern with a missing molecule allows to identify the features belonging to a single molecule. The center of a CuOEP molecule therefore corresponds with a minimum in the image and the eight maxima are located in correspondence with the ethyl legs. The six molecules surrounding the missing CuOEP have been highlighted. The molecule identified by a circle shows a little defect. Image (d) (2.4×2.4 nm, $U = -1.9$ V, $I = 25$ pA) is obtained by averaging over 18 cells. It allows to better resolve a single molecule. In images (e, f, g) the CPK model of a CuOEP molecule has been overlaid to image (d). Three of the most plausible adsorption conformations are given.

comprises two separate maxima. This is in perfect agreement with the presence of eight ethyl groups for each molecule. Based on these observations, it is clear that the molecules adsorb with their π -system lying more or less parallel to the surface. Furthermore, due to the high resolution achieved, it is possible to speculate about the precise adsorption geometry of CuOEP. Some of the feasible adsorption conformations are shown in fig. 4.8 (e), (f) and (g)). Among these, the most probable seems to be the configuration shown in fig. 4.8 (e) where the ethyl legs point outward from the surface. In fact the geometry of this configuration fits best with the observed one and furthermore it seems to justify the prominence of the legs in

4.3. High Resolution STM Imaging and Voltage Dependence.

the STM images.

Remarkably, the molecules in the adlayer do not show an exact four fold symmetry but they all seem to be elongated in one direction (e.g. for fig. 4.8 (d) this direction is nearly horizontal). This may be related with the low symmetry of the molecular assembly. As discussed in sec. 4.2, CuOEP arranges on Ag(001) in a deformed hexagonal pattern which is characterized by different periodicities along its different main directions. However, the deviation from a perfect hexagonal pattern is below 8% while the aspect ratio of the imaged molecules shows a deformation around 15%. Therefore, it seems that the molecules deform to better fit in a pattern which is not commensurate to the geometry of CuOEP. Such an alteration of the molecular shape is consistent with the observations reported for larger porphyrins on metals[122][123].

Furthermore, it can be observed that half of the observed protrusions look brighter than the others (fig. 4.8 (b)). In detail, the brighter maxima are the ones placed along the *stretching* direction of the molecules within the pattern. This effect is most probably linked to the deformation of the adsorbed molecules and therefore of their electronic structure. It can be observed that, along the *stretched* direction, the couples of legs of two neighboring molecules are very close. Therefore, the electronic states located on these legs are likely to *push-up* each other, which would explain their brighter appearance in STM.

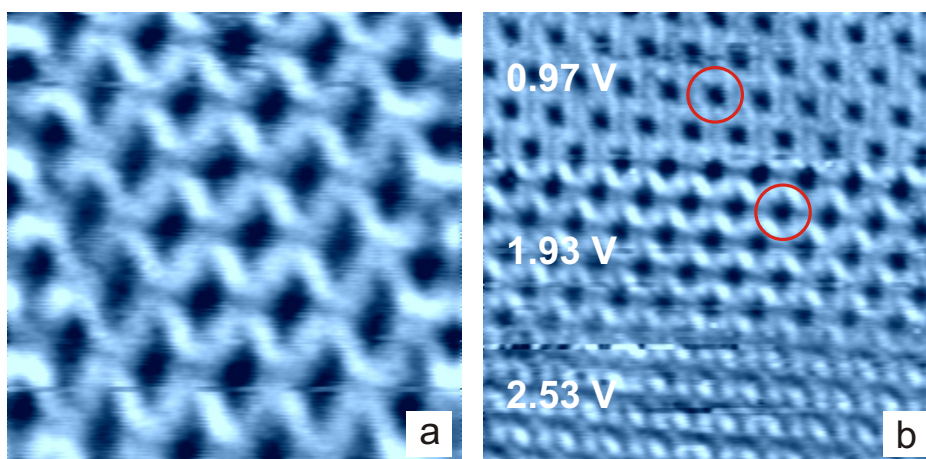


Figure 4.9.: CuOEP on Ag(001). Image (a) (8×8 nm, $U = 1.4$ V, $I = 20$ pA) shows the CuOEP pattern as it appears for voltages between 1.3 V and 2.0 V. Image (b) (15×15 nm, $I = 60$ pA) shows how the molecular appearance changes by using different bias voltages. For $U = 0.97$ V the same pattern as observed at negative bias (fig. 4.8) is found. This allows to identify the position of a CuOEP molecule in the pattern of image (a). As highlighted by the two circles in image (b), the center of each CuOEP corresponds with an imaged minimum while the maxima are located at the periphery of the molecule.

At positive sample bias (i.e. tunnelling from the tip into the unoccupied states of the sample) different molecular appearances are observed (fig. 4.9). The highest resolution images are obtained for voltages between 1.3 V and 2.0 V (fig. 4.9 (a)). Image 4.9 (b), where

4. CuOEP on Metals

the bias voltage has been changed while scanning, shows three different appearances discovered. Their simultaneous presence on the same STM image allows to establish a relation between them. For $U = 0.97$ eV the appearance essentially corresponds to the one observed at negative bias. Based on the previous discussion, it can be concluded that each molecule is centered on one of the square shaped minima. As highlighted by the two circles, fig. 4.9 (b) allows to conclude that, also in the pattern imaged at $1.3 \text{ V} < U < 2.0 \text{ V}$, the centers of the CuOEP molecules are located in correspondence with the minima of the image. However, the identification of a correspondence between the maxima and one molecule's legs is more complicated. In fact the four maxima surrounding each CuOEP appear to be merged with the maxima belonging to the neighboring molecules. Furthermore, analogously to what observed at negative bias, half of the maxima look brighter than the others.

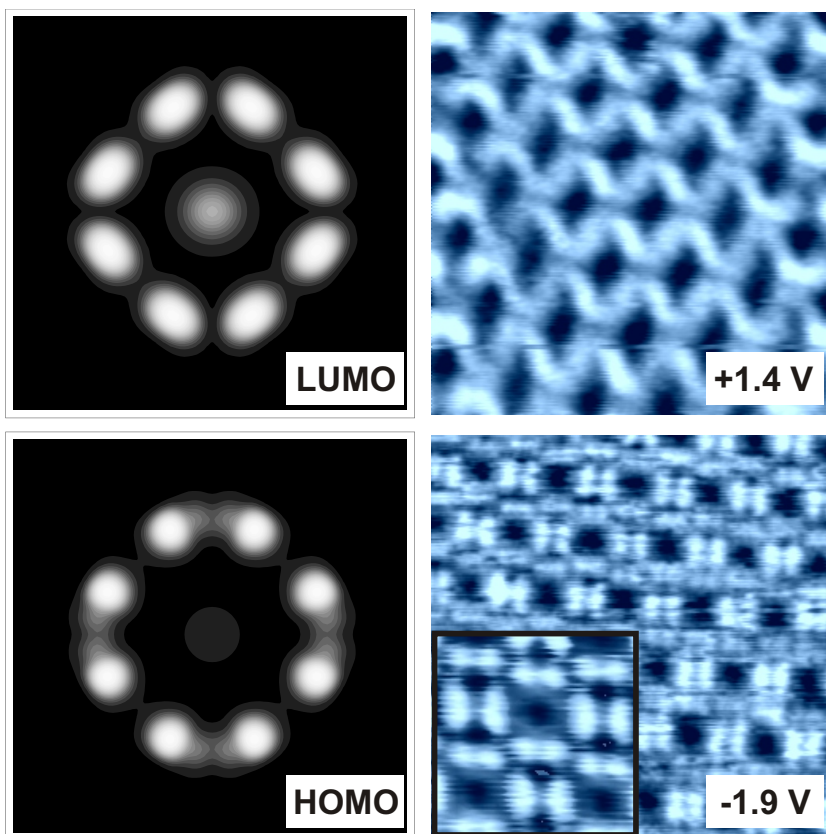


Figure 4.10.: CuOEP on Ag(001): DFT calculation *vs* experiment. The figure compares the simulated *constant height* STM images of the LUMO and HOMO states for a free CuOEP molecule with real STM images obtained at positive (tunnelling into unoccupied states) and negative (tunnelling from occupied states) sample bias. Details about the calculation are given in sec. 4.4. For the experimental parameters see figs. 4.9 (a), 4.8 (b) and 4.8 (d).

One of the most remarkable differences observed while changing the bias from negative (range between -1.5 V and -2 V) to positive (range between 1.3 V and 2.0 eV) is the change

4.3. High Resolution STM Imaging and Voltage Dependence.

of the symmetry in the molecular appearance. In both cases elongate maxima are visible but, by changing the bias, they *turn* by 45° . It is very instructive to compare these appearances with the results of a DFT calculation performed for a free CuOEP molecule (for further details see sec. 4.4). The calculation agrees very well with the experimental data and especially it seems to explain the change of symmetry previously described (fig. 4.10). However, it has to be remarked that the calculation has been performed for an isolated molecule, therefore neglecting any interactions with the substrate and the neighboring molecules. Nevertheless, its agreement with the experimental data offers a very likely explanation for the observed bias-related contrast changes and allows the identification of HOMO and LUMO.

4.3.2. CuOEP on Cu(111)

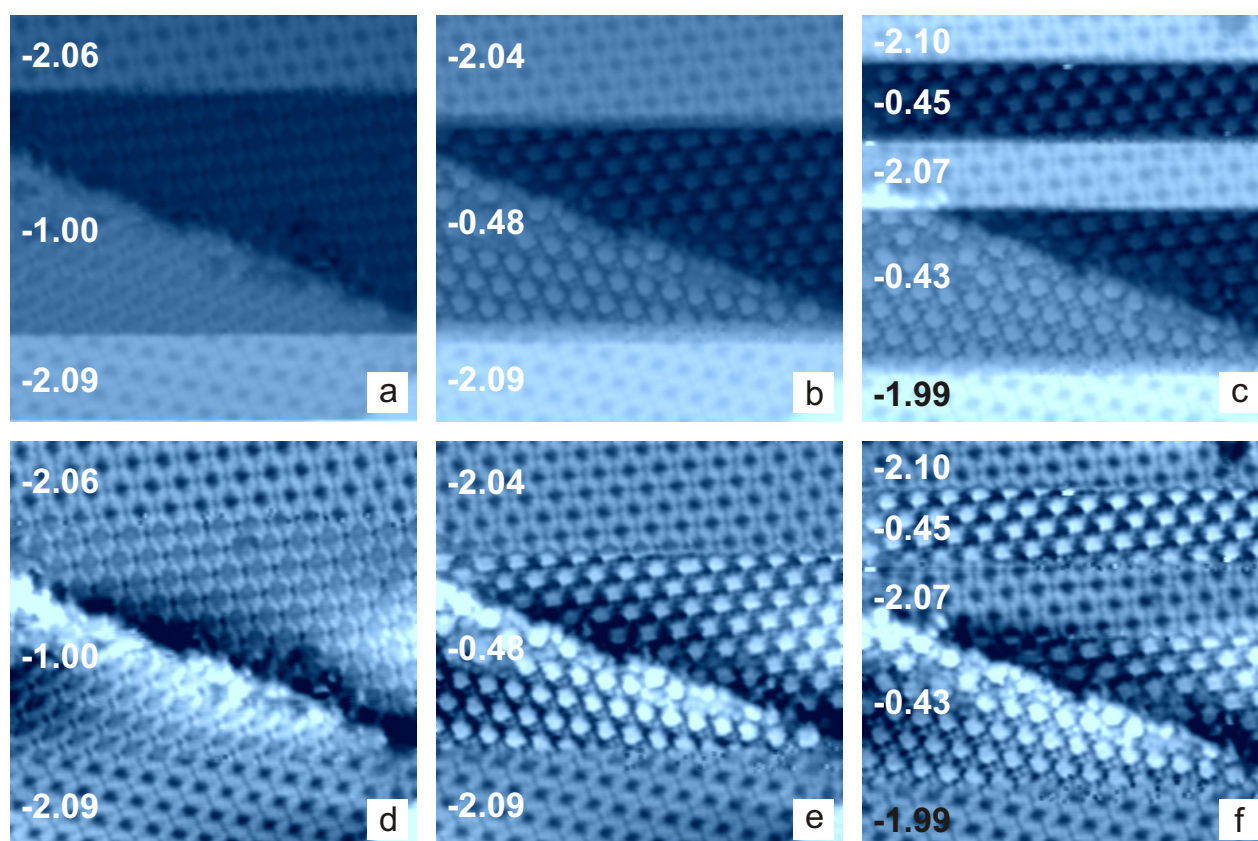


Figure 4.11.: STM images of CuOEP on Cu(111) (all 20×20 nm, $I = 24$ pA). The different bias voltages used are directly indicated (in volt) on the images. Images (d-f) are the same as (a-c) after applying a flattening filter (see sec. 1.2.1) used to emphasize the molecular appearance in each image section. The presence of different molecular appearances is evident.

The investigation of CuOEP on Cu(111) also reveals a strong dependence of the molecular appearance on the bias voltage. On this substrate the investigation has mainly been focussed

4. CuOEP on Metals

on the CuOEP occupied states (i.e. negative sample bias). Fig. 4.11 gives an overview on the most remarkable molecular appearances identified. The effect of the voltage on the molecular appearance is very strong and even reversal of contrast is observed. The reversibility and the reproducibility of the observed effects prove that they are not due to tip changes but that they indeed reflect genuine properties of the electronic structure of the adsorbed molecules.

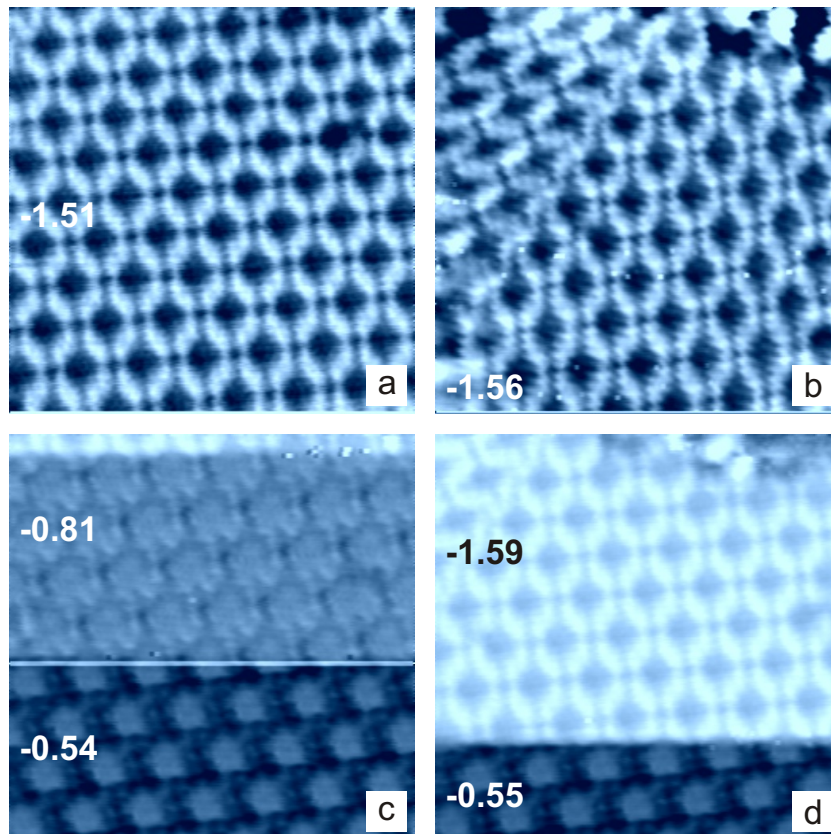


Figure 4.12.: CuOEP on Cu(111). STM images (all 10×10 nm, $I = 24$ pA) offer a close look on the molecular appearances observed for different biases (values in volt are indicated on the images). In (b) the observation of a border between two molecular domains indicates that for the appearances of image (a) and (b) the center of a CuOEP is located in correspondence to a minimum. Consequently, from (d) it can be inferred that for biases closer to zero CuOEP centers are imaged as maxima.

Fig. 4.12 gives a closer view on the different molecular appearances. In particular image 4.12 (b) shows the border between two differently oriented domains, which is very useful to identify the location of the CuOEP molecule centers within the imaged pattern. From the domain border shape and its position relative to the molecular pattern it can be concluded that the molecule centers are located at the minima of the STM image. Consequently, similarly to what observed for CuOEP on Ag(001), at voltages between 1.3 V and 2.0 eV, each elongate maximum arises from the cooperative effect of two neighboring molecules.

4.3. High Resolution STM Imaging and Voltage Dependence.

The appearance of the molecules shown in fig. 4.12 (a) and (b) is observed for biases between -2.5 V and -1.0 V. When approaching -1.0 V, the apparent height of the inner part of the molecule starts to increase. This trend is confirmed when the bias is further lowered and, at about -0.5 V, the inner part of the molecule appears as a maximum (fig. 4.12 (c)). A further insight in this change can be gained from high resolution STM images (fig. 4.13) obtained by applying an averaging filter (see sec. 1.2.1). Clearly, the CuOEP center can appear as a minimum (image 4.13 (d) taken at -1.51 V) as well as a maximum (image 4.13 (a) taken at -0.55 V). Images 4.13 (b) and (c), which have been acquired at -0.81 V and -1.00 V, present two intermediate situations, showing that the change between the different molecular appearances is smooth. This observation is consistent with the broadening of the molecular orbital levels, which is induced by the interaction with the metallic substrate.

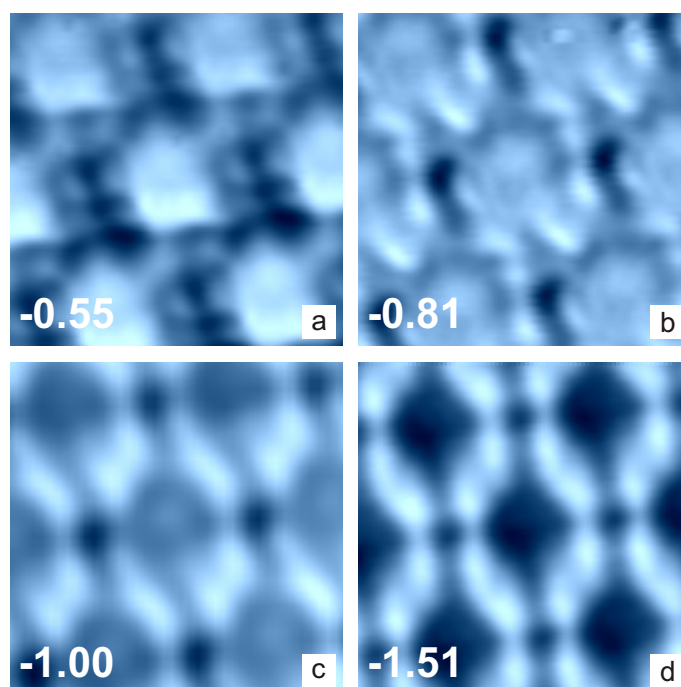


Figure 4.13.: CuOEP on Cu(111). These STM images (all 3.0×3.0 nm, $I = 24$ pA) are obtained by applying the averaging procedure described in sec. 1.2.1. Images (a) and (d) show two opposite features: the CuOEP center appears as a maximum in (a) and as a minimum in (d). Images (b) and (c) show two intermediate situations observed varying the voltage between -0.55 V (a) and -1.51 V (d).

In fig. 4.13 (a) some small spots are visible around the bright CuOEP core. Although the resolution achieved makes their identification quite difficult, it seems that on each side of the molecule core two of these local maxima are present. This suggests that each spot corresponds to one of the eight ethyl legs of CuOEP. The quality of the data does not allow to conclusively prove this hypothesis. However, the comparison with results reported in literature for analogous systems also supports this interpretation. For instance Scudiero *et*

4. CuOEP on Metals

al. show very similar STM images for NiOEP on Au(111)[124]. Analogous data are also published by Yoshimoto *et al.* for ZnOEP[147] and for FeClOEP[148] on Au(111). In all these publications a higher resolution of these intramolecular features is achieved by using a higher tunnelling current (0.3 nA for Scudiero *et al.*, over 1 nA for Yoshimoto *et al.*). Consequently, for these systems, the eight ethyl legs can be quite reliably identified in the STM images. Of special interest is the comparison with the publication of Scudiero *et al.* where the STM image shown has been acquired at a bias of -0.6 V, hence very close to the values used for the measurements reported here.

4.4. DFT Calculations

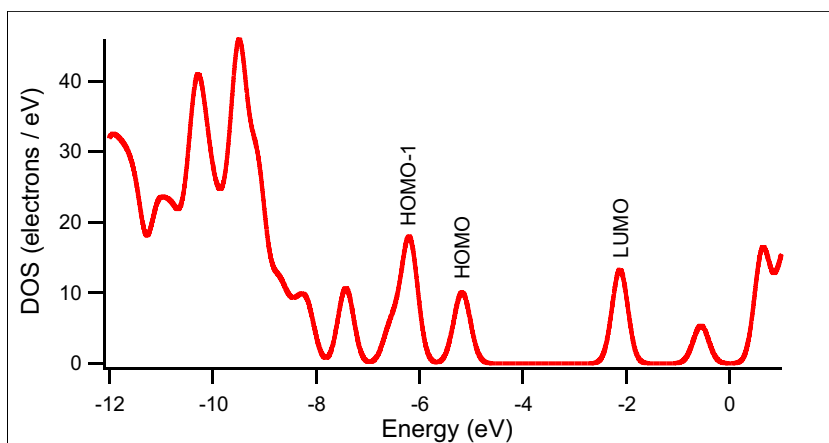


Figure 4.14.: CuOEP density of Kohn-Sham states calculated by DFT. The spectrum is obtained by the convolution of a normalized gaussian (width = 0.15 eV) for each calculated eigenstate.

In order to gain a deeper understanding of the measured data, they have been compared with DFT calculations. The computation has been carried out by Audrius Alkauskas at the Institute of Physics of the University of Basel. In this thesis only some of the conclusions useful to interpret the experimental results are reported.

The calculation deals with an isolated molecule, therefore neglecting any possible interaction with the substrate and with neighboring molecules. The calculation has been performed employing the B3LYP hybrid functional. D95V basis set was used for the light atoms, Lanl2DZ effective core potential and Lanl2DZ basis set for the central Cu atom.

First of all the influence of conformational flexibility on the electronic properties of the CuOEP molecule has been evaluated. Calculations show that the energy difference between different conformers is very small (few meV). The rotation of the ethyl legs does not influence the frontier orbitals of the CuOEP (as they are mainly of π -character) and only affects the states located more than 3 eV below the HOMO. The results reported here are obtained for a molecule with all eight legs pointing up. For this configuration the molecule has a small dipole moment of 0.5 debye, due to the fact that the ethyl legs are positively charged.

4.5. UPS Spectra: HOMO and HOMO-1 Positions

Fig. 4.14 shows the density of states obtained from the calculation. Here the terms HOMO, HOMO-1 and LUMO are used for convenience to indicate bunches of states lying very close in energy. In particular, the HOMO is composed of two near-degenerate states with a_1 and a_2 symmetry. The LUMO consists of two degenerate e states. The Cu $d_{x^2-y^2}$ -derived b_1 state belongs to the LUMO.

Furthermore, the results of the DFT calculation have been used to simulate the STM images of the HOMO and the LUMO (fig. 4.10). The images show a cut of the partial electron density in a plane lying 3 Å over the porphyrin plane. According to Tersoff-Hamann approximation[16][17] this simulates the result of a *constant height* STM image.

4.5. UPS Spectra: HOMO and HOMO-1 Positions

Based on the STM and LEED experiments described so far, not much can be learned about the adsorbate-substrate interaction. Therefore, UPS measurements have been performed to complete the characterization and understanding of CuOEP adsorption on metal.

Spectra have been acquired for different CuOEP coverages, from the submonolayer range up to the multilayer regime, as well as for the clean metal substrates. The evolution of the spectra for increasing coverages, starting from the bare metal case, allows the identification of the spectral features characteristic of the CuOEP layer. Fig. 4.15 shows the low binding energy part of the UPS spectra for CuOEP on Cu(111), Ag(111) and Ag(001). As a reference, the spectra acquired on the clean metals are reported as well. The detailed evolution of the complete (measured over the full energy range available) UPS spectra as a function of the CuOEP coverage is shown in Appendix B.

For clean Cu(111) and Ag(111) the surface states are clearly visible while for Ag(001) the typical metal Fermi edge is observed. Upon CuOEP deposition the HOMO and HOMO-1 states can be identified and it is evident that both states lie at different energies on the three substrates (values are summarized in table 4.2). However, it has to be remarked that in fig. 4.15 the spectra are shifted in order to keep their Fermi edges aligned, hence all energies are referred to the substrate Fermi level. As explained in the following (see sec. 4.6), their *absolute position* (i.e. with respect to the vacuum level) can be determined as well.

Here it is important to note that the energy difference between HOMO and HOMO-1 is nearly the same on all substrates (1.1-1.2 eV) and that it is very close to the value of 1.0 eV obtained from the calculation for a free molecule (fig. 4.14). This indicates that the interaction with the substrates shifts HOMO and HOMO-1 levels (see discussion in sec. 4.6) but does not significantly modify the structure of these states. This therefore suggests that there is no chemical binding between CuOEP and the metal substrate.

This conclusion is also supported by the fact that the relative intensities of the two peaks predicted by the DFT calculation (fig. 4.15) agree very well with the observed intensities. Furthermore, on Cu(111) where, due to the higher CuOEP coverage, the best quality of the signal is achieved, the HOMO-1 peak shows a shoulder on its higher binding energy side, which is also predicted by the computation.

4. CuOEP on Metals

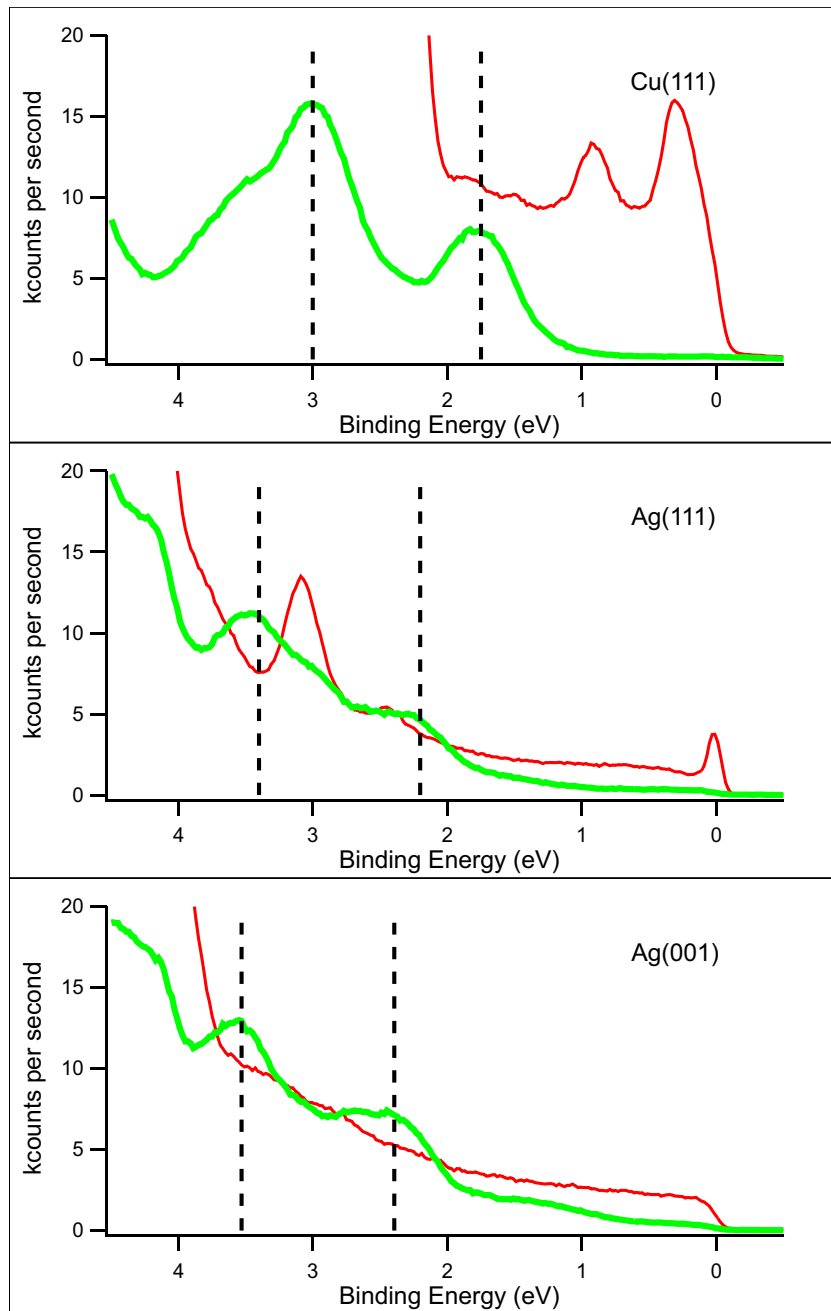


Figure 4.15.: UPS measurements for CuOEP on metals. The spectra (thick lines) are measured for a *nominal coverage* (see discussion in Appendix B) of 34 Å, 45 Å and 31 Å for Cu(111), Ag(111) and Ag(001), respectively. As a reference, the UPS spectra for the clean metals are reported as well (thin lines). The dashed vertical lines indicate the positions of HOMO and HOMO-1 states.

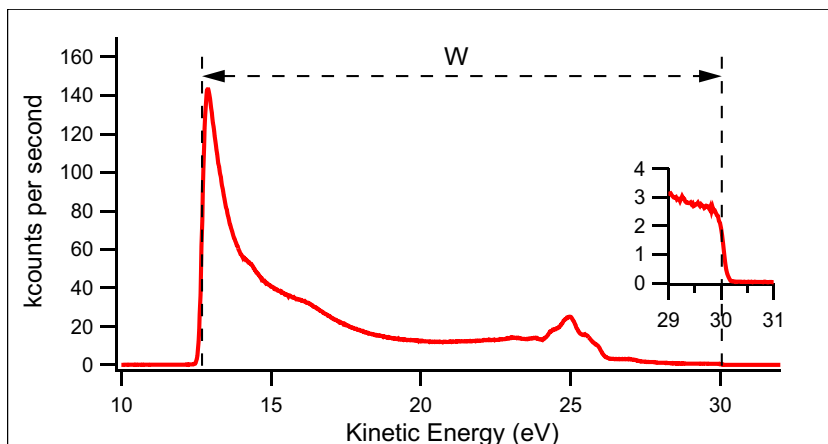


Figure 4.16.: Work function measurement by means of UPS. The graph shows the spectrum obtained for 2.0 Å CuOEP on Ag(001). By keeping the sample at negative bias voltage, the position of the low energy cutoff of the emitted photoelectrons can be measured. The inset shows a zoom of the spectrum around the Fermi edge. As shown, the low energy cutoff and of the Fermi edge allow to determine the spectrum width W .

4.6. Work Function Change and Charge Transfer

UPS can also be profitably used to measure the work function of a sample. For this purpose UPS spectra have been measured by applying a negative voltage (-10.0 V) to the sample in order to measure the whole width of the UPS spectrum, including the low-energy cutoff of the emitted photoelectrons (fig. 4.16). The work function can then be determined according to the following relation

$$h\nu = W + \Phi \quad (4.1)$$

where ν , W , Φ are the frequency of the incident UV light, the spectrum width and the sample work function, respectively.

It is well known that adsorbates can modify the work function of their supporting surface. Such effects have been thoroughly investigated and particular attention has been devoted to organic adsorbates. Detailed reviews of this field have been published by Ishii *et al.*[25] and Knupfer *et al.*[149]. Our experiments, confirming the tendency reported for other porphyrins and many other organic compounds, show that CuOEP adsorption lowers the sample work function. Fig. 4.17 shows a sequence of UPS spectra acquired at increasing CuOEP coverage. For different coverages, diverse spectrum widths W are found, hence the work function depends on the coverage.

The graph of fig. 4.18 shows the work function shifts, extracted from the UPS measurements for the three different substrates, as a function of the CuOEP *nominal coverage*. A complete set of the measured data is given in tables B.1, B.2 and B.3 in Appendix B. The data show that the work function decreases with the coverage until, at a CuOEP coverage of 4-6 Å (around 2 ML), a saturation point is reached.

4. CuOEP on Metals

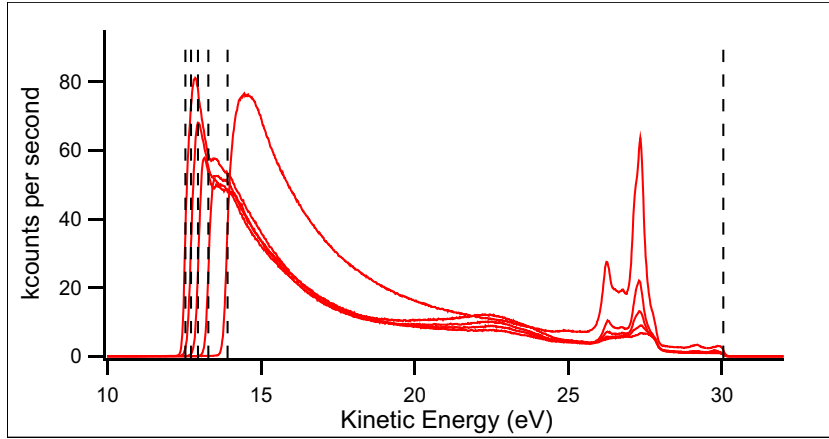


Figure 4.17.: UPS spectra for CuOEP on Cu(111) at various coverages. Due to the instrumental set-up, the acquired spectra are shifted in order to keep their Fermi edges aligned. Hence, a variations in the spectrum width is reflected in a shift of the low energy cutoff peak.

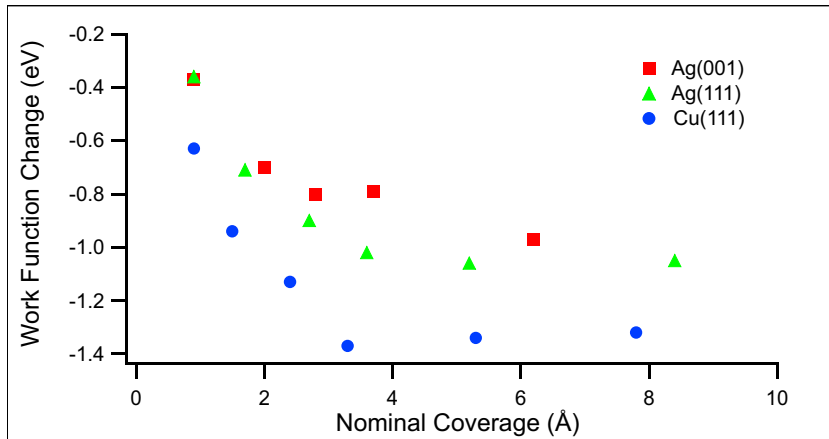


Figure 4.18.: Work function change as a function of the *nominal coverage*. The graph groups the data measured for Cu(111), Ag(111) and Ag(001). The complete series of the measured values of the work function change as a function of the coverage for all three investigated substrates are given in table B.1, B.2 and B.3.

In literature three main mechanisms have been identified to be responsible for the adsorbate-induced work function shift[150][143][151]. Consequently it has been suggested that the work function change $\Delta\Phi$ can approximatively be written as the sum of three terms:

$$\Delta\Phi = \Delta\Phi_{met} + \Delta\Phi_{dip} + \Delta\Phi_{charge} \quad (4.2)$$

A first mechanism ($\Delta\Phi_{met}$) is common to all closed shell adsorbates and it is the so called *pillow effect*. It is well known that at the metal-vacuum interface the electron density tends to spread from the metal into the vacuum[152]. This leads to the formation of a surface

4.7. Level Alignment: Substrate Dependence

dipole (oriented towards the metal), which increases the energy barrier to be overcome in order to extract an electron from the metal, hence increasing the work function. Closed shell adsorbates tend to *push* electrons back in the metal therefore reducing the surface dipole. Hence $\Delta\Phi_{met}$ is always negative.

A second mechanism ($\Delta\Phi_{dip}$) regards polar adsorbates. If the polar adsorbates order on the surface in an uniform way, aligning their dipole moments in the same direction, an additional surface dipole layer is formed. Hence it holds $\Delta\Phi_{dip} > 0$ if the dipole moments point towards the metal and $\Delta\Phi_{dip} < 0$ if they point towards the vacuum. As found from the DFT calculation (see sec. 4.4), the CuOEP molecule gains a dipole moment of 0.5 debye if all the ethyl legs point out of the molecular plane. The effect of such a dipole moment on $\Delta\Phi_{dip}$ can be calculated for the case of 1 ML coverage by means of the Helmholtz relationship

$$\Delta\Phi_{dip} = \frac{e}{\epsilon_0 A} p_{mol} \quad (4.3)$$

where A is the area per molecule, and p_{mol} the dipole moment of an individual molecule. Using the molecular densities found in sec. 4.2, for all three substrates investigated, a value for $|\Delta\Phi_{dip}|$ of about 0.1 eV is obtained. The fact that the observed work function changes are around one order of magnitude bigger than the maximum $|\Delta\Phi_{dip}|$ allowed for CuOEP, indicates that this mechanism is not relevant for the system investigated here.

Finally, work function changes can be induced by charge transfer ($\Delta\Phi_{charge}$). An adsorbate may accept/donate an electron from/to the substrate, which again would lead to the formation of a surface dipole and therefore to an alteration of the work function. Evidently it holds $\Delta\Phi_{charge} > 0$ for acceptor adsorbates and $\Delta\Phi_{charge} < 0$ for donors. Most organic molecules and especially porphyrins have been shown to have a donor character, i.e. to induce a work function decrease[25][149].

From this discussion it can be deduced that mainly $\Delta\Phi_{met}$ and $\Delta\Phi_{charge}$ play a significant role for the CuOEP/metal system. The dependence on the coverage does not help to discriminate between the two. Both mechanisms are expected to lower the work function and in all cases the induced change should increase monotonically with the coverage up to 1 ML, while a saturation is expected at higher coverage. Detailed analysis and discussions[150][143] suggest that, for a molecule like CuOEP, $\Delta\Phi_{met}$ should reach a value around -0.4 eV for a full monolayer. Hence, the *pillow effect* alone is not strong enough to explain the measured values of $\Delta\Phi$. This proves that, for CuOEP on Cu(111), Ag(111) and Ag(001), $\Delta\Phi_{charge} < 0$ and a significant charge transfer from the molecule to the substrate takes place.

4.7. Level Alignment: Substrate Dependence

In the previous sections the UPS data acquired for different CuOEP coverages have been discussed. Here the attention is focussed on the positioning of the molecular levels as a function of the different substrates. In order to simplify this discussion, only the values measured at high coverage are considered. More precisely the data discussed in the following have been obtained at a molecular coverage of 34 Å, 45 Å and 31 Å for Cu(111), Ag(111) and Ag(001), respectively. As explained in detail in Appendix B, for comparably thick molecular

4. CuOEP on Metals

layers the quantitative determination of the coverage is only approximative. However, for all the three metal substrates investigated, the number of layers can reliably be estimated to be within the range 5-15 ML. This is a broad range, but, as shown in fig. 4.18, the shift of molecular levels is characterized by a saturation which occurs after the multilayer regime is surpassed. Therefore, although the real coverages are known only approximatively, the comparison of the measurements performed on different substrates is still appropriate.

By the same technique described in sec. 4.6 the position of all peaks in the spectra (e.g. HOMO and HOMO-1) referred to the vacuum level (instead of the Fermi level) can be obtained. This technique is especially interesting in the case of the HOMO because it allows to measure the ionization potential (IP) of CuOEP within the molecular layer. The values obtained for the different substrates are reported in table 4.2.

	$\Delta\Phi$ (eV)	E_{HOMO} (eV)	E_{HOMO-1} (eV)	IP (eV)
Cu(111)	-1.28 ± 0.05	-1.8 ± 0.2	-3.0 ± 0.2	5.6 ± 0.2
Ag(111)	-1.08 ± 0.05	-2.2 ± 0.2	-3.4 ± 0.2	5.7 ± 0.2
Ag(001)	-0.86 ± 0.05	-2.3 ± 0.2	-3.4 ± 0.2	6.0 ± 0.2
gas phase	-	-	-	6.5 ref. [153]

Table 4.2.: CuOEP on metal: summary of the orbital energy levels as determined by UPS. The data reported have been measured at the highest molecular coverage reached: 34 Å, 45 Å and 31 Å for Cu(111), Ag(111) and Ag(001), respectively

Considering the experimental uncertainty, the IP values measured for the different substrates are very similar. This is in agreement with the conclusion drawn in sec. 4.15, where it was found that the HOMO and HOMO-1 levels are shifted but no significant modification of their structure takes place upon adsorption. This agreement further suggests that no chemical bonding between CuOEP and the metal substrate occurs. The bonding is therefore of ionic type. The charge transfer shifts the molecular levels without significantly affecting their structure.

The IP measured on the three metal surfaces differs from the one measured by Kitagawa *et. al.* for CuOEP in gas phase (6.5 eV)[153]. On the surface the IP is 0.5 to 0.9 eV lower than the one measured in gas phase. However, differences of this order have often been found for similar organic/metal systems[154].

While the IP values of adsorbed CuOEP molecules show only a small dependence on the metal substrate, a strong dependence is observed for the work function change. An analysis of this dependence is interesting as it allows to gain further insight into the processes occurring at the organic-metal interface.

The molecules adsorbed on the metal and the substrate tend to align their chemical potentials. For the metal it holds

$$\mu_{met} = -\Phi_{met} \quad (4.4)$$

If the molecule-adsorbate interaction is not too strong, it can be assumed that the chemical

4.7. Level Alignment: Substrate Dependence

potential lies at the so called *mid-gap* point. Therefore

$$\mu_{mol} = -\frac{IP + EA}{2} \quad (4.5)$$

where EA is the CuOEP electron affinity. The alignment of the chemical potentials is responsible for the charge transfer described in sec. 4.6 (Δ_{charge} term of eq. 4.2). Hence, the work function of the metal substrate (Φ_{met}) affects Δ_{charge} and ultimately the total work function change $\Delta\Phi$.

Using the calculated gas phase values of IP (7.22 eV) and EA (0.60 eV), the resulting chemical potential for CuOEP is $\mu_{mol} = -3.91$ eV. Therefore, given the respective work functions ($\Phi_{Cu(111)} = 4.94$ eV, $\Phi_{Ag(111)} = 4.74$ eV, $\Phi_{Ag(001)} = 4.64$ eV), for all metal substrates investigated it holds $\mu_{mol} > \mu_{met}$. Hence, to achieve the alignment of the chemical potentials, electrons have to be transferred from the adsorbate molecules to the substrate. This prediction is in agreement with the observed lowering of the sample work function induced by CuOEP adsorption.

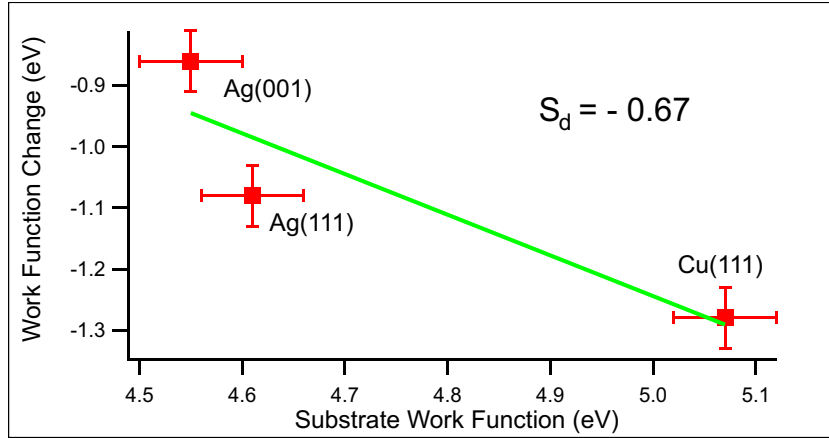


Figure 4.19.: Work function change (measured upon the deposition of a CuOEP multilayer) plotted versus the measured work function of the clean metal substrate. Assuming a linear dependence, a least square fit yields $S_d = -0.67$.

According to this simple picture, the charge transfer needed to align the chemical potentials depends on the metal work function. In detail, if $\mu_{mol} > \mu_{met}$, the charge transfer should be bigger for substrates with high work functions. This prediction has already been verified in a number of publications (see for instance the reviews published by Ishii *et al.*[25] and Knupfer *et al.*[149]) and it is confirmed here for CuOEP. In fig. 4.19 the measured work function changes are plotted against the work function values measured for the clean metal substrates. Commonly a linear dependence of $\Delta\Phi$ on Φ_{met} is assumed[25]. Hence, defining $S_d = d\Delta\Phi/d\Phi_{met}$, a least square fit for the data measured on Cu(111), Ag(111) and Ag(001) gives $S_d = -0.67$. Of course a total of three data points is far from ideal for a proper fit. However, it is interesting to note that the resulting value of S_d is consistent with the results already published for other organic systems and especially for other porphyrins[25][149].

4. CuOEP on Metals

Finally, the difference between the $\Delta\Phi$ measured on Ag(111) and on Ag(001) is specially remarkable. The big majority of the published work dealing with the $\Delta\Phi$ dependence on Φ_{met} is based on measurements performed on polycrystalline substrates. Measuring on single crystals opens up the possibility to judge the role played by a specific surface orientation. The measurement of different $\Delta\Phi$ values on Ag(111) and on Ag(001) proves that the surface orientation does play a significant role in the work function shift induced upon CuOEP adsorption. Hence, it can be stated that the work function change does not only depend on the chemical nature of the substrate but also on the details of its surface electronic structure.

5. Conclusion and Outlook

Copper(II) octaethyl porphyrin (CuOEP) is a molecule with an extended π -electron system comprising 24 delocalized electrons. Together with the central metal ion, this π -system is responsible for the very interesting electrochemical and photophysical properties characteristic of porphyrin molecules. Among other porphyrins, CuOEP is a comparably simple system, which makes it an ideal candidate for detailed investigations with the ultimate aim to fully understand its properties and behavior on defined model surfaces.

In this thesis the adsorption of CuOEP has carefully been studied both on metal surfaces and on NaCl thin films. Special attention has been paid to compare the behavior of the molecules on the bare metal and on NaCl layers of different thickness.

An extensive investigation has been carried out by combining scanning tunnelling microscopy (STM), ultraviolet electron spectroscopy (UPS) and low energy electron diffraction (LEED). In order to achieve a more general understanding, all experiments have been repeated on three different metal substrates (Cu(111), Ag(111) and Ag(001)). Moreover, DFT calculations have been used to assist the analysis and the interpretation of the experimental data.

The most original result is the observation of molecular self assembly on an insulator material. In fact, in literature there are few examples of molecular self-assembly of small molecules on non-conductive substrates, while larger organic molecules either do not show any ordering or condense in comparably large crystallites. For CuOEP on NaCl films instead, the epitaxial assembly in an ordered structure takes place already at the monolayer regime.

This distinctive feature makes CuOEP/NaCl a very interesting model system for the investigation of the electronic properties of molecular adsorbates. It is well known that these properties can be strongly affected by the interaction with the substrate. Therefore, the low reactivity proper of insulator surfaces offers the unique chance to bring molecules onto a substrate which does not strongly influence the electronic structure of the molecular adsorbates.

The system investigated is of particular interest in the context of *molecular electronics*, as it demonstrates the feasibility of self assembly of complex organic molecules on a non conductive surface, hence with virtually no electronic coupling to the substrate. This achievement represents a fundamental step towards the development of any in-plane electronic device based on molecules supported on a solid substrate. Moreover, the simultaneous presence on the surface of free metal areas, salt structures of various thickness and molecules organized in ordered patterns is very interesting as it represents a first step towards the development of more complex heterogeneous structures comprising specific functionalities.

The observed surface heterogeneity allows the direct comparison of the CuOEP adsorption energy on the clean metal and on salt structures 1-3 ML thick. As expected, the adsorption

5. Conclusion and Outlook

energy is lowered by introducing an insulator monolayer and decreases stepwise by increasing the salt layer thickness. These observations point out another notable property of the investigated system, namely the possibility to tune the substrate-adsorbate interaction by controlling the thickness of the NaCl structures. This tunability is a real benefit as it represents an additional degree of freedom in tailoring the properties of molecular structures on surfaces.

To improve the understanding of CuOEP adsorption, series of experiments have also been performed on clean metal substrates. In particular, high resolution STM images performed at different bias voltages, in conjunction with DFT calculations, allow to gain insight in the adsorption conformation of CuOEP on Ag(001). UPS measurements demonstrate that, for all three metal substrates, a charge transfer occurs and CuOEP molecules donate electrons to the substrate. Together with the results of the DFT calculations, the UPS data show that the CuOEP-metal binding is mainly of ionic nature and no chemisorption occurs.

Finally, a dependence of the charge transfer on the work function of the metal substrate has been found. This is highly interesting, as the control of the level alignment at the metal-organic interface is of primary importance for a number of relevant applications such as organic light emitting diodes and thin film transistors. All in all, the experimental findings presented in this thesis clearly show that metal-insulator-molecule model systems can reliably be produced in a bottom up approach. The investigation of their properties, with a clear focus on how the molecular electronic structure is affected upon adsorption, yields some fundamental insight, which is highly relevant for any research aimed at the development of molecular electronics devices supported on solid substrates.

A. Triangular NaCl Structures

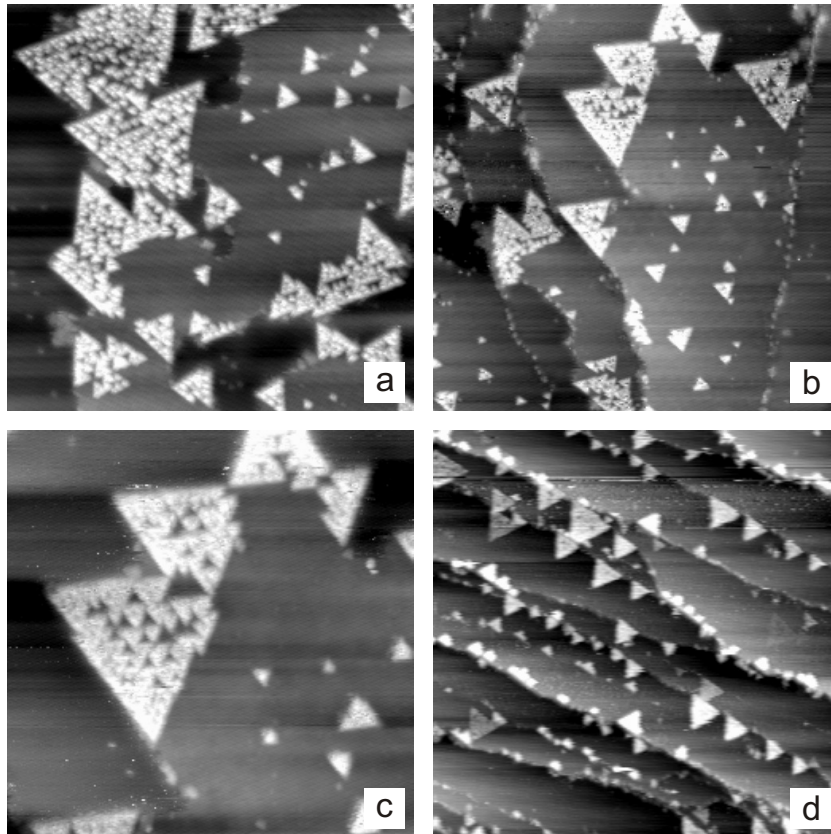


Figure A.1.: NaCl triangular islands on Ag(111) (a-c) and on Cu(111) (d). Images (a) (100×100 nm, $U = -1.6$ V, $I = 10$ pA) and (b) (100×100 nm, $U = -3.0$ V, $I = 25$ pA) show overviews of different areas. Especially in (a) a layer (looking like a *brighter carpet*) laying under and in between the island can be identified. Most likely it is formed by NaCl. The internal structure of each island, formed by many smaller triangles, is well visible in (c) (50×50 nm, $U = -3.0$ V, $I = 25$ pA) which is a zoom-in on the same area of (a). Image (d) (150×150 nm, $U = -3.0$ V, $I = 36$ pA) shows an example of the observations performed on Cu(111). In this case the tendency of the islands to be located aside the metal substrate step edges is very clear.

This appendix is dedicated to report about the observation of an unexpected phenomenon observed only very seldom on NaCl/metal samples. After the preparation of a sodium chloride film according to the standard recipe described in sec. 2.3, a few times the NaCl

A. Triangular NaCl Structures

structures imaged by STM looked different than usual. Instead of the characteristic rectangular shape, the salt structures showed a very distinct triangular shape. This observation was made on two Cu(111) and one single Ag(111) sample.

As shown in fig. A.1, the NaCl aggregates in triangular islands whose borders seem to be aligned along some specific directions. A closer look reveals that each island is formed by the aggregation of smaller NaCl triangular structures. Many of the islands (see for instance fig. A.1 (d)) are aligned along substrate step edges. Sometimes the triangular salt structures seem to grow on top of a normal salt layer, as for instance shown in image A.1 (a).

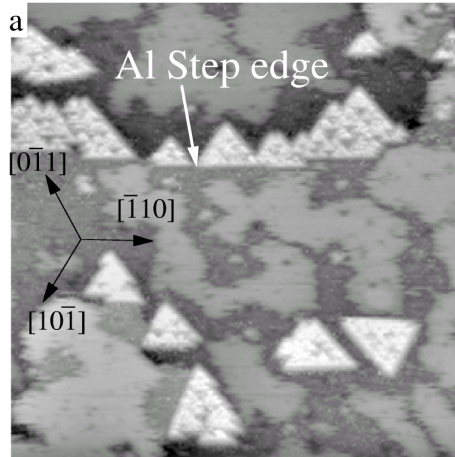


Figure A.2.: Image 2 (a) from ref. [74]. STM constant current topography (50×50 nm, $U = 1.2$ V, $I = 60$ pA) of Al(111) after adsorption of 0.35 ML Na and a dose of Cl_2 corresponding to 0.2 ML.

The triangular shape does not only contradict the usual results repeatedly obtained for NaCl on Cu(111), Ag(111) and Ag(001) (see sec. 2.4.2) but also a large number of observations reported in literature (see sec. 2.2 and the references therein). However, there is a single publication by Hebenstreit *et al.* reporting a very similar phenomenon, namely the growth of triangular NaCl islands on Al(111)[74]. Very remarkably, Hebenstreit *et al.* report that “some of the islands consist of smaller triangles with defects between them” and describe how “the islands are preferentially located at the lower side of substrate step edges”. Also the comparison of fig. A.2, extracted from that publication, with the measurements reported here (fig. A.1) reveals impressive similarities.

Hebenstreit *et al.* explain their observations with the formation of a polar (111) surface of the NaCl crystal. More precisely they suggest the formation of a 3-layer system (Na-Cl-Na) terminating like the NaCl(111) surface. This model relies on a non equilibrated stoichiometry between Na and Cl, namely an excess of Na on the Al(111) surface. To support this hypothesis Hebenstreit *et al.* explain that the triangular structures are obtained depositing Na on Al(111) and subsequently dosing Cl_2 on the surface. Moreover they report that controlling the dosing of Cl_2 and adding more Na has clear effects on the nucleation of triangular structures.

Considering this explanation our results seem somehow surprising. All samples have been

prepared by evaporating NaCl from bulk and, as discussed in sec. 2.2, this should ensure a ratio of 1 between the amount of Na^+ and Cl^- ions deposited on the surface. The formation of a NaCl(111) surface seems therefore quite unlikely. However, some chlorine desorption from the surface cannot completely be ruled out. For instance, as explained in sec. 2.6, it is known that X-ray irradiation of alkali halides may induce the desorption of anions, consequently leading to the formation of defects such as color centers[80][81]. For one of the samples, where triangular islands have been observed, the STM measurements were performed after electron irradiation (LEED) which is a potential source for chlorine desorption. On the other hand, other samples did not show any triangular feature after prolonged LEED measurement sessions. Moreover, for two of the samples showing triangular islands, no LEED measurement had been performed and no alternative reason for a chlorine desorption could be identified.

B. CuOEP on Metal: Collection of the UPS Data

During this thesis a series of UPS measurements for CuOEP on metals have been performed. In secs. 4.5, 4.6 and 4.7 only some of the most significant results are presented and discussed. In detail, the attention is focussed on those results which are more closely related with the STM data and the DFT calculations there presented. This appendix shows an extended collection of the UPS measurements performed for CuOEP on Ag(001), Ag(111) and Cu(111).

The full UPS spectra of CuOEP have been investigated as a function of the CuOEP coverage from the submonolayer to the multilayer regime. The deposition has been monitored with a quartz microbalance (see sec. 3.4). For coverages up to 1 ML the system could be very reliably calibrated by means of STM. On the other hand, for coverages exceeding 1 ML, getting STM images becomes problematic and the evaluation of the molecular film thickness by means of XPS is not straightforward either. In a first approximation it can be assumed that the sticking rates of CuOEP on a preexisting molecular layer and on a clean metal substrate are the same. All the film thicknesses reported in this work have been calculated in this approximation. However, combined XPS and LEED analysis show that, in the multilayer regime, this approximation is leading to overestimate the effective CuOEP coverage. In particular XPS suggests that this overestimation is larger for Ag(111) and Ag(001) than for Cu(111). Consistently, by means of LEED it is observed that on Ag(111) and Ag(001) CuOEP layers of nominal thickness bigger than 30 Å (1 ML \sim 2.2 Å) show the same crystalline structure as the first monolayer (see sec. 4.2). For Cu(111) instead, at similar nominal coverage, no surface periodic structure can be anymore identified by LEED. For all three substrates it has to be considered that the indicated thicknesses are not very accurate and can only be used in the frame of a qualitative discussion.

The UPS spectra measured for different coverages are shown in fig. B.1. For all the clean metal substrates the d bands are visible and for Cu(111) and Ag(111) the surface state is observed. While increasing the CuOEP coverage, the intensity of the metal d bands decreases and additional peaks begin to rise. The contribution of the metal to the spectra remains predominant until some Å of CuOEP are deposited. This implies that states originating from the CuOEP layer can univocally be identified only at coverages over 1 ML. For this reason an analysis of the evolution of the peaks for increasing coverages is very convenient as it allows to discriminate the spectral features related to the adsorbates and to the substrate.

Aside the already described HOMO and HOMO-1 states (see sec. 4.5), a very broad peak is approximatively placed at a binding energy between 6 eV and 10 eV with a maximum around 8 eV. The peak is clearly the result of the convolution of several states and it is therefore difficult to interpret. However, this broad peak is quite in good agreement with

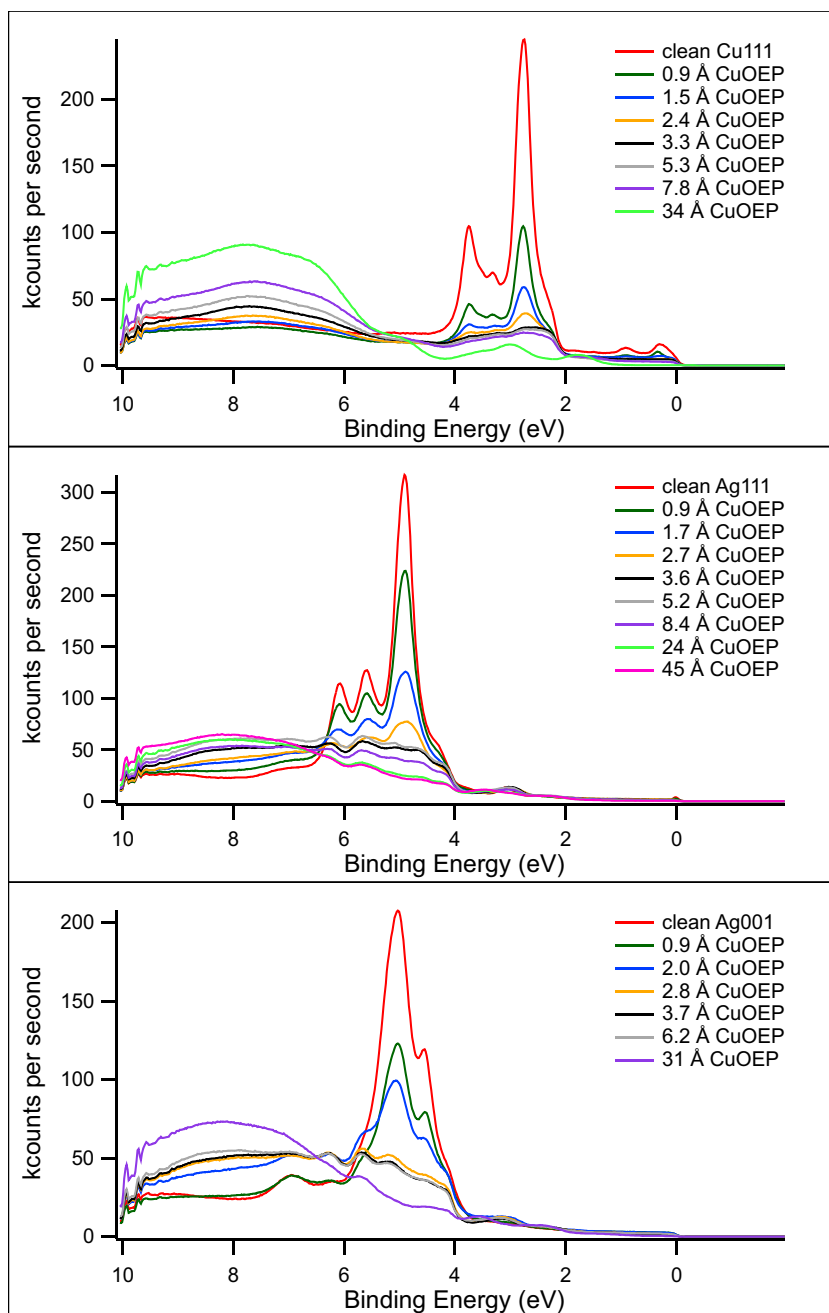


Figure B.1.: Complete set of UPS measurements for CuOEP on Cu(111), Ag(111) and Ag(001) as a function of the molecular coverage. (Due to the large number of spectra acquired a good legibility of the graphs can only be obtained in the color print version).

the calculations presented before. The calculated spectrum (fig. 4.14) predicts the presence of two big bunches of states with their maxima approximately 4.4 eV and 5.1 eV below the HOMO. These peaks, which are very broad and partially convoluted, produce a large

B. CuOEP on Metal: Collection of the UPS Data

increase in the DOS starting about 4 eV below the HOMO. Being $E_{HOMO} \simeq -2$ eV, the right shoulder of the resulting broad peak happens to be placed at a binding energy of about 6 eV, in good agreement with the experimental data. However, the calculated peak is not as broad as the measured one. This discrepancy can have different explanations but the most plausible is that, as already mentioned, the calculation has been performed for a free CuOEP molecule, neglecting any interaction with the substrate as well as with neighboring molecules.

coverage	sec. elec. peak (eV)	WF shift (eV)
clean Cu(111)	13.92	WF=5.07 (4.94)
0.9 Å CuOEP	13.29	-0.63
1.5 Å CuOEP	12.96	-0.94
2.4 Å CuOEP	12.73	-1.13
3.3 Å CuOEP	12.55	-1.37
5.3 Å CuOEP	12.58	-1.34
7.8 Å CuOEP	12.60	-1.32
34 Å CuOEP	12.64	-1.28

Table B.1.: Work function change for CuOEP on Cu(111). The table reports the position of the secondary electron peak and of the corresponding work function change as a function of the CuOEP coverage. For the case of clean Cu(111) the measured work function value and the one known from literature (in brackets) are reported. For the secondary electron peak positions and for the work function values an uncertainty of ± 0.05 eV is estimated.

In sec. 4.6 the work function changes observed upon CuOEP deposition on the metal surfaces have been discussed. In detail fig. 4.18 shows that the work function change depends on the CuOEP coverage. A more complete set of the measured data is given here. Tables B.1, B.2 and B.3 summarize all the values of the sample work function measured for different CuOEP coverages on Cu(111), Ag(111) and Ag(001), respectively.

coverage	sec. elec. peak (eV)	WF shift (eV)
clean Ag(111)	13.46	WF=4.61 (4.74)
0.9 Å CuOEP	13.10	-0.36
1.7 Å CuOEP	12.75	-0.71
2.7 Å CuOEP	12.56	-0.90
3.6 Å CuOEP	12.42	-1.02
5.2 Å CuOEP	12.38	-1.06
8.4 Å CuOEP	12.39	-1.05
24 Å CuOEP	12.38	-1.06
45 Å CuOEP	12.36	-1.08

Table B.2.: Work function change for CuOEP on Ag(111). The table reports the position of the secondary electron peak and of the corresponding work function change as a function of the CuOEP coverage. For the case of clean Ag(111) the measured work function value and the one known from literature (in brackets) are reported. For the secondary electron peak positions and for the work function values an uncertainty of ± 0.05 eV is estimated.

coverage	sec. elec. peak (eV)	WF shift (eV)
clean Ag(001)	13.40	WF=4.55 (4.64)
0.9 Å CuOEP	13.03	-0.37
2.0 Å CuOEP	12.70	-0.70
2.8 Å CuOEP	12.60	-0.80
3.7 Å CuOEP	12.61	-0.79
6.2 Å CuOEP	12.43	-0.97
31 Å CuOEP	12.54	-0.86

Table B.3.: Work function change for CuOEP on Ag(001). The table reports the position of the secondary electron peak and of the corresponding work function change as a function of the CuOEP coverage. For the case of clean Ag(001) the measured work function value and the one known from literature (in brackets) are reported. For the secondary electron peak positions and for the work function values an uncertainty of ± 0.05 eV is estimated.

Bibliography

- [1] M. Schulz, *The end of the road for silicon?*, Nature **399**, 729 (1999).
- [2] G. Binnig and H. Rohrer, *Scanning tunneling microscopy*, Helvetica Physica Acta **55**, 762 (1982).
- [3] G. Binnig, H. Rohrer, Ch. Gerber, and E. Weibel, *Surface studies by scanning tunneling microscopy*, Physical Review Letters **49**, 57 (1982).
- [4] A. M. Baró, G. Binnig, H. Rohrer, Ch. Gerber, E. Stoll, A. Baratoff, and F. Salvan, *Real-Space Observation of the 2×1 Structure of Chemisorbed Oxygen on Ni(110) by Scanning Tunneling Microscopy*, Physical Review Letters **52**, 1304 (1984).
- [5] G. Binnig, H. Rohrer, Ch. Gerber, and E. Weibel, *(111) facets as the origin of reconstructed Au(110) surfaces*, Surface Science **131**, L379 (1983).
- [6] G. Binnig, H. Rohrer, Ch. Gerber, and E. Weibel, *7×7 Reconstruction on Si(111) Resolved in Real Space*, Physical Review Letters **50**, 120 (1983).
- [7] G. Binnig, C. F. Quate, C. Gerber, and E. Weibel, *Atomic Force Microscope*, Physical Review Letters **56**, 930 (1986).
- [8] Y. Martin and H. K. Wickramasinghe, *Magnetic imaging by “force microscopy” with 1000 Å resolution*, Applied Physics Letters **50**, 1455 (1987).
- [9] Y. Martin, D. W. Abraham, and H. K. Wickramasinghe, *High-resolution capacitance measurement and potentiometry by force microscopy*, Applied Physics Letters **52**, 1103 (1988).
- [10] D. W. Pohl, W. Denk, and M. Lanz, *Optical stethoscopy: image recording with resolution $\lambda/20$* , Applied Physics Letters **44**, 651 (1984).
- [11] U. Dürig, D. W. Pohl, and F. Rohner, *Near-field optical-scanning microscopy*, Journal of Applied Physics **59**, 3318 (1986).
- [12] C. J. Chen, *Introduction to Scanning Tunneling Microscopy*, Oxford University Press (1993).
- [13] R. Wiesendanger and H.-J. Güntherodt, eds., *Introduction to Scanning Tunneling Microscopy*, Springer-Verlag (1996).

- [14] D. Drakova, *Theoretical modelling of scanning tunneling microscopy, scanning tunneling spectroscopy and atomic force microscopy*, Reports on Progress in Physics **64**, 205 (2001).
- [15] J. Bardeen, *Tunneling from a many-particle point of view*, Physical Review Letters **6**, 57 (1961).
- [16] J. Tersoff and D. R. Hamann, *Theory and Application for the Scanning Tunneling Microscope*, Physical Review Letters **50**, 1998 (1983).
- [17] J. Tersoff and D. R. Hamann, *Theory of the scanning tunneling microscope*, Physical Review B **31**, 805 (1985).
- [18] A. Zangwill, *Physics at surfaces*, Cambridge University Press (1988).
- [19] E. J. Scheibner, L. H. Germer, and C. D. Hartman, *Apparatus for Direct Observation of Low-Energy Electron Diffraction Patterns*, Review of Scientific Instruments **31**, 112 (1960).
- [20] C. Davisson and L. H. Germer, *Diffraction of Electrons by a Crystal of Nickel*, Physical Review **30**, 705 (1927).
- [21] M. A. Van Hove, W. H. Weinberg, and C.-M. Chan, *Low-Energy Electron Diffraction, Experiment, Theory and Surface Structure Determination*, Springer (1986).
- [22] K. Heinz, *Structural analysis of surfaces by LEED*, Progress in Surface Science **27**, 239 (1988).
- [23] H. Hertz, *Über einen Einfluss des ultravioletten Lichtes auf die elektrische Entladung*, Annalen der Physik und Chemie **31**, 983 (1887).
- [24] A. Einstein, *Über einen die Erzeugung und Verwandlung des Lichts betreffenden heuristischen Gesichtspunkt*, Annalen der Physik **17**, 132 (1905).
- [25] H. Ishii, K. Sugiyama E. Ito, and K. Seki, *Energy Level Alignment and Interfacial Electronic Structures at Organic/Metal and Organic/Organic Interfaces*, Advanced Materials **11**, 605 (1999).
- [26] S. Hüfner, *Photoelectron Spectroscopy*, Springer (1996).
- [27] R. G. Musket, W. Mc Lean, C. A. Colmenares, D. M. Makowiecki, and W. J. Siekhaus, *Preparation of atomically clean surfaces of selected elements: a review*, Application of Surface Science **10**, 143 (1982).
- [28] S. Berner, *Molecular diffusion and self-organization on metal surfaces : sub-phthalocyanine on Ag(111)*, Ph.D. thesis, Universität Basel (2002).

Bibliography

- [29] T. M. Schaub, *Untersuchung nichtperiodischer Oberflächen im Ultrahochvakuum mittels Rastertunnelmikroskopie*, Ph.D. thesis, Universität Basel (1994).
- [30] D. E. Bürgler, C. M. Schmidt, J. A. Wolf, T. M. Schaub, and H.-J. Güntherodt, *Ag films on Fe/GaAs(001): from clean surfaces to atomic Ga structures*, *Surface Science* **366**, 295 (1996).
- [31] C. M. Schmidt, *Magnetic Interlayer Exchange Coupling in Fe/Cr/Fe(001) Trilayers is Correlated to Nanometer Scale Lateral Interface Structure*, Ph.D. thesis, Universität Basel (1988).
- [32] F. Meisinger, *Rastersondenmikroskopie an magnetischen Systemen*, Ph.D. thesis, Universität Basel (2000).
- [33] O. W. Richardson, *On the Negative Radiation from Hot Platinum*, *Proceedings of the Cambridge Philosophical Society* **11**, 286 (1901).
- [34] U. Barjenbruch, S. Fölsch, and M. Henzler, *Surface states on epitaxial thin films of NaCl and KCl*, *Surface Science* **211-212**, 749 (1989).
- [35] J. Viernow, D. Y. Petrovykh, A. Kirakosian, J.-L. Lin, F. K. Men, M. Henzler, and F. J. Himpsel, *Chemical imaging of insulators by STM*, *Physical Review B* **59**, 10356 (1999).
- [36] J. Viernow, D. Y. Petrovykh, F. K. Men, A. Kirakosian, J.-L. Lin, and F. J. Himpsel, *Linear arrays of CaF₂ nanostructures on Si*, *Applied Physics Letters* **74**, 2125 (1999).
- [37] M. Klaua, D. Ullmann, J. Barthel, W. Wulfhekel, J. Kirschner, R. Urban, T. L. Monchisky, A. Enders, J. F. Cochran, and B. Heinrich, *Growth, structure, electronic, and magnetic properties of MgO/Fe(001) bilayers and Fe/MgO/Fe(001) trilayers*, *Physical Review B* **64**, 134411 (2001).
- [38] H. Oh, S. B. Lee, J. Seo, H. G. Min, and J.-S. Kim, *Chemical structure of the interface between MgO films and Fe(001)*, *Applied Physics Letters* **82**, 361 (2003).
- [39] M.-C. Wu, J. S. Corneille, C. A. Estrada, J.-W. He, and D. W. Goodman, *Synthesis and characterization of ultra-thin MgO films on Mo(100)*, *Chemical Physics Letters* **182**, 472 (1991).
- [40] M. C. Gallagher, M. S. Fyfield, J. P. Cowin, and S. A. Joyce, *Imaging insulating oxides: scanning tunneling microscopy of ultrathin MgO films on Mo(001)*, *Surface Science* **339**, L909 (1995).
- [41] S. C. Street, C. Xu, and D. W. Goodman, *The physical and chemical properties of ultrathin oxide films*, *Annual Review of Physical Chemistry* **48**, 43 (1997).
- [42] S. Altieri, L. H. Tjeng, and G. A. Sawatzky, *Electronic structure and chemical reactivity of oxide-metal interfaces: MgO(100)/Ag(100)*, *Physical Review B* **61**, 16948 (2000).

- [43] C. Li, R. Wu, A. J. Freeman, and C. L. Fu, *Energetics, bonding mechanism, and electronic structure of metal-ceramic interfaces: Ag/MgO(001)*, Physical Review B **48**, 8317 (1993).
- [44] S. Schintke, S. Messerli, M. Pivetta, F. Patthey, L. Libiouille, M. Stengel, A. De Vita, and W.-D. Schneider, *Insulator at the ultrathin limit: MgO on Ag(001)*, Physical Review Letters **87**, 276801 (2001).
- [45] S. Schintke and W.-D. Schneider, *Insulators at the ultrathin limit: electronic structure studied by scanning tunneling microscopy and scanning tunneling spectroscopy*, Journal of Physics: Condensed Matter **16**, R49–R81 (2004).
- [46] A. Wiltner, A. Rosenhahn, J. Schneider, C. Becker, P. Pervan, M. Milun, M. Kralj, and K. Wandelt, *Growth of copper and vanadium on a thin Al₂O₃ film on Ni₃Al(111)*, Thin Solid Films **400**, 71 (2001).
- [47] T. Maroutian, S. Degen, C. Becker, K. Wandelt, and R. Berndt, *Superstructures and coincidences of a thin oxide film on a metallic substrate: a STM study*, Physical Review B **68**, 155414 (2003).
- [48] R. Franchy, J. Masuch, and P. Gassmann, *The oxidation of the NiAl(111) surface*, Applied Surface Science **93**, 317 (1996).
- [49] X. H. Qiu, G. V. Nazin, and W. Ho, *Vibrationally resolved fluorescence excited with submolecular precision*, Science **299**, 542 (2003).
- [50] M. Bäumer and H.-J. Freund, *Metal deposits on well-ordered oxide films*, Progress in Surface Science **61**, 127 (1999).
- [51] C. Dietrich, H.-G. Boyen, and B. Koslowski, *Characterization of ultrathin insulating Al₂O₃ films grown on Nb(110)/sapphire(0001) by tunneling spectroscopy and microscopy*, Journal of Applied Physics **94**, 1478 (2003).
- [52] R. M. Jaeger, J. Libuda, M. Bäumer, K. Homann, H. Kuhlenbeck, and H.-J. Freund, *Vibrational structure of excited states of molecules on oxide surfaces*, Journal of Electron Spectroscopy and Related Phenomena **64-65**, 217 (1993).
- [53] M. Gautier, J. P. Duraud, L. Pham Van, and M. J. Guittet, *Modifications of α -Al₂O₃(0001) surfaces induced by thermal treatments or ion bombardment*, Surface Science **250**, 71 (1991).
- [54] T. Bertrams and H. Neddermeyer, *Growth of NiO(100) layers on Ag(100): characterization by scanning tunneling microscopy*, Journal of Vacuum Science & Technology B **14**, 1141 (1996).
- [55] I. Sebastian, T. Bertrams, K. Meinel, and H. Neddermeyer, *Scanning Tunneling Microscopy on the Growth and Structure of NiO(100) and CoO(100) Thin Films*, Faraday Discussions **114**, 129 (1999).

Bibliography

- [56] M. R. Castell, P. L. Wincott, N. G. Condon, C. Muggelberg, G. Thornton, S. L. Dudarev, A. P. Sutton, and G. A. D. Briggs, *Atomic-resolution STM of a system with strongly correlated electrons: NiO(001) surface structure and defect sites*, Physical Review B **55**, 7859 (1997).
- [57] M. Bäumer, D. Cappus, H. Kuhlenbeck, H.-J. Freund, G. Wilhelmi, A. Brodde, and H. Neddermeyer, *The structure of thin NiO(100) films grown on Ni(100) as determined by low-energy-electron diffraction and scanning tunneling microscopy*, Surface Science **253**, 116 (1991).
- [58] C. Hagendorf, R. Shantyr, K. Meinel, K.-M. Schindler, and H. Neddermeyer, *Scanning tunneling microscopy and spectroscopy investigation of the atomic and electronic structure of CoO islands on Ag(001)*, Surface Science **532-535**, 346 (2003).
- [59] M. Hassel, H. Kuhlenbeck, H.-J. Freund, S. Shi, A. Freitag, V. Staemmler, S. Lutkehoff, and M. Neumann, *Electronic surface states of CoO(100) an electron energy loss study*, Chemical Physics Letters **240**, 205 (1995).
- [60] A. Gorschlüter and H. Merz, *Localized d-d excitations in NiO(100) and CoO(100)*, Physical Review B **49**, 17293 (1994).
- [61] F. M. Pan, L. K. Verheij, R. David, and R. Franchy, *Temperature dependence of the growth of gallium oxide on CoGa(100)*, Thin Solid Films **400**, 22 (2001).
- [62] U. Berner and K. Schierbaum, *Cerium oxide layers on Pt(111): a scanning tunneling microscopy study*, Thin Solid Films **400**, 46 (2001).
- [63] S. Fölsch, U. Barjenbruch, and M. Henzler, *Atomically thin epitaxial films of NaCl on germanium*, Thin Solid Films **172**, 123 (1989).
- [64] C. Schwennicke, J. Schimmelpfennig, and H. Pfnür, *Morphology of NaCl thin films grown epitaxially on Ge(100)*, Surface Science **293**, 57 (1993).
- [65] K. Glöckler, M. Sokolowski, A. Soukopp, and E. Umbach, *Initial growth of insulating overlayers of NaCl on Ge(100) observed by scanning tunneling microscopy with atomic resolution*, Physical Review B **54**, 7705 (1996).
- [66] R. Bennewitz, V. Barwich, M. Bammerlin, C. Loppacher, M. Guggisberg, A. Baratoff, E. Meyer, and H.-J. Güntherodt, *Ultrathin films of NaCl on Cu(111): a LEED and dynamic force microscopy study*, Surface Science **438**, 289 (1999).
- [67] J. Repp, *Rastertunnelmikroskopie und -spektroskopie an Adsorbaten auf Metall- und Isolatoroberflächen*, Ph.D. thesis, Freie Universität Berlin (2002).
- [68] H. Hebenstreit, J. Redinger, Z. Horozova, M. Schmidt, R. Poudloucky, and P. Varga, *Atomic resolution by STM on ultra-thin films of alkali halides: experiment and local density calculations*, Surface Science **424**, L321 (1999).

- [69] J. G. Roberts, S. Hoffer, M. A. Van Hove, and G. A. Somorjai, *Tensor low-energy electron diffraction analysis of the surface structure of NaCl(100) thin films grown on Pd(100) and Pt(111)*, Surface Science **437**, 75 (1999).
- [70] Ch. Loppacher, M. Bammerlin, M. Guggisberg, F. Battiston, R. Bennewitz, S. Rast, A. Baratoff, E. Meyer, and H.-J. Güntherodt, *Phase variation experiments in non-contact dynamic force microscopy using phase locked loop techniques*, Applied Surface Science **140**, 287 (1999).
- [71] G. M. Rothberg, M. Eisenstadt, and P. Kusch, *Free evaporation of alkali halide crystals*, Journal of Chemical Physics **30**, 517 (1959).
- [72] N. W. Ashcroft and N. D. Mermin, *Solid state physics*, Saunders College Publishing (1976).
- [73] C. Tegenkamp, H. Pfnür, W. Ernst, U. Malaske, J. Wollschläger, D. Peterka, K. M. Schröder, V. Zielasek, and M. Henzler, *Defects in epitaxial insulating thin films*, Journal Physics: Condensed Matter **11**, 9943 (1999).
- [74] H. Hebenstreit, M. Schmidt, J. Redinger, R. Poudloucky, and P. Varga, *Bulk terminated NaCl(111) on aluminum: a polar surface of an ionic crystal?*, Physical Review Letters **85**, 5376 (2000).
- [75] S. Fölsch, A. Helms, S. Zöphel, J. Repp, G. Meyer, and K. H. Rieder, *Self-Organized patterning of an insulator-on-metal system by surface faceting and selective growth: NaCl/Cu(211)*, Physical Review Letters **84**, 123 (2000).
- [76] R. Bennewitz, A. S. Foster, L. N. Kantorovich, M. Bammerlin, Ch. Loppacher, S. Schär, M. Guggisberg, E. Meyer, and A. L. Shluger, *Atomically resolved edges and kinks of NaCl islands on Cu(111): experiment and theory*, Physical Review B **62**, 2074 (2000).
- [77] R. M. Feenstra, J. A. Stroscio, J. Tersoff, and A. P. Fein, *Atom-selective imaging of the GaAs(110) surface*, Physical Review Letters **58**, 1192 (1987).
- [78] A. F. Wells, *Structural inorganic chemistry*, Oxford University Press (1984).
- [79] D. Briggs and M.P. Seah, eds., *Practical Surface Analysis*, Wiley (1983).
- [80] F. Seitz, *Color centers in alkali halide crystals*, Review of Modern Physics **18**, 384 (1946).
- [81] B. R. Sever, N. Kristianpoller, and F. C. Brown, *F-center production in alkali halide crystals by monocromatic x-ray and ultraviolet radiation*, Physical Review B **34**, 1257 (1986).
- [82] J. F. Moulder, W. F. Stickle, P. E. Sobol, and K. D. Bomben, *Handbook of X Ray Photoelectron Spectroscopy*, Perkin-Elmer Corporation (1992).

Bibliography

- [83] J. H. Burroughes, D. D. C. Bradley, A. R. Brown, R. N. Marks, K. MacKay, R. H. Friend, P. L. Burn, and A. B. Holmes, *Light Emitting Diodes based on Conjugated Polymers*, *Nature* **347**, 359 (1990).
- [84] S. R. Forrest, *Ultrathin Organic Films Grown by Organic Molecular Beam Deposition and Related Techniques*, *Chemical Reviews* **97**, 1793 (1997).
- [85] W. Brütting, S. Berleb, and A. Mückl, *Device physics of organic light-emitting diodes based on molecular materials*, *Organic Electronics* **2**, 1 (2001).
- [86] H. E. Katz, *Organic Molecular Solids as Thin Film Transistor Semiconductors*, *Journal of Materials Chemistry* **7**, 369 (1997).
- [87] G. Horowitz, *Organic Field-Effect Transistors*, *Advanced Materials* **10**, 365 (1998).
- [88] G. Ertl, H. Knözinger, and J. Weitkamp, eds., *Handbook of Heterogeneous Catalysis*, vol. 1-5, Wiley-VCH (1997).
- [89] A. Aviram and M. A. Ratner, *Molecular Rectifiers*, *Chemical Physics Letters* **29**, 277 (1974).
- [90] R. Lloyd Carroll and C. B. Gorman, *The Genesis of Molecular Electronics*, *Ange wandte Chemie International Edition* **41**, 4378 (2002).
- [91] C. Joachim, J. K. Gimzewski, and A. Aviram, *Electronics using Hybrid-Molecular and Mono-molecular Devices*, *Nature* **408**, 541 (2008).
- [92] S. De Feyter and F. C. De Schryver, *Two-dimensional supramolecular self-assembly probed by scanning tunneling microscopy*, *Chemical Society Review* **32**, 139 (2003).
- [93] D. E. Hooks, T. Fritz, and M. D. Ward, *Epitaxy and molecular organization on solid substrates*, *Advanced Materials* **13**, 231 (2001).
- [94] F. Rosei, M. Schunack, Y. Naitoh, P. Jiang, A. Gourdon, E. Lægsgaard, I. Stensgaard, C. Joachim, and F. Besenbacher, *Properties of large organic molecules on metal surfaces*, *Progres Surface Science* **71**, 95 (2003).
- [95] J. Repp, G. Meyer, F. E. Olsson, and M. Petersson, *Controlling the Charge State of Individual Gold Adatoms*, *Science* **305**, 493 (2004).
- [96] X. H. Qiu, G. V. Nazin, and W. Ho, *Vibronic States in Single Molecule Electron Transport*, *Physical Review Letters* **92**, 206102 (2004).
- [97] J. Repp, G. Meyer, S. M. Stojković, A. Gourdon, and C. Joachim, *Molecules on insulating films: scanning-tunneling microscopy imaging of individual molecular orbitals*, *Physical Review Letters* **94**, 026803 (2005).

- [98] J. Schimmelpfennig, S. Fölsch, and M. Henzler, *LEED studies of the adsorption of CO₂ on thin epitaxial NaCl films*, Surface Science **250**, 198 (1991).
- [99] J. Vogt and H. Weiss, *The monolayer structure of CO₂ adsorbed on the NaCl(100) single crystal surface: A tensor low-energy electron diffraction analysis*, Journal of Chemical Physics **119**, 1105 (2003).
- [100] J. A. Edling, H. H. Richardson, and G. E. Ewing, *Infrared spectroscopy of CH₄, CH₂D₂ and CD₄ adsorbed on sodium chloride films*, Journal of Molecular Structure **157**, 167 (1987).
- [101] L. M. Quattrocci and G. E. Ewing, *Infrared spectroscopy of monolayer CH₄ on NaCl(001)*, Journal of Chemical Physics **96**, 4205 (1992).
- [102] J. Heidberg, O. Schönekas, H. Weiss, G. Lange, and J. P. Toennies, *A PIR, HAS and LEED study of the monolayer CH₄-NaCl(001)*, Berichte der Bunsengesellschaft für Physikalische Chemie **99**, 1370 (1995).
- [103] S. Hayashi, H. Ikuno, H. Yanagi, and M. Ashida, *Epitaxial growth and molecular orientation of tetra(4-pyridyl)porphyrin thin film vacuum-evaporated on KCl*, Journal of Crystal Growth **123**, 35 (1992).
- [104] H. Yanagi, K. Takemoto, S. Hayashi, and M. Ashida, *Crystal growth of tetraphenylporphyrin thin films*, Journal of Crystal Growth **99**, 1038 (1990).
- [105] H. Yanagi and T. Shibutani, *Orientation-dependent phosphorescence from nanocrystals of platinum tetraphenylporphyrin grown on alkali halides*, Thin Solid Film **438-439**, 33 (2003).
- [106] J. R. Fryer and C. Ewins, *Epitaxial growth of thin films of perylene*, Philosophical Magazine A **66**, 889 (1992).
- [107] R. Lüthi, E. Meyer, H. Haefke, L. Howald, W. Gutmannsbauer, and H.-J. Güntherodt, *Sled-type motion on the nanometer scale: determination of dissipation and cohesive energies of C₆₀*, Science **266**, 1979 (1994).
- [108] F. Balzer and H.-G. Rubahn, *Chain-length dependent para-phenylene film- and needle-growth on dielectrics*, Surface Science **548**, 170 (2004).
- [109] M. Möbus, N. Karl, and T. Kobayashi, *Structure of perylene-tetracarboxylic-dianhydride thin films on alkali halide crystal substrates*, Journal of Crystal Growth **116**, 495 (1992).
- [110] L. Nony, R. Bennowitz, O. Pfeiffer, E. Gnecco, A. Baratoff, E. Meyer, T. Eguchi, A. Gourdon, and C. Joachim, *Cu-TBPP and PTCDA molecules on insulating surfaces studied by ultra-high-vacuum non-contact AFM*, Nanotechnology **15**, S91 (2004).

Bibliography

- [111] H. Rauscher, T. A. Jung, J.-L. Lin, A. Kirakosian, F. J. Himpsel, U. Rohr, and K. Mullen, *One-dimensional confinement of organic molecules via selective adsorption on CaF_1 versus CaF_2* , Chemical Physics Letters **303**, 363 (1999).
- [112] C. Tegenkamp and H. Pfnür, *Correlation of electronic and local structure of 4-hydroxythiophenol on $\text{NaCl}(100)$ and $\text{Ag}(100)$* , Journal of Chemical Physics **118**, 7578 (2003).
- [113] L. Nony, E. Gnecco, A. Baratoff, A. Alkauskas, R. Bennewitz, O. Pfeiffer, S. Maier, A. Wetzol, E. Meyer, and Ch. Gerber, *Observation of Individual Molecules Trapped on a Nanostructured Insulator*, Nanoletters **4**, 2185 (2004).
- [114] H. W. Kroto, J. R. Heath, S. C. O'Brien, R. F. Curl, and R. E. Smalley, *C_{60} : Buckminsterfullerene*, Nature **318**, 162 (1985).
- [115] W. Kratschmer, L. Lamb, K. Fostiropoulos, and D. Huffman, *Solid C_{60} : A New Form of Carbon*, Nature **347**, 354 (1990).
- [116] S. Modesti, S. Cerasari, and P. Rudolf, *Determination of charge states of C_{60} adsorbed on metal surfaces*, Physical Review Letters **71**, 2469 (1993).
- [117] J. K. Gimzewski, S. Modesti, and R. R. Schlittler, *Cooperative self-assembly of Au atoms and C_{60} on $\text{Au}(110)$ surfaces*, Physical Review Letters **72**, 1036 (1994).
- [118] K. Motai, T Hashizume, H. Shinohara, Y. Saito, H.W. Pickering, Y. Nishina, and T. Sakurai, *C_{60} grown on the $\text{Cu}(111)1 \times 1$ surface*, Japanese Journal of Applied Physics **32**, L450 (1993).
- [119] E. I. Altman and R. J. Colton, *Determination of the orientation of C_{60} adsorbed on $\text{Au}(111)$ and $\text{Ag}(111)$* , Physical Review B **48**, 18244 (1993).
- [120] S. Berner, M. Brunner, L. Ramoino, H. Suzuki, H.-J. Güntherodt, and T. A. Jung, *Time evolution analysis of a 2D solid-gas equilibrium: a model system for molecular adsorption and diffusion*, Chemical Physics Letters **348**, 175 (2001).
- [121] S. Berner, M. de Wild, L. Ramoino, S. Ivan, A. Baratoff, H.-J. Güntherodt, H. Suzuki, D. Schlettwein, and T. A. Jung, *Adsorption and two-dimensional phases of a large polar molecule: Sub-phthalocyanine on $\text{Ag}(111)$* , Physical Review B **68**, 115410 (2003).
- [122] T. A. Jung, R. R. Schlittler, and J. K. Gimzewski, *Conformational identification of individual adsorbed molecules with the STM*, Nature **386**, 696 (1997).
- [123] T. A. Jung, R. R. Schlittler, J. K. Gimzewski, H. Tang, and C. Joachim, *Controlled room temperature positioning of individual molecules: molecular flexure and motion*, Science **271**, 181 (1996).

- [124] L. Scudiero, D. E. Barlow, and K. W. Hipps, *Scanning tunneling microscopy, orbital-mediated tunneling spectroscopy, and ultraviolet photoelectron spectroscopy of Nickel(II) Octaethylporphyrin deposited from vapor*, Journal of Physical Chemistry B **106**, 996 (2002).
- [125] R. Pak and W. R. Scheidt, *Structure of (2,3,7,8,12,13,17,18-octaethylporphinato)copper(II)*, Acta Crystallographica **C47**, 431 (1991).
- [126] M. Böhringer, W.-D. Schneider, and R. Berndt, *Scanning tunneling microscope-induced molecular motion and its effect on the image formation*, Surface Science **408**, 72 (1998).
- [127] S. Yim, S. Heutz, and T. S. Jones, *Influence of intermolecular interactions on the structure of phthalocyanine layers in molecular thin film heterostructures*, Physical Review B **67**, 165308 (2003).
- [128] H. C. Hamaker, *The London-van der Waals Attraction between Spherical Particles*, Physica **4**, 1058 (1937).
- [129] J. Israelachvili, *Intermolecular and Surface Forces*, Academic Press (1985).
- [130] E. M. Lifshitz, *The Theory of Molecular Attractive Forces Between Solids*, Soviet Physics JETP **2**, 73 (1956).
- [131] I. E. Dzyaloshinskii, E. M. Lifshitz, and L. P. Pitaevskii, *The general theory of van der Waals forces*, Advances in Physics **10**, 165 (1959).
- [132] L. Bergström, *Hamaker constants of inorganic materials*, Advances in Colloids and Interface Science **70**, 125 (1997).
- [133] V. A. Parsegian and G. H. Weiss, *Spectroscopic Parameters for Computation of van der Waals Forces*, Journal of Colloid and Interface Science **81**, 285 (1981).
- [134] D.-H. Wei, D. C. Skelton, and S. D. Kevan, *Lateral interactions and corrugation in physisorption systems: CH₄/Cu(100)*, Journal of Chemical Physics **105**, 7808 (1996).
- [135] G. S. Elliott, D. H. Wei, K. J. Wu, and S. D. Kevan, *Substrate-mediated dispersion interaction effects in the properties of a physisorbed gas*, Journal of Chemical Physics **99**, 4152 (1993).
- [136] G. Vidali, G. Ihm, H.-Y. Kim, and M. W. Cole, *Potentials of physical adsorption*, Surface Science Reports **12**, 133 (1991).
- [137] F. E. Olsson and M. Persson, *A density functional study of adsorption of sodium-chloride overlayers on a stepped and a flat copper surface*, Surface Science **540**, 172 (2003).

Bibliography

- [138] M. Böhringer, W.-D. Schneider, R. Berndt, K. Glöckler, M. Sokolowski, and E. Umbach, *Corrugation reversal in scanning tunneling microscope images of organic molecules*, Physical Review B **57**, 4081 (1998).
- [139] K. Morgenstern, E. Lægsgaard, I. Stensgaard, F. Besenbacher, M. Böhringer, W.-D. Schneider, R. Berndt, F. Mauri, A. De Vita, and R. Car, *Stability of two-dimensional nanostructures*, Applied Physics A **69**, 559 (1999).
- [140] M. Böhringer, W.-D. Schneider, and R. Berndt, *Two-dimensional self-assembly of supramolecular structures*, Surface Review and Letters **7**, 661 (2000).
- [141] D. M. Eigler, P. S. Weiss, E. K. Schweizer, and N. D. Lang, *Imaging Xe with a low-temperature scanning tunneling microscope*, Physical Review Letters **66**, 1189 (1991).
- [142] H. Peisert, M. Knupfer, and J. Fink, *Energy level alignment at organic/metal interfaces: Dipole and ionization potential*, Applied Physics Letters **81**, 2400 (2002).
- [143] H. Peisert, M. Knupfer, T. Schwieger, G. G. Fuentes, D. Olligs, and J. Fink, *Fluorination of copper phthalocyanines: Electronic structure and interface properties*, Journal of Applied Physics **93**, 9683 (2003).
- [144] I. H. Campbell, S. Rubin, T. A. Zawodzinski, J. D. Kress, R. L. Martin, D. L. Smith, N. N. Barashkov, and J. P. Ferraris, *Controlling Schottky energy barriers in organic electronic devices using self-assembled monolayers*, Physical Review B **54**, R14321 (1996).
- [145] I. H. Campbell, J. D. Kress, R. L. Martin, D. L. Smith, N. N. Barashkov, and J. P. Ferraris, *Controlling charge injection in organic electronic devices using self-assembled monolayers*, Applied Physics Letters **71**, 3528 (1997).
- [146] S. Yoshimoto, J. Inukai, A. Tada T. Abe T. Morimoto, A. Osuka, H. Furuta, and K. Itaya, *Adlayer Structure of and Electrochemical O₂ Reduction on Cobalt Porphine-Modified and Cobalt Octaethylporphyrin-Modified Au(111) in HClO₄*, Journal of Physical Chemistry B **108**, 1948 (2004).
- [147] S. Yoshimoto, E. Tsutsumi, Y. Honda, Y. Murata, M. Murata, K. Komatsu, O. Ito, and K. Itaya, *Controlled Molecular Orientation in an Adlayer of a Supramolecular Assembly Consisting of an Open-Cage C₆₀ Derivative and Zn^{II} Octaethylporphyrin on Au(111)*, Angewandte Chemie International Edition **43**, 3044 (2004).
- [148] S. Yoshimoto, A. Tada, and K. Itaya, *In Situ Scanning Tunneling Microscopy Study of the Effect of Iron Octaethylporphyrin Adlayer on the Electrocatalytic Reduction of O₂ on Au(111)*, Journal of Physical Chemistry B **108**, 5171 (2004).
- [149] M. Knupfer and H. Peisert, *Electronic properties of interfaces between model organic semiconductors and metals*, physica status solidi (a) **201**, 1055 (2004).

- [150] X. Crispin, V. Geskin, A. Crispin, J. Cornil, R. Lazzaroni, W. R. Salaneck, and J.-L. Brédas, *Characterization of the Interface Dipole at Organic/Metal Interfaces*, Journal of the American Chemical Society **124**, 8131 (2002).
- [151] L. Lindell, M. P. de Jong, W. Osikowicz, R. Lazzaroni, M. Berggren, W. R. Salaneck, and X. Crispin, *Characterization of the interface dipole at the paraphenylenediamine-nickel interface: A joint theoretical and experimental study*, Journal of Chemical Physics **122**, 084712 (2005).
- [152] N. D. Lang and W. Kohn, *Theory of Metal Surfaces: Charge Density and Surface Energy*, Physical Review B **1**, 4555 (1970).
- [153] S. Kitagawa, I. Morishima, T. Yonezawa, and N. Sato, *Photoelectron spectroscopic study on metalloctaethylporphyrins*, Inorganic Chemistry **18**, 1345 (1979).
- [154] I. G. Hill, A. Kahn, J. Cornil, D. A. dos Santos, and J. L. Brédas, *Occupied and unoccupied electronic levels in organic π -conjugated molecules: comparison between experiment and theory*, Chemical Physics Letters **317**, 444 (2000).

List of Publications

Publications

- S. Berner, M. Brunner, L. Ramoino, H. Suzuki, H.-J. Güntherodt, and T. A. Jung, *Time evolution analysis of a 2D solid-gas equilibrium: a model system for molecular adsorption and diffusion*, Chem. Phys. Lett. **348** (2001) 175-181
- L. Ramoino, M. Labardi, N. Maghelli, L. Pardi, M. Allegrini, and S. Patanè, *Polarization-modulation near-field optical microscope for quantitative local dichroism mapping*, Rev. Sci. Instr. **73** (2002) 2051-6
- M. de Wild, S. Berner, H. Suzuki, L. Ramoino, A. Baratoff, and T. A. Jung, *Molecular Assembly and Self-Assembly: Molecular Nanoscience for Future Technologies*, Chimia **56** (2002) 500-505
- S. Berner, M. de Wild, L. Ramoino, S. Ivan, A. Baratoff, H.-J. Güntherodt, H. Suzuki, D. Schlettwein and T. A. Jung, *Adsorption and two-dimensional phases of a large polar molecule: Sub-phthalocyanine on Ag(111)*, Phys. Rev. B **68** (2003) 115410
- M. de Wild, S. Berner, H. Suzuki, L. Ramoino, A. Baratoff, and T. A. Jung, *Molecular Assembly and Self-Assembly: Molecular Nanoscience for Future Technologies*, Ann. N. Y. Acad. Sci. **1006** (2003) 291305
- S. Berner, S. Schintke, L. Ramoino, M. de Wild and T. A. Jung, *Two-dimensional structural transition controlled by the electric field*, US Patent Application Nr. 20050002222 A1 (2005)
- L. Ramoino, M. von Arx, S. Schintke, A. Baratoff, H.-J. Güntherodt, and T. A. Jung, *Layer-selective epitaxial self-assembly of porphyrins on ultrathin insulators*, submitted to Chem. Phys. Lett.
- A. Alkauskas, L. Ramoino, M. von Arx, S. Schintke, A. Baratoff, H.-J. Güntherodt, and T. A. Jung, *Energy level alignment at the metal - octaethylporphyrin interfaces*, manuscript in preparation

Conference Presentations

- L. Ramoino, S. Berner, M. Brunner, L. Gade, C. Galka, T. A. Jung and H.-J. Güntherodt, *Deposition system for single molecule experiments with scanning tunneling microscope*, Sci & Ski Conference 01, Andermatt (Switzerland), March 19-23, 2001
- L. Ramoino, S. Berner, M. Brunner, H. Suzuki, H. Yanagi, D. Schlettwein, H.-J. Güntherodt and T. A. Jung, *Molecular Adsorption and Motion in a 2D GasSolid Equilibrium*, Thin Film & Crystal Growth Mechanisms, Williamstown MA, July 1-6, 2001.
- L. Ramoino, S. Berner, M. de Wild, L. Gade, C. Galka, T. A. Jung and H.-J. Güntherodt, *STM Study of Perylene Molecules Adsorbed on Ag(100)*, Twannberg Workshop on Nanoscience, Twannberg (Switzerland), October 16-19, 2001
- L. Ramoino, S. Schintke, S. Berner, M. de Wild, T. A. Jung and H.-J. Güntherodt, *Scanning Tunnelling Microscopy and Spectroscopy of Organic Molecules on Thin NaCl(001) Films: A model System for Single Molecular Tunnelling*, Meeting of the NCCR on Nanoscale Science, Pontresina (Switzerland), September 3-6, 2002
- L. Ramoino, S. Schintke, S. Berner, M. de Wild, T. A. Jung and H.-J. Güntherodt, *Organic molecules on thin NaCl(001) films and on Cu(111) investigated by STM*, TNT2002 (Trends in Nanotechnology), Santiago de Compostela (Spain), September 9-13, 2002
- L. Ramoino, S. Berner, M. de Wild, S. Schintke, H. Suzuki, H.-J. Güntherodt, and T. A. Jung, *Reversible 2D Molecular Phase Transition Induced by STM Tip*, STM'03, Eindhoven (the Netherlands), July 21-25, 2003
- L. Ramoino, S. Schintke, S. Berner, M. de Wild, H.-J. Güntherodt, and T. A. Jung, *Thin insulator layers and molecular wires on a metallic substrate*, STM'03, Eindhoven (the Netherlands), July 21-25, 2003
- L. Ramoino, S. Berner, M. de Wild, A. Heuri, D. Haldemann, A. Scheybal, H.-J. Güntherodt, and T. A. Jung. *Nano-Patterns Explored for Molecular Scale Storage (Acronym SADS, Self Assembled Data Storage)*, Nanofair, St Gallen (Switzerland), September 9-11, 2003

Acknowledgments

I'd like to take here the opportunity to thank all the people which made my Ph.D. possible.

First of all, I'm grateful to Prof. H.-J. Güntherodt and to my supervisor Dr. T. A. Jung for giving me the opportunity to work in Basel. Here I had a great time and I had the possibility to work in a really interesting and stimulating environment.

I also want to thank Prof. E. Meyer for accepting to be a referee of this thesis.

I then want to express my gratitude to all the past and present members of the NANOLAB: Simon Berner, Michael de Wild, Alex Heuri, Silvia Schintke, Diego Haldemann, Matthias von Arx, Hannes Spillmann, Markus Wahl, Andreas Kiebele, Meike Stöhr and Tomas Samuely. In particular I'd like to thank Simon Berner and Michael de Wild for teaching me all the *secrets* of the complex NANOLAB's experimental equipment. I also want to thank Silvia Schintke and Matthias von Arx which closely assisted me in my Ph.D. work and carefully read this thesis.

I'm grateful to our theorists Alexis Baratoff and Audrius Alkauskas. The frequent and fruitful discussions I had with them have been invaluable. In particular I want to acknowledge Audrius Alkauskas for the DFT calculations whose results are also presented in this thesis.

I'd like to thank the present and past members of the whole Güntherodt and Meyer group for the friendly atmosphere and the numerous and very interesting discussions.

I also want to acknowledge the kind and helpful collaboration received during my work from all the people of the electronic workshop and especially from H.-R. Hidber and A. Tonin.

A particular mention goes to Remo Hofer for his helpful support on all kind of informatics problems and for his patience in sharing the office all this time.

I'd like to thank J. Vetter, G. Weaver, A. Fischer, A. Kalt and B. Kammermann for their administrative work and for their effective collaboration in making simple also complicated bureaucratic issues.

Finally I must thank here my family and all the friends which supported me during this time. It is not possible to mention here all their names but my sincere and deepest gratitude goes to all of them.

Curriculum Vitae

Luca Ramoino

01.07.1975	geboren in Imperia (Italien)
1981-1986	Besuch der <i>Scuola Elementare</i> in Imperia
1986-1989	Besuch der <i>Scuola Media</i> in Imperia
1989-1994	Besuch der <i>Liceo Scientifico</i> in Imperia
Jul. 1994	Maturität
Okt. 1994	Beginn des Studiums in Physik an der Universität Pisa
Jul. 1999 – Jul 2000	Diplomarbeit in der Forschungsgruppe von Prof. M. Allegrini am Institut für Physik der Universität Pisa mit dem Thema: “ <i>Study and application of polarization contrast in optical near field microscopy</i> ”
Okt. 2000	Diplom Abschluss <i>Laurea in Fisica</i>
Dez. 2000 – Mai 2005	Doktorarbeit und Assistententätigkeit unter der Leitung von Dr. T. A. Jung in der Gruppe von Prof. H.-J. Güntherodt am Institut für Physik der Universität Basel

Folgenden Dozentinnen und Dozenten verdanke ich meine Ausbildung:

M. Allegrini (PI), E. Arimondo (PI), A. Baratoff (BS), R. Bennowitz (BS), G. Cicogna (PI), E. d’Emilio (PI), M. Giordano (PI), S. Goedecker (BS), G. Grosso (PI), E. Guadagnini (PI), H.-J. Güntherodt (BS), M. Hegner (BS), T. A. Jung (BS), M. Labardi (PI), D. Leporini (PI), R. Mannella (PI), P. Menotti (PI), E. Meyer (BS), P. Minguzzi (PI), S. Servadio (PI).

PI: Universität Pisa

BS: Universität Basel

